

AD-A066 280

FOREIGN TECHNOLOGY DIV WRIGHT-PATTERSON AFB OHIO
EXPERIMENTAL AEROMECHANICS (SELECTED CHAPTERS), (U)
JAN 79 S M GÖRLIN

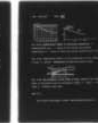
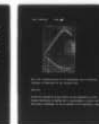
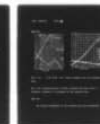
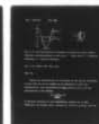
F/G 20/4

UNCLASSIFIED

FTD-ID(RS)T-2011-78

NL

1 OF 4
ADA
066280



①

AD-A066280

FOREIGN TECHNOLOGY DIVISION



EXPERIMENTAL AEROMECHANICS
(Selected Chapters)

by

S. M. Gorlin



Approved for public release;
distribution unlimited.



79 03 06 117

UNEDITED MACHINE TRANSLATION

FTD-ID(RS)T-2011-78

8 January 1979

MICROFICHE NR: *AD-79-C-000065*

EXPERIMENTAL AEROMECHANICS (SELECTED CHAPTERS)

By: S. M. Gorlin

English pages: 349

Source: Eksperimental'naya Aeromekhanika,
Moscow, 1970, pp. 1-8; 111-146;
294-420.

Country of origin: USSR

This document is a machine translation.

Requester: FTD/TQTA

Approved for public release; distribution unlimited.

ACCESSION NO.	
RTIS	Write Section <input checked="" type="checkbox"/>
RDS	Ref. Section <input type="checkbox"/>
UNANNOUNCED	<input type="checkbox"/>
JUSTIFICATION	
BY	
DISTRIBUTION/AVAILABILITY CODE	
Dist.	AVAIL. REQ. BY SPECIAL
A	

THIS TRANSLATION IS A RENDITION OF THE ORIGINAL FOREIGN TEXT WITHOUT ANY ANALYTICAL OR EDITORIAL COMMENT. STATEMENTS OR THEORIES ADVOCATED OR IMPLIED ARE THOSE OF THE SOURCE AND DO NOT NECESSARILY REFLECT THE POSITION OR OPINION OF THE FOREIGN TECHNOLOGY DIVISION.

PREPARED BY:

TRANSLATION DIVISION
FOREIGN TECHNOLOGY DIVISION
WP-AFB, OHIO.

79 03 06 117

TABLE OF CONTENTS

U. S. Board on Geographic Names Transliteration System, Russian and English Trigonometric Functions.....	1
Preface.....	3
Introduction.....	6
Chapter V. Boundary Layer.....	12
Chapter VIII. Aerodynamic Characteristics of Different Bodies.....	93
Chapter IX. Characteristics of Profiles and Wings.....	209
Chapter X. Flow in Channels.....	314
References.....	349

U. S. BOARD ON GEOGRAPHIC NAMES TRANSLITERATION SYSTEM

Block	Italic	Transliteration	Block	Italic	Transliteration
А а	А а	A, a	Р р	Р р	R, r
Б б	Б б	B, b	С с	С с	S, s
В в	В в	V, v	Т т	Т т	T, t
Г г	Г г	G, g	У у	У у	U, u
Д д	Д д	D, d	Ф ф	Ф ф	F, f
Е е	Е е	Ye, ye; E, e*	Х х	Х х	Kh, kh
Ж ж	Ж ж	Zh, zh	Ц ц	Ц ц	Ts, ts
З з	З з	Z, z	Ч ч	Ч ч	Ch, ch
И и	И и	I, i	Ш ш	Ш ш	Sh, sh
Й й	Й й	Y, y	Щ щ	Щ щ	Shch, shch
К к	К к	K, k	Ъ ъ	Ъ ъ	"
Л л	Л л	L, l	Ы ы	Ы ы	Y, y
М м	М м	M, m	Ь ь	Ь ь	'
Н н	Н н	N, n	Э э	Э э	E, e
О о	О о	O, o	Ю ю	Ю ю	Yu, yu
П п	П п	P, p	Я я	Я я	Ya, ya

*ye initially, after vowels, and after Ъ, Ь; e elsewhere.
When written as ё in Russian, transliterate as yě or ě.

RUSSIAN AND ENGLISH TRIGONOMETRIC FUNCTIONS

Russian	English	Russian	English	Russian	English
sin	sin	sh	sinh	arc sh	sinh ⁻¹
cos	cos	ch	cosh	arc ch	cosh ⁻¹
tg	tan	th	tanh	arc th	tanh ⁻¹
ctg	cot	cth	coth	arc cth	coth ⁻¹
sec	sec	sch	sech	arc sch	sech ⁻¹
cosec	csc	csch	csch	arc csch	csch ⁻¹

Russian	English
rot	curl
lg	log

Page 2.

In the book are set forth the physical bases of experimental aeromechanics, the methods of aeromechanical tests under varied conditions. Is given description of the devices of different wind tunnels and installations, intended for experimental investigations at subsonic, supersonic and hypersonic speeds. Are set forth methods and are described instruments for determining the flow parameters during aerodynamic tests, and also experimental procedure and introduction of corrections to the results of experiments. The considerable place in the book occupies the presentation of the results of investigations in the experimental determination of the aerodynamic wing characteristics of aircraft, rockets, different bluff bodies, ground-based transport and above-ground structures and elements of structures.

The book is intended for the students of VUZ [Institute of Higher Education], who study aerohydrodynamics and gas dynamics and their application/appendix to different branches of technology. It will be also useful for the workers of design bureaus and scientific organizations, which directly conduct experimental research in the field of aeromechanics or using results aeromechanical experiments, and also for persons, occupied with

equipping of different aeromechanical installations and with the development of equipment to them.

Figures 447. Tables 21. Bibliographies 8.

Reviewers:

MAI

department of the aerohydrodynamics of LPI im. Kalinin prof. I.
Ya. Fabrikant.

Experimental aeromechanics is connected to theoretical processes not from one or the other mechanical analogs, but it invests the behavior of bodies under the actual conditions of their interaction with the fluid flow and gases and transfers the results of experiments for other analogous cases with the aid of the laws of similarity.

The object/subject of its experiments are physical bodies.

Page 3.

Preface.

Experimental aeromechanics in contrast to theoretical proceeds not from one or the other mechanical analogs, but it investigates the behavior of bodies under the actual conditions of their interaction with the fluid flow and gases and transfers the results of experiments for other analogous cases with the aid of the laws of similarity.

The object/subject of its experiments are physical bases, experimental methods and results of aeromechanical investigations.

In this work special attention is devoted to the examination high velocities whose study in recent years occupies the increasing place both in theoretical ones and in experimental aeromechanical investigations. In the book are consecutively presented the physical properties of liquid and gases, the fundamental laws of movement of air at small and high rates of flow, the cell/elements of gas dynamics, the laws of the flow around the bodies of various forms, similarity and simulation in aeromechanical experiments, methods, ways and results of different aeromechanical measurements, air foil data, wings, bodies of revolution, flow in ducts, nozzles and exit cone/diffusers.

Page 4.

The limited size of the book will not make it possible to present some, although specific questions of aeromechanics as that: the characteristic of bodies with unsteady motion, etc. In all possible cases the aeromechanical phenomena and the processes are characterized not only physically, but are given also the quantitative data, which make it possible to rate/estimate the specific gravity/weight of different factors, which affect the flow around diverse bodies of the flow of gas.

The dimensional values, given in the book, are given in the majority of the cases in MKGSS system since aeromechanical measurements and processing of their results are adapted to the system indicated. When dimensional values are not connected directly with measurements it is utilized international system (SI).

For the facilitation of the conversion of ones of one system into another in text, is given the table of the dimensionality, which are encountered in aeromechanics of physical quantities in MKGSS system and international system (SI).

Page 5.

The author expresses deep appreciation to the reviewers Prof. Nicholas Yakovlevich Fabrikant and Prof. Leo Gerasimovich Loytsyanskiy, who made is many observations, which contributed to an improvement in the book, V. V. Nazarenko and G. E. Khidyakov - for the useful discussion the manuscripts, and also by N. A. Mironovoy and G. I. Antonova after aid in preparation for the manuscript for press/printing.

Author.

Page 6.

Introduction.

Aeromechanics is called the science, which is occupied by the study of the laws of the motion of gases (air) under varied conditions and investigating their effect with the contacted bodies. In this narrow sense aeromechanics is the part of the hydromechanics, i.e., the mechanics of the unsteady bodies which can be subdivided into three groups:

- 1) fluid bodies with high viscosity (glycerin);
- 2) fluid bodies with small ductility/toughness/viscosity (water, gasoline, mercury);
- 3) gaseous substances (air, nitrogen, oxygen, etc.).

Between these groups there are no sharp boundaries. However, it is difficult to establish/install the boundary between solids and liquids. The basic difference between them lies in the fact that solid bodies change form approximately proportional to the affecting

them force, unsteady - are deformed even under the effect how conveniently of small forces, if the deformation rate is low. The forces which must be overcome in this case, are called of the viscous forces.

Liquid and gaseous substances essentially differ from each other in terms of the degree of compressibility. While the liquids exert extremely high resistance to a change in their volume and because of this are considered in hydromechanics as incompressible, gases are compressed during comparatively small changes in the pressure. On these reasons for the investigations, connected taking into account the compressibility effect of air and gases, they occupy in aeromechanics the exclusively important place.

The properties of gases, liquids and solid bodies are connected with their molecular structure. As is known, between molecules there are attracting forces. In solid bodies they are most significant, and it is necessary to greatly strengthen in order to overcome them (to change form, but those more to divide solid body on part). In liquids these forces are much less; therefore liquids do not have their own form, they are flowing and always is taken the form of the container in which they are located. In gases of the force of the mutual attraction, barely they are exhibited and become noticeable only at very high pressures and low temperatures when the intermolecular

distances strongly decrease.

Page 7.

At sufficiently low (for this pressure) temperature the gases are converted into liquid (for example, nitrogen with -195.8°C ; oxygen with -183°C).

The basic difference for gases from liquids consists: first, in the insignificance of cohesive forces between the molecules of gas, caused by the large distances between them and which leads to the fact that the molecules fly off in different directions, and gas is spread by entire given to it volume, liquid, filled into container, is formed floating surface; in the second place, in the large intermolecular distances of gas, which causes its powerful compressibility in comparison with the negligible compressibility of liquids.

The liquid, deprived of the viscous forces, is called ideal. The examination of the courses of ideal fluid makes important sense because many phenomena in aeromechanics (in real liquids and gases) little depend on the viscous forces whose effect is substantial near body surface and therefore in the first approximation, they can be considered as the phenomena in ideal fluid. Although gases consist of

the molecules, between which there are interval/gaps however for convenience in their theoretical study, they consider that the substance of gas is continuously distributed in all volume, i.e., that gas is continuous medium. As a result of the smallness of the particles, which compose substance, this representation (simulation) of gases and liquids are not virtually affected the obtained results.

In 1 cm^3 of air it is found at normal atmospheric pressure $2.7 \cdot 10^{19}$ molecules (number of Loschmidt). Examining, for example, cube with fin/edges 0.01 mm , we will obtain that in this volume it is contained $2.7 \cdot 10^{10}$ molecules. Under these conditions air can be considered continuous medium. Such position will not occur at the very low values of density (pressure), so, at a pressure of approximately one billionth standard atmosphere ($1 \cdot 10^{-9} \text{ mm Hg}$) into of 1 cm^3 will be located $2.7 \cdot 10^{10}$ molecules, but in cube with fin/edges 0.01 mm - 27 molecules. On these reasons with the motion of the strongly rarefied gases or during flights at very high altitudes (for example, at the height/altitude of 200 km and higher) already it is not possible to consider gas as continuous medium.

Under normal conditions the pressure gas on barrier/obstacle (wall) on the average remains time-constant, since a number of molecules is very great, is also great and a number of collisions of molecules with wall. For example, at temperature of 0°C and pressure

760 mm Hg the velocity of the motion of the molecules of air is equal about 450 m/s, the collision frequency per second of each molecule with other or with wall comprises $7.5 \cdot 10^9$, and the mean free path of molecules - about one decamillion part of the meter ($\sim 5.9 \cdot 10^{-6}$ cm). With a decrease of pressure, which corresponds to elevation to height/altitude, it decreases both number of molecules and collision rate, and increases the average path of their mean free path which reach at the height/altitude of 100 km - 10 cm, at the height/altitude of 150 km - 8 m, but at the height/altitude of 200 km - more than thousand meters.

Page 8.

At similar height/altitudes separate molecules is clashed with the flying apparatus only one time. The laws of the effect of air on this apparatus will be others, rather than at the low altitudes where the mean free path of molecules is negligible in comparison with the size/dimensions of the flying bodies.

Thus, aeromechanics studies air circulation and its interaction with bodies under the manifold conditions, characterized by both the different state of the gas (pressure, temperature, density, etc.) and by different forms of bodies.

The tasks, connected with aeromechanics, are encountered in many areas of science and technology; however, principal direction is connected with the study of relative motion of liquid (gas) and solid body. Here first of all it is necessary to note the cases when the streamlined bodies are completely immersed in liquid (aircraft, submarines, rockets, etc.) and the conditions, under which the liquid or gas flows within different channels (gas pipes, wind tunnels, ventilation systems, compressors, turbines of jet engines, etc.).

Although theoretical aeromechanics achieved large successes, it not always can be used for solving the manifold practical tasks, advanced by the development of technology and industry. On these reasons in aeromechanics, intensely are developed the experimental methods of the studies which actually can be considered as independent important discipline. The experimental methods of aeromechanics are utilized not only for checking the developed theory, but also they are the source of the creation of more precise theories on the basis of the phenomena and facts, detected experimentally.

Page 111.

Chapter V.

BOUNDARY LAYER.

§V.1. Laminar and turbulent boundary layers.

Until now, was examined, mainly, the motion of ideal fluid, i.e., the liquid, not having internal frictional forces. the forces of internal friction or ductility/toughness/viscosity exist in all real liquids and gases. As a result of their effect, all strict conclusions, made for an ideal fluid, for real liquids and gases are these approximate, that need some corrections and refinements. One of primary tasks of aeromechanics (in particular, experimental) is the determination of the corrections into theory which introduce the forces of viscosity of liquids or gases.

The viscous forces attempt to inhibit the rapidly driving/moving particles of liquid and to accelerate the motion of slower particles.

They are in essence forces of periphery and it is especially great where the liquid flows by layers with a large difference in the rates. Ductility/toughness/viscosity serves as a reason for the education/formation of eddy/vortices, very substantially affecting flow of liquid or gases. On the other hand, the formed eddy/vortices due to ductility/toughness/viscosity gradually are resolved.

If we take the liquid between two parallel plates and to give to upper plate rate u (Fig. V.1), then observation they make it possible to establish/install following:

- 1) liquid adheres to surfaces so that the particles which directly fit closely to plates, have rates, equal to the rates of plate;
- 2) the rate of the liquid between plates along the normal to them changes according to linear law;
- 3) internal fluid friction is resisted to motion, proportional to the velocity gradient.

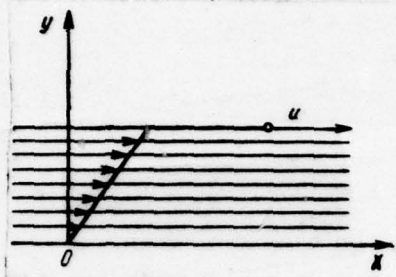


Fig. V.1. Flow of liquid between plates.

Page 112.

Analogous experiments show that during the flow around body of liquid on very body surface the liquid is motionless, it "adheres", and at certain small distance from it, it acquires already the rate, comparable with the local velocity of inleakage (Fig. V.1). This thin layer, in which takes place the increase of velocity from zero to the local velocity of flow, is called boundary layer.

Ductility/toughness/viscosity in liquids and gases is the consequence of their molecular structure. The molecules of gases and liquids according to kinetic theory possess the completely definite average random velocities, which depend only on temperature. In each more rapidly driving/moving layer I (Fig. V.2) molecule, they have, except the velocity of irregular molecular motion, even additional ordered velocity of overall forward motion. Thus, the velocity of

molecules in layer I will be more than in layer II. With the mixing of layers, the more rapidly driving/moving molecules, falling into the slow layer II, transfer to the molecules of this layer certain momentum/impulse/pulse and they will accelerate them, and themselves to brake. And vice versa, "slow" molecules, falling into rapid layers, will be brake them, and themselves somewhat accelerated.

Newton assumed, and further investigations justified this assumption that the forces of viscosity dX , acting along two closely spaced area/sites (or layers) in the boundary layer of liquid (Fig. V. 3) :

$$dX = -\mu \left(\frac{\partial v}{\partial y} \right) dS,$$

where μ - the coefficient of dynamic viscosity, characterizing physical properties of liquid;

dS - area;

$\frac{\partial v}{\partial y}$ - velocity gradient along the normal to body surface.

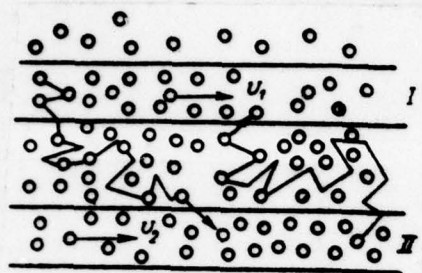


Fig. V.2.

Fig. V.2. Molecular motion as the reason for ductility/toughness/viscosity.

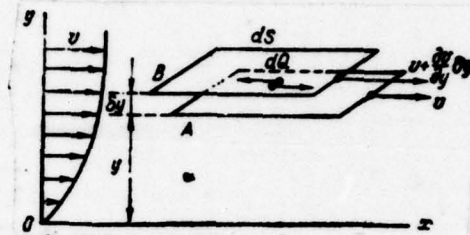


Fig. V.3.

Fig. V.3. Interaction of layers according to Newton.

Page 113.

The forces, which act on two adjacent pads, are equal in magnitude, but they are oppositely directed.

If we divide force dX into area dS , then we will obtain voltage equal to

$$\tau = \frac{dX}{dS} = \mu \left(\frac{\partial v}{\partial y} \right)_{y=0}$$

This voltage directed along area/site is therefore tangential (tangent).

The coefficient of ductility/toughness/viscosity there is a value dimensional (see table III.1):

$$[\mu] = \frac{\left[\frac{dX}{dS} \right]}{\left[\frac{\partial v}{\partial y} \right]} = \frac{\left[\frac{\text{кг}}{\text{м}^2} \right]^{(1)}}{\left[\frac{\text{м} \cdot \text{с}}{\text{сек} \cdot \text{м}} \right]} = \left[\frac{\text{кг} \cdot \text{сек}}{\text{м}^3} \right]^{(2)} = \left[\frac{\text{н} \cdot \text{сек}}{\text{м}^3} \right]^{(3)}.$$

Key: (1). kgf. (2). kg·s. (3). N·s. (4). m/s. In the examination of the flow of liquid or gases, it is very frequently necessary to compare the viscous forces, which depend on μ , with the inertial forces, the proportional ones to mass density ρ . Therefore proves to be advisable to introduce an additional one coefficient of the ductility/toughness/viscosity

$$\nu = \frac{\mu}{\rho},$$

that characterizing the acceleration of single mass from the viscous forces. This coefficient is called kinematic modulus of viscosity. Its dimensionality

$$[\nu] = \left[\frac{\text{м}^2}{\text{сек} \cdot \text{с}} \right].$$

Key: (1). m²/s. All calculations in aeromechanics are conducted usually in system of practical units, and values μ and ν one should represent in the same system. However, the majority of the laboratory investigations of ductility/toughness/viscosity is conducted in the absolute system of ones. As ones of ductility/toughness/viscosity, is

accepted one poise, which corresponds to value τ , equal to 1 dynes to of 1 cm² under the assumption $\frac{\partial v}{\partial y} = 1$, that velocity from area/site to area/site, removed to a distance of 1 cm, changes on 1 cm/s. Under these conditions

$$\mu = \frac{\tau}{\frac{\partial v}{\partial y}} = 1.$$

Page 114.

Are used also small/finer one of ductility/toughness/viscosity - centipoises and millipoise. Transition from poises to working standard of ductility/toughness/viscosity can be found from the relationship/ratio

$$\left| \frac{\kappa \Gamma \cdot \text{сек}}{\text{м}^2} \right| = \frac{981,000 \overset{(1)}{\text{дин}} \cdot \text{сек}}{10\,000 \text{ с.м}^2} = 98,1 \left| \frac{\overset{(2)}{\text{дин}} \cdot \text{сек}}{\text{с.м}^2} \right| = 98,1 \overset{(2)}{\text{пуаз}}$$

Key: (1). dyn·s. (2). poise.

or

$$\mu \left| \frac{\kappa \Gamma \cdot \text{сек}}{\text{м}^2} \right| = \frac{\overset{(1)}{\mu} \overset{(2)}{\text{пуаз}}}{98,1}.$$

Key: (1). kg·s. (2). poise.

In exactly the same manner for a kinematic modulus of viscosity let us find

$$\nu \left| \frac{\text{m}^2}{\text{сек}} \right| = \nu \left| \frac{\text{см}^2}{\text{сек}} \right| \cdot \frac{1}{100\,000}$$

Key: (1). m^2/s .

In practice value μ is determined in the majority of the cases by viscosimeters, gauging consumption of the liquid through the capillary or capillary tubes flows in which are subordinated to poiseuille equation, into honor of whom is named one of ductility/toughness/viscosity. Poiseuille flow - this is the flow of viscous fluid along the duct of a small diameter. In examination in the glass duct of flow of water, to which are mixed small solid suspended particles, it is possible at considerable rate of flow to note that together with main x x-motion of duct are clearly visible the incidental particle motions in the direction, normal to the axle/axis of duct. If the rate of motion in duct is decreased, then at certain rate will become the evident that the particles of liquid move with separate layers over the trajectories, to and walls. This flow is called laminar. If we examine laminar flow in the tube of so small a diameter, that the boundary layer thickness is more than a radius, then boundary layer will be linked on axle/axis and will fill entire tube. The law of rate change in a radius is determined by

Poiseuille equation (Fig. V.4)

$$v = \frac{\Delta p}{4\mu l} (R^2 - r^2),$$

where l - distance of the section in question from the beginning of duct;

Δp - jump/drop in the pressure under action of which occurs the flow;

R - radius of duct;

r - variable radius.



Fig. V.4. Rate change across duct during Poiseuille flow.

Page 115.

From this formula it follows that the rate changes according to parabolic law. This flow is called Poiseuille flow. Fluid flow rate through the tube is equal to

$$U = \frac{\pi \Delta p}{8 \mu l} R^4,$$

where U - a volume of the liquid, which escape/ensued for time unit;

Δp - the pressure differential at the length of the capillary of tube;

l - length of capillary;

R - radius of tube.

Value of the coefficient of ductility/toughness/viscosity for

the air

$$\mu = (1,745 \cdot 10^{-6} + 5,03 \cdot 10^{-9} t^{\circ}\text{C}) \text{ kg}\cdot\text{s}/\text{m}^2$$

of $t=15^{\circ}\text{C}$ $\mu=1.82 \cdot 10^{-6} \text{ kgf s}/\text{m}^2$. Hence $\nu=1,45 \cdot 10^{-5}$ (with $t=15^{\circ}\text{C}$ $p=760 \text{ mm Hg}$). For the water

$$\mu = \frac{0,0178\rho}{1 + 0,0337t^{\circ} + 0,00022t^{\circ 2}}$$

at 15°C

$$\mu = 1,164 \cdot 10^{-4} \text{ kg}\cdot\text{s}/\text{m}^2.$$

The kinematic viscosity of water is small:

$$\nu = \frac{\mu}{\rho} = \frac{\mu g}{\gamma} = \frac{1,164 \cdot 10^{-4} \cdot 9,81}{1000} = 0,1145 \cdot 10^{-6} \text{ m}^2/\text{s} \text{ (at } 15^{\circ}\text{C)}.$$

Comparing this value with value ν for air, we obtain

$$\frac{\nu_{\text{air}}}{\nu_{\text{water}}} = \frac{1,45 \cdot 10^{-5}}{0,1145 \cdot 10^{-6}} = 12,7.$$

i.e. the kinematic viscosity of air 12.7 times of more than the kinematic viscosity of water.

The ductility/toughness/viscosity of air and other gases increases with temperature. A change in the kinematic modulus of

viscosity during a change in the temperature and pressure for air is shown on Fig. V.5. The viscosity of true liquids from a temperature rise falls.

Under the effect of viscosity (internal friction) the gas velocity on the surface of the streamlined plate becomes equal to zero. During removal/distance from plate along the normal to its surface, the speed grow/rises to the value, which corresponds to the speed of undisturbed flow (v_0). The same occurs, also, during the flow around other bodies despite the fact that the speed along them can be changed.

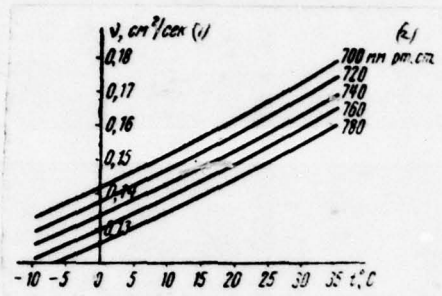


Fig. V.5. Curve/graph $\nu = f(t)$ for air.

Key: (1) . cm²/s. (2) . mm Hg.

Page 116.

In laminar boundary layer the flow occurs by the nonmiscible layers (Fig. V.6), but in this case the flow is whirled (Fig. V.7), and boundary layer occasionally referred to as also the layer of surface turbulence. Despite the fact that the particles in this layer rotate, there is no their transverse mixing.

If boundary-layer flow is accompanied by the random movement of particles and their mixing in transverse direction (perpendicular to flow direction), then this boundary layer is called turbulent. Single particles in it describe complex curved paths, which do not coincide with the flow lines of the averaged flow (Fig. V.8).

This state of boundary-layer flow and connected with frictional resistance to motion, and also all the aerodynamic properties of the streamlined bodies depend on Reynolds number, which characterizes the ratio of inertial forces to frictional forces. To number $Re_x = 2 \cdot 10^5$ for a flat/plane plate, the boundary layer retains its laminar structure. Hence it follows that the length of the laminar part of the boundary layer

$$l_x = \frac{Re_x v}{v} = 2 \cdot 10^5 \frac{v}{v}.$$

For standard air

$$l_x = 2 \cdot 10^5 \frac{1,45 \cdot 10^{-3}}{v} = \frac{29,0}{v}.$$

The increase of velocity or boundary layer velocity profile can be described by the approximate theoretical expressions

$$v = v_0 \left[2 \left(\frac{y}{\delta} \right) - 5 \left(\frac{y}{\delta} \right)^2 + 6 \left(\frac{y}{\delta} \right)^3 - 2 \left(\frac{y}{\delta} \right)^4 \right]$$

or

$$v = v_0 \left(2 \frac{y}{\delta} - \frac{y^2}{\delta^2} \right).$$

where y - point, in which the velocity is equal v ;

δ - thickness of the entire boundary layer (Fig. V.9), with $y = \delta$
 $v = v_0$.



Fig. V.6. Diagrammatic representation of viscous motion in boundary layer.

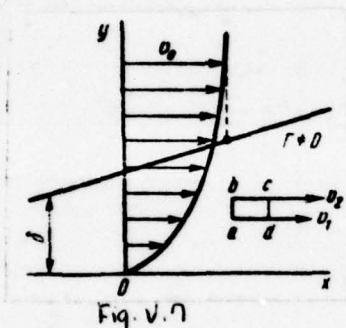


Fig. V.7

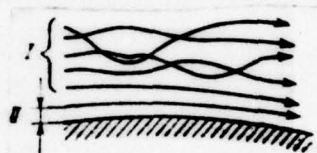


Fig. V.8.

Fig. V.7. Eddying of laminar boundary layer.

Fig. V.8. The schematic of turbulent motion in the boundary layer: I - turbulent boundary layer; II - laminar sublayer.

Page 117.

These airfoil/profiles satisfy the condition of adhesion on wall and the condition of steady transition to the velocity of the inviscid flow v_0 . However, virtually the increase of the velocity in boundary layer occurs on its larger part almost linearly, and

beginning approximately with the half of thickness of the layer it begins bending of the velocity profile. The thickness of laminar boundary layer along plate, as show experimental data, is changed according to parabolic law, i.e., it is proportional \sqrt{x} :

$$\frac{\delta}{x} = \frac{5,83}{\sqrt{Re_x}} \text{ or } \delta = 6 \sqrt{\frac{\nu x}{u_0}}$$

here Re_x - Reynolds number at a distance x from leading edge plate.

Friction stress for a flat/plane plate variably decreases inversely proportionally \sqrt{x} :

$$\tau_{\text{sum}} = 0,382 \sqrt{\frac{\mu \rho u_0^3}{x}}$$

which is confirmed well by experimental data.

Coefficient of friction drag of smooth plate, in reference to its complete surface:

$$c_{f_{\text{sum}}} = \frac{X_{\text{sum}}}{\rho \frac{u_0^2}{2} S'}$$

where X_{sum} - frictional force, which acts on both of sides (surface) of the plate

$$X_{\text{sum}} = 1,33 \sqrt{\mu \rho l} u_0^{3/2},$$

$$(X_{\text{sum}} = 2 \int_0^l \tau \Delta S); \Delta S = l \cdot \Delta X; S = l \cdot l,$$

hence

$$c_{f_{\text{sum}}} = \frac{1,33 \sqrt{\mu \rho l} u_0^{3/2}}{\rho \frac{u_0^2}{2} 2l} = 1,33 \sqrt{\frac{\mu}{\rho l u_0}} = 1,33 \sqrt{\frac{1}{Re_x}}$$

The velocity of single particles in laminar boundary layer along plate at certain constant distance from its beginning (with $Y=\text{const}$) due to friction decreases. Kinetic energy of these particles also decreases, and laminar layer becomes unstable.

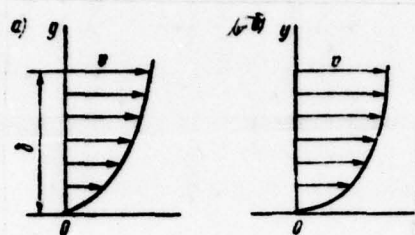


Fig. V.9. Comparison of the velocity profiles in laminar (a) and turbulent (b) boundary layers.

Page 118.

At certain distance from the leading edge of plate, called x_{cr} and corresponding to this distance $Re_{cr} = \frac{x_{cr} v_0}{\nu}$, the flow becomes turbulent. The transition of the stream-line conditions of flow to turbulent occurs in the so-called transition region where the flow mixed.

Near wall remains the very thin $\left(\delta = \frac{16\nu}{\sqrt{c_{тр\delta}}}\right)$ laminar sublayer, in which the velocity gradient is very great, which produces an increase of the frictional resistance in boundary layer. For a turbulent boundary layer the velocity along the normal to surface (wall) grow/rises approximately of proportionally to the root seventh degree of distance from the wall (see Fig. V.9):

$$v = v_0 \left(\frac{y}{\delta}\right)^{\frac{1}{7}}.$$

The thickness of turbulent boundary layer along wall grow/rises more rapid than the thickness of the laminar boundary layer:

$$\frac{\delta}{x} = \frac{0.37}{5\sqrt{Re_{xp}}}.$$

Friction stress and coefficient of friction drag in turbulent boundary layer is also more, rather than with the laminar boundary layer:

$$\tau = 0.0225 \rho v_*^{\frac{7}{4}} \left(\frac{v}{v_* \delta} \right)^{\frac{1}{4}},$$

$$c_{f, \text{typ6}} = \frac{0.074}{Re} \left(\text{is more precise, } \frac{0.455}{(\lg Re_x^{0.44})} \right).$$

In transient coefficient domain of friction (Fig. V.10)

$$c_{f, \text{nep}} = \frac{0.074}{\sqrt{Re}} - \frac{1700}{Re}.$$

Ratio of the coefficients of friction drag for a flat/plane plate of purely turbulent and purely laminar flows following:

Re	10 ⁵	10 ⁶	10 ⁷	10 ⁸	10 ⁹
$\frac{c_{f, \text{typ6}}}{c_{f, \text{lam}}}$	1.71	3.36	7.15	16.03	37.04



Fig. V.10. Comparison of the coefficient of friction c_f of different flow conditions: I - $c_{f_{\text{lam}}}$; II - $c_{f_{\text{typ}}}$; III - $c_{f_{\text{sep}}}$

Page 119.

As can be seen from that presented, with an increase in Reynolds number turbulent resistance increasingly more exceeds laminar. By this is caused tendency how it is possible longer (at the larger length of body) to preserve the stream-line conditions of flow during the flow around different bodies (airfoil/profiles and fuselages of aircraft, rockets, ships, etc.), since thus it is possible to decrease their resistance and to increase the velocity of motion (at given power).

Frictional resistance depends substantially on the compressibility of air. For a laminar boundary layer this effect can be estimated for a flat/plane plate on G. P. Burago's approximation formulas

$$\frac{c_{f_{\text{lam. ch}}}}{c_{f_{\text{lam. bezk}}}} = \frac{1}{(1 + 0.1 M_{\infty}^2)^{1/2}}$$

while for turbulent

$$\frac{c_{x_{\text{турб. см}}}}{c_{x_{\text{турб. несм}}}} = \frac{1}{\left(1 + \frac{1}{15} M_{\infty}^2\right)^{\frac{2}{3}}}$$

The dependence of turbulent friction on Mach number is given in Fig. V.11. For determination of the position of the transition point of laminar boundary layer into turbulent for smooth airfoil/profiles, it is possible to use the curve/graph, given in Fig. V.12, in which is given the dependence $(\bar{x}_T - \bar{x}_m) = f(Re)$

$$\bar{x}_T = \frac{x_{T, \text{ср}}}{b},$$

$$\bar{x}_m = \frac{x_{\text{min. сср}}}{b},$$

where b - a chord.

$x_{\text{min. сср}}$ is determined usually from dependence $\bar{P}=f(\alpha)$ for this airfoil/profile, obtained from experiment or by theoretical method.

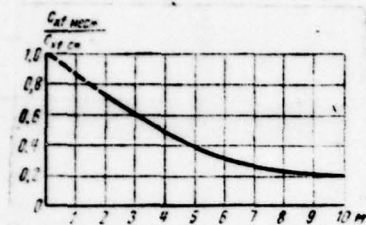


Fig. V.11

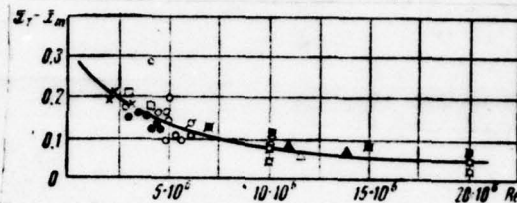


Fig. V.12

Fig. V.11. Dependence of the coefficient of friction of turbulent boundary layer on Mach number.

Fig. V.12. Curve/graph for determining the position of transition point.

Page 120.

It must be noted that with an increase of the angle of attack within small limits the transition point with increase c_y is displaced on the upper surface of airfoil/profile forward, and on lower - back/ago, and its mid-position for this Re number does not virtually change. With an increase in Reynolds number the transition point is displaced forward, the region of laminar flow is reduced, and drag coefficient increases (Fig. V.13).

The initial turbulence of flow. The flow, which encounters to bodies, is usually filled by small/fine eddy/vortices. In wind

tunnels the source of vortex formation, or turbulence, are different cell/elements, which are located in flow (diffuser grids, blades of elbows, etc.), and also very walls of duct.

In the presence of small/fine vortex flows, the velocity its always fluctuates (Fig. V.14), since the carried by flow eddy/vortices they will first increase, then decrease the local velocity in dependence on their direction of rotation and position relative to flow-rate meter (nozzle). The usual meters (besides hot-wire ones), used during aerodynamic investigations, give only the averaged velocity of flow. True airspeed

$$v_{\text{net}} = v_{cp} \pm \bar{v},$$

where \bar{v} - average quadratic value of the pulsating velocity of flow; can be positive (i.e. directed to the same side, as v_{cp}) and negative.

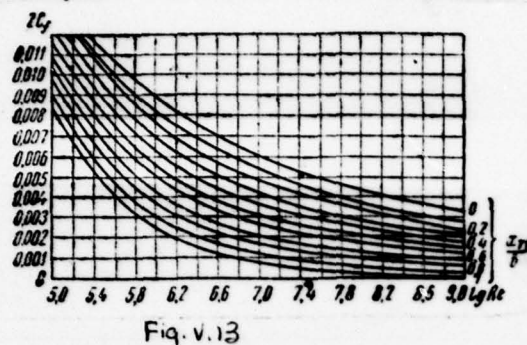


Fig. V.13

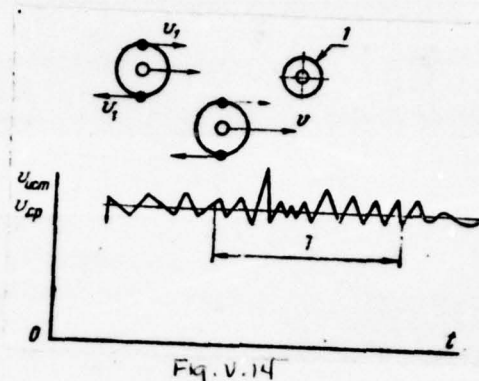


Fig. V.14

Fig. V.13. Effect of a number Re and of a position of transition point for frictional resistance.

Fig. V.14. Stream-velocity fluctuation: 1 - speed/rate meter.

Page 121.

The initial turbulence of flow the greater, the greater the value \bar{v} , determined according to the expression

$$\bar{v} = \sqrt{\frac{1}{t_2 - t_1} \int_{t_1}^{t_2} v dt},$$

here $(t_2 - t_1)$ - certain period of time for which falls the large number of pulsations of velocity (Fig. V.14). For measure, or degree, turbulences acquire the value

$$\varepsilon = \frac{\bar{v}}{v_{cp}}.$$

The value of the degree of initial turbulence expresses

frequently in the percentages

$$\epsilon\% = \frac{v}{v_{cp}} 100.$$

Investigations showed that in wind tunnels the initial turbulence of flow oscillates within limits by 0.1-20/o. Turbulence of natural atmospheric air at the height/altitude of several hundred meters is equal to $\epsilon \approx 0.02\%$. In spite of its low value the initial turbulence of flow in duct strongly affects the character of flow. If in flow is initial turbulence, then, as show experiments, the laminar part of boundary layer on body sharply is reduced, since laminar layer little is stable, and initial turbulence of its flow easily "swings". Frictional resistance in plate, wing profile and similar bodies in this case strongly grow/rises. Increases also overall drag c_x (Fig. V.15).

Not always, however, the increase of initial turbulence increases the resistance of body. An increase in the resistance is obtained in such bodies, whose main thing it is comprise friction, but not the resistance, caused by forces of pressure. The bodies of good streamline shape include the plates, placed by fin/edge to flow, fuselages and wings of aircraft, missile body, dirigibles, ships, etc. In such bodies friction reaches 70-80o/o of total resistance.

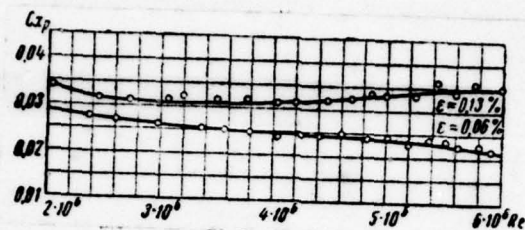


Fig. V.15. Effect of the intensity of turbulence ϵ and of number Re on the drag coefficient of bodies of revolution.

Page 122.

In the bodies whose resistance depends, mainly, on pressures (shape drag), caused by boundary-layer separation, in the turbulent flow sometimes is created smaller resistance than in laminar flow. An example is sphere. Its coefficient c_x strongly depends on Reynolds number (see Fig. V.19). An incidence/drop in the drag coefficient occurs simultaneously with the transition of boundary layer from laminar state into turbulent. With the small Re numbers, the laminar boundary layer in sphere blows away from its surface almost over the greatest transverse section (diameter).

According to the available experiments, at the first torque/moment the flow flows about the sphere without breakaways (Fig. V.16a), in front and from behind it is obtained elevated

pressure, while on transverse to flow - equator, - lowered/reduced, i.e., flow pattern the same as for the case of ideal fluid. In the following instant the boundary layer begins leak from regions with elevated pressure (i.e. from front/leading and rear ends) into region with lowered/reduced (i.e. to equatorial cross section). About maximum (transverse) cross section these layers collide (Fig. V.16b). As a result of collision, occurs the flow breakaway from the surface of sphere and air begins leak as shown in Fig. V.16c, moreover pressure after sphere decreases, that also creates pressure difference from the front and from behind sphere is caused the high resistance, measured by coefficient $\bar{c}_x \approx 0.48$.

With the large Re numbers, the boundary layer in sphere transfer/converts into turbulent state. It in exactly the same manner blows away from surface, but only at the point, which lies further along flow, than with laminar boundary layer. This is explained by the fact that on the boundary of turbulent boundary layer occurs the energetic mixing of air of this layer with the driving/moving above its surface of layer external flow. Therefore the layer, which flows from the front back/ago (along flow), is carried along by external flow, and the layer, which flows forward, it is braked by it.

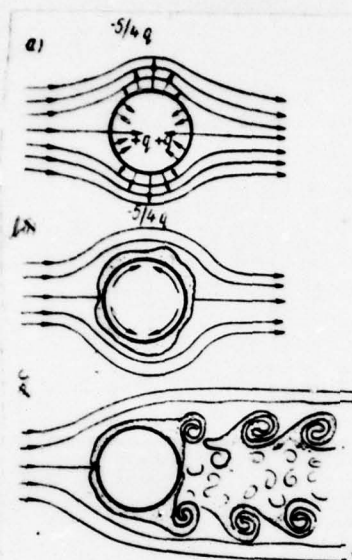


Fig. V.16. Flow around sphere at different moment of time.

Page 123.

As a result the first layer pushes aside separation point back/ago. During this displacement of separation point, the picture of the distribution of pressure according to sphere becomes more favorable (Fig. V.17) and approaches a flow pattern of ideal fluid. In this case, the coefficient to flow pattern of ideal fluid. In this case, the drag coefficient of sphere falls to very low value ($c_x = 0,1$) despite even the fact that the frictional resistance against the surface of sphere in turbulent layer will be increased.

Sphere is very sensitive to initial turbulence. Sufficient before the sphere to place several thin wires so that the boundary layer would pass into turbulent state. Is very exponential the following experience in Prandtl. If we Jan to the front of sphere (Fig. V.18) place fine/thin wire ring, then it not only will not increase the drag coefficient of sphere, but it vice versa decreases it more than twice (at low speeds).

Sphere they use for the indirect determination of the initial turbulence of flow in wind tunnels. Graphically the results of the tests of sphere in ducts with different initial turbulence of flow take the form, depicted in Fig. V.19. This curve/graph can be changed in the form $c_x = f(Re_{sp})$, where Re_{sp} - there is Reynolds number, with whom $c_x = 0.3$. This curve is very steady and on it satisfactorily lie down all experiments in different ducts.

For the determination of the degree of initial turbulence in the newly constructed duct, it is necessary to test there sphere at different velocities and to construct curve $c_x = f(Re)$. After finding Re with which $c_x = 0.3$, it is possible on curve/graph, given on Fig. V.20, to find the value of the initial turbulence of flow $\epsilon\%$.

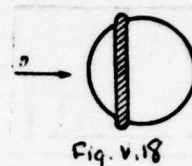
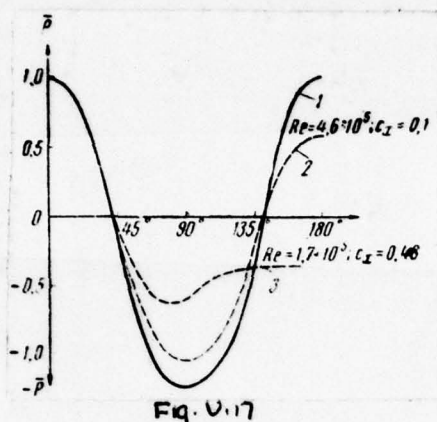


Fig. V.17. The distribution of pressure according to sphere during different conditions/modes of the flow: 1 - ideal flow; 2 - turbulent breakaway; 3 - laminar breakaway.

Fig. V.18. Sphere with wire ring.

Page 124.

During the determination of the degree of the initial turbulence of flow with the aid of sphere, it is necessary to take into consideration, that dependence $\epsilon\% = f(Re)_{sp}$, shown on Fig. V.20 and approximated by the formula

$$\epsilon\% = \frac{5}{\left[\frac{Re_{sp}}{100000} \right]^{0.11}} - 2,$$

is obtained according to the experiments, carried out in the 1940s with the spheres with a diameter of 12-22 cm in ducts with the

relatively high degree of initial turbulence (0.5-30/o). In recent years the quality of flow in wind tunnels increased and the degree of initial turbulence in them was lowered to 0.2-0.30/o. Furthermore, it was noticed, that the obtained value $\epsilon\%$ depends on the diameter of sphere and size/dimension of the test section of the duct.

The experiments conducted regarding initial turbulence with the use of spheres of different diameter and hot-wire anemometers showed following. Value Re_{xp} in duct with the size/dimension of the test section of 3 m varies from 400,000 for sphere $d=100$ mm to 310,000 for sphere $d=500$ mm, with respect varies and value $\epsilon\%$. The greater the diameter of sphere with the assigned/prescribed diameter of test section, those the more obtained from it value $\epsilon\%$, which corresponds to the larger frequency band of the pulsations of the velocity, "recovered" by sphere. So, sphere $d\approx 300-350$ mm covers entire range of pulsations and gives great value $\epsilon\%$, sphere $d=100$ mm gives the reduced value $\epsilon\%$, which corresponds to the range of pulsations from 1000-2000 Hz and it is above.

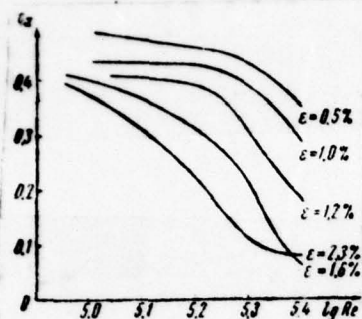


Fig. V.19

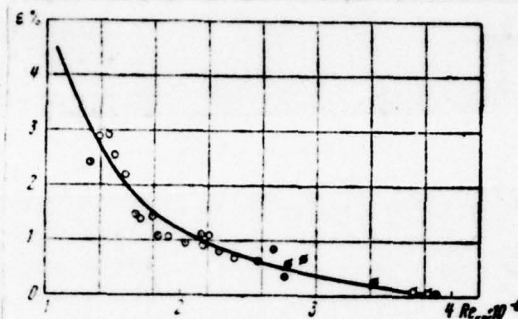


Fig. V.20

Fig. V.19. Dependence c_x of sphere on Re numbers and $\epsilon\%$ Fig. V.20. Dependence $\epsilon\%$ on Re_{sp} for a sphere. Different small circles showed different wind tunnels.

Page 125.

It is necessary to keep in mind that the spectrum of stream-velocitys fluctuation covers very wide frequency band: from ones to hundreds of thousand hertz. However, those determining the intensities of turbulence are low frequencies (Fig. V.21). On these reasons during the determination of values Re_{sp} and $\epsilon\%$ with the aid of sphere, it is necessary to introduce correction $\Delta\epsilon\% = f(d_m)$ for the ratio of its diameter to the diameter of test section, but in the case of the measurement by hot-wire anemometer - to consider its frequency characteristic, frequency band of the pulsations of

velocity, measured by hot-wire anemometer.

Taking into account the results of experiments in recent years, it is possible for determining initial turbulence of flow in wind tunnels¹ with the aid of sphere to use the following dependences.

FOOTNOTE 1. There are in the form of duct with the relatively small initial turbulence of flow in test section ($\epsilon\% = 0.5 \div 0.7$). ENDFOOTNOTE.

1. Expected critical Reynolds number is connected with size/dimensions of tested sphere and test section

$$10^{-5} Re_{cr} = 0,8e^{14,6x - 200x^2} + 3,$$

where

$$x = \frac{d_w}{D_{p.v.}}$$

here d_w - diameter of tested sphere;

$D_{p.v.}$ - diameter of test section of duct.

2. Intensity value of initial turbulence of flow in terms of obtained in experiments value Re_{sp} :

$$\epsilon\% = \frac{10^{-4}}{Re_{sp} \left(0,1 \frac{d_w}{D_{p.v.}}\right)^{\frac{1}{5}}}$$

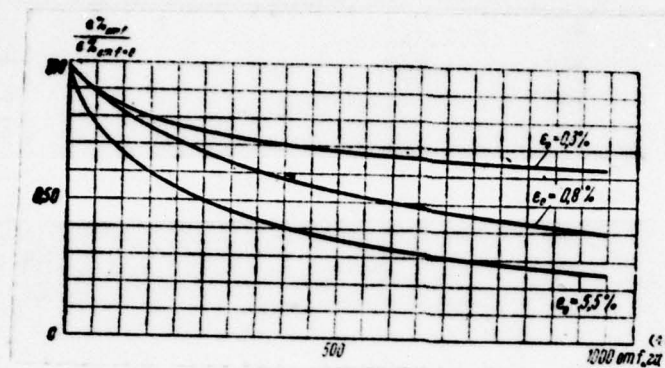


Fig. V.21. Dependence of the intensity of turbulence on the spectrum of the measured frequencies and the turbulence equipment/devices.

Key: (1) . Hz.

Page 126.

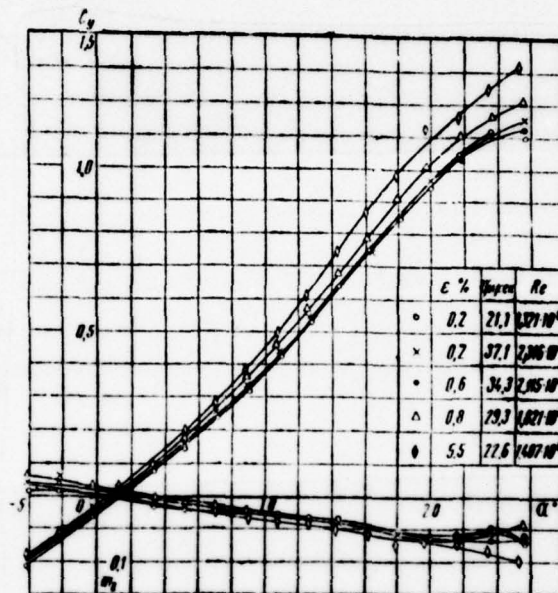
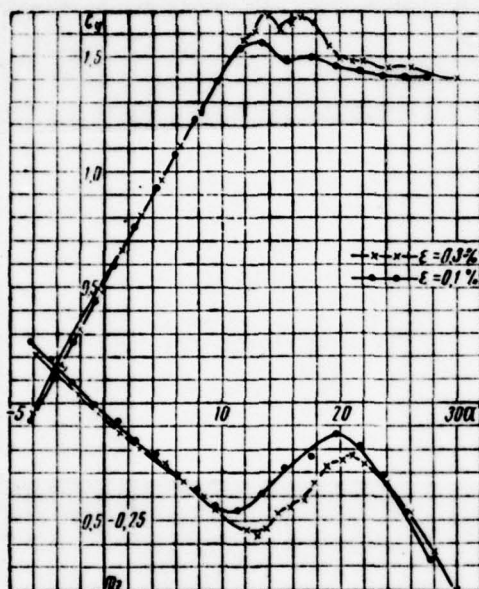


Fig. V.22. $C_L, m_z = f(\alpha, \epsilon\%)$ for a model airplane with the sweptback wing.

Fig. V.23. Characteristics of model airplane with delta wing at different intensity of turbulence of the incident flow.

Page 127.

The initial turbulence of flow affects also such aerodynamic

characteristics as lift coefficient $c_{y \max}$ and coefficient of pitching moment. Figure V.22 and V. 23 gives values $c_y = f(\alpha)$ and $m_z = f(\alpha)$ for aircraft with swept and delta wing, in Fig. V.24 for rectangular and in Fig. V.25 for a laminar wing, obtained with different initial turbulence levels of flow. As can be seen from diagram (Fig. V.22), at the high angles of attack of larger initial turbulence, corresponds the larger value of coefficient $c_{y \max}$ and m_z . This is explained by the fact that with the large initial turbulence of flow and at angle of attack of wing the flow around upper surface is steadier (the same effect, as during the flow around sphere). The same effect of increase $c_{y \max}$ gives an increase in Re number.

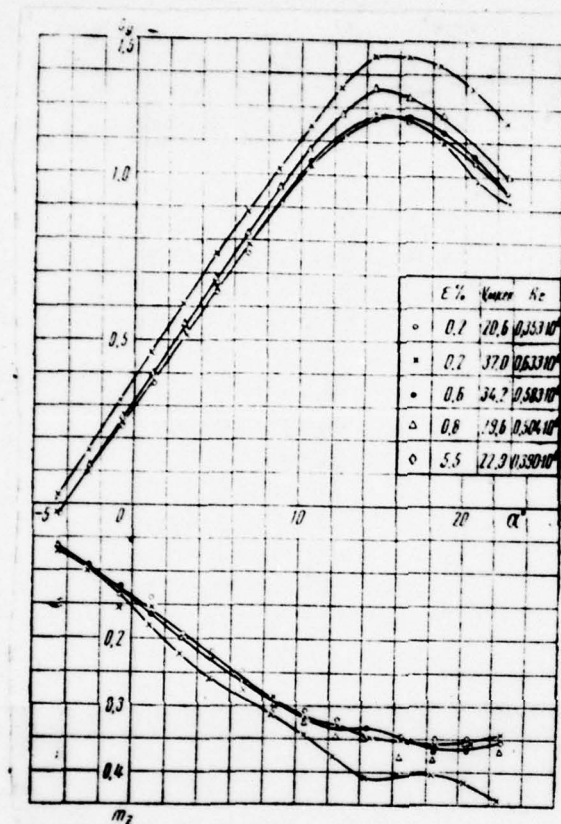


Fig. V.24. Characteristics of the rectangular wing at different intensity of turbulence of the incident flow.

Page 128.

During the evaluation of the results of the experiments in wind tunnels importantly to divide and to rate/estimate an effect both of the initial turbulence $\epsilon\%$ and Re numbers of the experiment. Figure

V.26 shows the effect of the intensity of turbulence on the resistance of some bluff bodies.

Taking into account the considerable eddying effect of flow in wind tunnels on the results of experiments in them and the fact that the contemporary forms of flight vehicles are very ideal, and frictional resistance for them plays the significant role, they attempt during tests in ducts to have the initial turbulence of flow, as close to atmospheric.

Boundary-layer separation. As a whole to the position of the transition of laminar boundary layer into turbulent state, besides Re number, the form of wall (airfoil/profile), local bendings, angle of attack, that cause pressure gradient in the direction of the motion of gas and the initial turbulence of flow, are exerted effect and state of fairing (degree of its roughness). Figure V.27 gives changes in the value of the coefficient of friction for ducts from different by roughness surface in dependence on Re number.

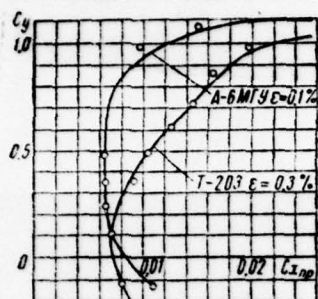


Fig. V.25

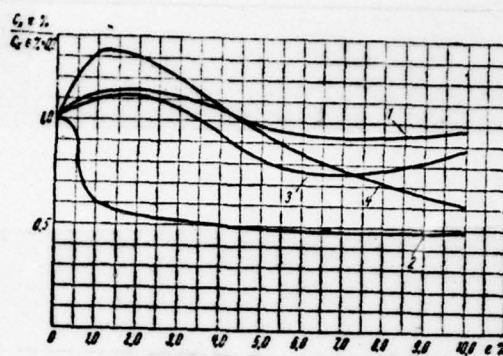


Fig. V.26

Fig. V.25. Polars of laminar-flow profile NACA63₂=616 at different intensity of turbulence of incident flow ($Re=1.25 \cdot 10^6$).

Fig. V.26. The dependence of the relative resistance of different bodies on the intensity of turbulence of the incident flow: 1 - cylinder after crisis ($Re=4 \cdot 10^5$); 2 - cylinder to crisis ($Re=2 \cdot 10^5$); 3 - cube ($Re=4 \cdot 10^5$); 4 - model of electric locomotive on screen ($Re=4 \cdot 10^6$).

Page 129.

As can be seen from figure, by good surface finishing it is possible to attain the decrease of frictional resistance several times. An especially important value this fact has for the aircraft of rockets, ships and the similar bodies, frictional resistance in which comprises the considerable portion of total resistance.

The effect of different inequalities (rivet head, slot, surface waviness, heavy graininess in coloration) lies in the fact that they agitate laminar flow, move transition point into turbulent flow forward (to the leading edge of body), increase section with turbulent boundary layer and, consequently, also resistance. The degree of the surface roughness is called the ratio of height/altitude k of the prominence/protuberances of roughness to radius r of duct or to wing chord (to length of body). this roughness is called of relative. Absolute roughness is measured in millimeters or portions of millimeters. Values in the millimeters of the height/altitude of the projections of the roughness of different materials following:

clean drawn tubes from brass, copper, lead. 0.0015-0.001

new steel seamless pipes. 0.04-0.17

zinc-coated iron ducts. 0.39

new cast-iron pipes. 0.25-0.42

birch plywood. 0.025-0.05

pinewood plywood. 0.1

wooden ducts. 0.25-1.25

wooden planed blades. 0.25-2.0

surface from clean cement. 0.25-1.25

plasterings by cement mortar. 0.45-3.0

concreted channels. 0.8-9.0

covered with glaze earthenware ducts. 0.25-6.0

ducts from glass. 0.0015-0.01

coating with oil paint over the puttied surface. 0.1.

The permissible degree of roughness, not calling change in the resistance, is given for a wing profile in Fig. V.28. In the free flow out of boundary layer, air friction is not virtually exhibited, and the total pressure in all points is equal. In boundary layer it is less than in the free flow, and it changes from one point to the next due to the losses of the kinetic energy, which converts into heat.

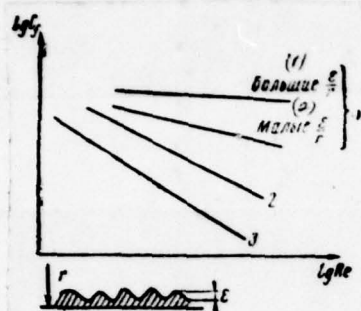


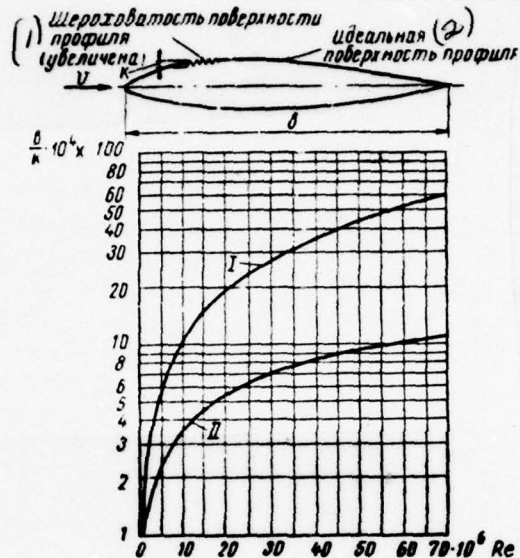
Fig. V.27. The dependence of the coefficient of friction of ducts on roughness and Re number: 1 - rough; 2 - corrugated; 3 - smooth.
Key: (1). Large. (2). Small.

Page 130.

Heating by boundary-layer friction of the surface of the driving/moving at a high speed bodies reaches the significant magnitudes (Fig. V.29) and it is commensurable with heating from the compression of gas at critical point.

The flow pattern into boundary layer and stability of this layer is had considerable effect on interaction of flow and streamlined body. Boundary layer stability, its thickness and tendency toward breakaway on body depend, mainly, on the distribution of the velocities in the free flow out of boundary layer. If above it due to the curvature of body velocity grow/rises (flow is accelerated) or camber of velocity does not change its sign, then boundary layer will be stable. This flow pattern occurs on the nose sections of the profiles of wings, in nozzles, etc.

If the velocity in the direction of flow due to the expansion of jets (channel, etc.) decreases, then in accordance with this grow/rises pressure.



V.28.
Fig. depending on Re number and flow conditions: I - b/k for turbulent motion (aerodynamic smooth surface); II - b/k for viscous motion.

Key: (1). Roughness of the surface of the airfoil/profile (it is increased). (2). Ideal surface of airfoil/profile.

Page 131.

The particles in boundary layer, which lost due to friction their kinetic energy, at certain distance from leading edge cannot move into high-pressure area and are stopped. Further with an increase in the distance from leading edge, appears reverse/inverse

boundary-layer flow, which will entail change in the velocity profile, education/formation of eddy/vortices and breakaway of layer from wall (Fig. V.30).

The point of boundary layer, at which the frictional force turns into zero and after which begins reverse flow, it is called the separation point of flow. The detached laminar boundary layer rapidly transfer/converts into turbulent state (Fig. V.30) and can with small curvature of walls again adhere to body. Turbulent boundary layer longer does not blow away from body, since it scoops energy from external flow, but also it after breakaway can adhere to body. After the breakaway of layer, somewhat descends frictional resistance, but considerably is raised pressure drag.

The detached away from body eddy/vortices at certain distance from it are linked and is formed "trace" - the region of that braked, several chamfered and vortex flow (Fig. V.31). The controls, arrange/located in trace, have the lowered/reduced effectiveness and are tested the shocks of the disappearing from body eddy/vortices. Flow breakaway causes not only sharp increase in the resistance, but also lift breakdown.

The state of boundary layer has high value, also, for the characteristics of the flow of liquid and gases in of various kinds

channels, conduit/manifolds, nozzles and exit cone/diffusers (see in detail Chapter X).

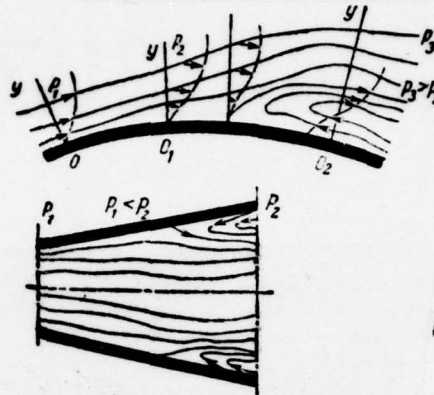
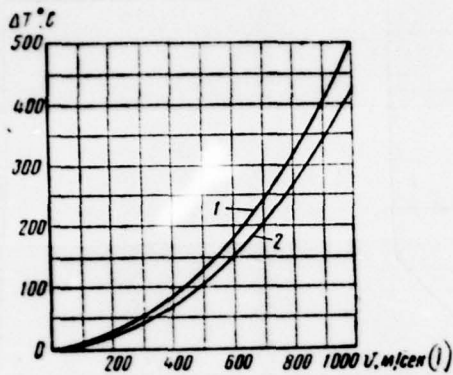


Fig. V.30.

Fig. V.29. The dependence of heating rubbing surfaces against the air: 1 - heating at the point of zero velocity $\Delta T = v^2/2000$; 2 - heating the surfaces of aircraft $\Delta T = v^2/2320$; $Pr = 0.74$.

Key: (1) . m/s.

Fig. V.30. Flow with breakaway in boundary layer.

Page 132.

Boundary layer control. Elimination or weakening of all undesirable phenomena, connected with boundary-layer flow, is possible with the aid of control of this layer.

One of the simplest methods of the "tightening" of the transition of laminar boundary layer into turbulent state is

imparting to the body (for example, to the wing profile or fuselage) of such forms, with which the point of the minimum of pressure it is displaced to the rear portion. This method makes it possible to decrease the frictional resistance. However, in many instances, for example for an increase in the lift of wing at high angles of attack, it is not effective. Recently increasing propagation receive the forced methods of boundary layer control (UPS) with the aid of suction or blowing. These methods pursue the target/purposes of prevention or tightening of boundary-layer separation and transition delay of boundary layer from laminar into turbulent state (Fig. V.32).

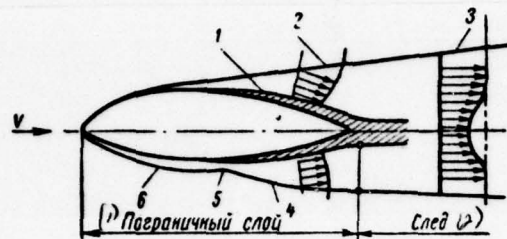


Fig. V.31. The edication/formation of wake after the body: 1 - real thickness; 2 - high-speed/velocity boundary-layer profile; 3 - high-speed/velocity airfoil/profile of trace; 4 - turbulent boundary layer; 5 - transition point; 6 - laminar boundary layer.

Key: (1) . Boundary layer. (2) . wake.

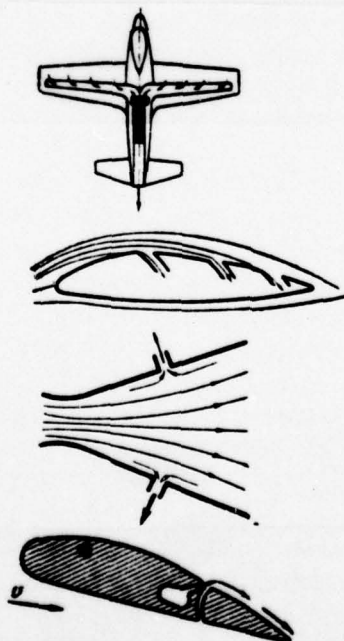


Fig. V.32. Schematics of suction and blowing of boundary layer.

Page 133.

If we exhaust from laminar boundary layer its those particles which to a considerable degree lost their kinetic energy, then boundary layer velocity profile will become more "filled": in layer remain the particles, earlier more distant from wall and which possess high kinetic energy, which raises the stability of the newly formable after place suction of layer. During the sitting of the suction slots or opening/apertures and of corresponding expenditure/consumption through them, it is possible to attain so that the boundary layer thickness nowhere would exceed critical. Laminar boundary-layer flow in this case succeeds in preserving to the large Re numbers ($\sim 10^7$). This method of laminarization is actually directed toward the distance (displacement) of transition point and has important value for decreasing the frictional resistance and heating of surface, which is substantial during motion with high velocities. Tightening or prevention of boundary-layer separation has the important value for an improvement in the characteristics during the flow around bodies at angles of attack or flow of liquid in expanding ducts.

To the position of separation point, it is possible to affect

both suction and blowing of boundary layer. With suction (after the place of breakaway) is reduced the pressure in the region between the detached layer and the body surface.

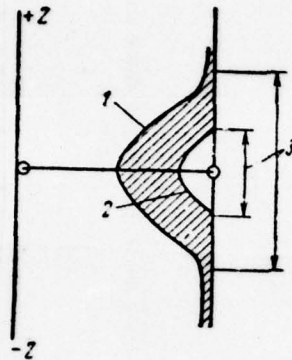


Fig. V.33. The effect of boundary-layer bleed on the trace: 1 - velocity profile without suction; 2 - airfoil/profile with suction; 3 - trace; z - vertical distance from leading edge.

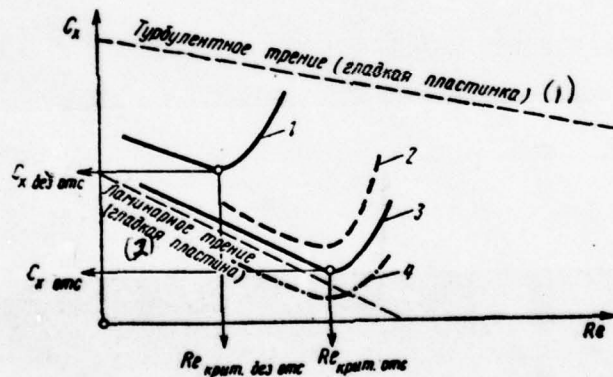


Fig. V.34. The effect of boundary-layer bleed on the drag coefficient of different Re numbers: 1 - airfoil/profile without suction; 2 - partial suction; 3 - suction from an entire surface of airfoil/profile; 4 - recuperation of trace.

Key: (1). Turbulent friction (smooth plate). (2). laminar friction (smooth plate).

Page 134.

The detached boundary layer in this case again adheres to body, its flow becomes steadier and the breakaway of layer occurs in point, which is located further along flow, than this would be without suction. Boundary-layer bleed, displacing separation point, attenuate of boundary layer and thickness of trace (Fig. V.33), of being basic source resistance, which can be substantially decreased (for example, Fig. V.34). If the exhausted air is discarded into the trace which in this case will obtain supplementary energy, then this recuperation (restoration/reduction) of trace, as can be seen from Fig. V.34, additionally is decreased resistance.

In connection with the wings of aircraft suction it is possible to produce with one or several slots, arrange/located usually for thick wings ($\bar{c}=10-12\%$) before the flap, and for fine/thin ones - additionally, near nose section. The character of lift increment for a wing with UPS depending on expenditure/consumption is shown on Fig. V.35. With this

$$c_l = \frac{Q}{S v_\infty},$$

where Q - expenditure/consumption; S - wing area, operated by boundary-layer bleed.

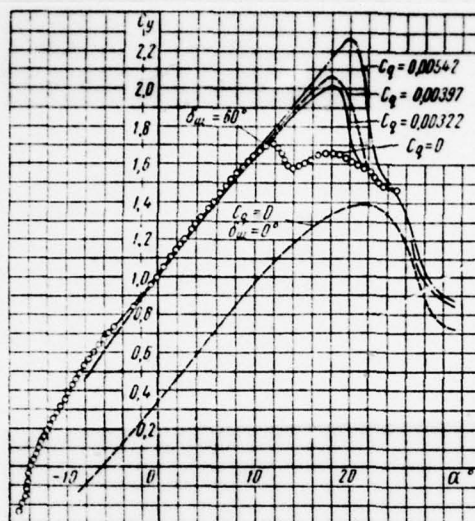


Fig. V.35. Dependence of the lift coefficient when boundary layer control system is present,.

Page 135.

In recent years are conducted the investigations in suction through opening/apertures for the laminarization of the flow around entire surface wing, fuselage, etc. These investigations showed the possibility of realization similarly of the laminarization of boundary layer virtually on all wing and considerable reduction for this count of wing drag. However, transfer of the results of laboratory tests for nature meets with great structural/design and technological difficulties, since the preservation/retention/maintaining of laminar boundary layer requires

careful surface finishing, precise execution of geometric forms of opening/apertures for suction, uniformity of the air bleed of other factors which on real aircraft to carry out is complicated.

Another method of the distance of separation point is boundary layer injection. This makes it possible to increase kinetic energy of the stagnation particles, to decrease the frictional resistance and to shift/shear separation point in flow. It should be noted that UPS has especially important value for an increase in the aerodynamic lift of aircraft.

Figure V.36 shows a change in the lift coefficient for model airplane with the sweptback wing in dependence on angle of attack with blowing and without blowing of the deflected on 60° flap.

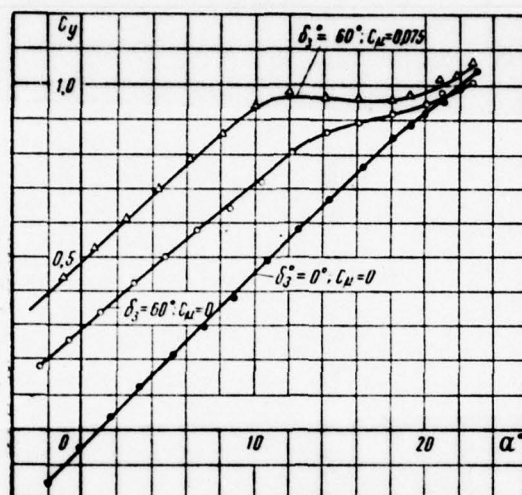


Fig. V.36. the effect of blowing on $c_y = f(\alpha)$ for a model airplane.

Page 136.

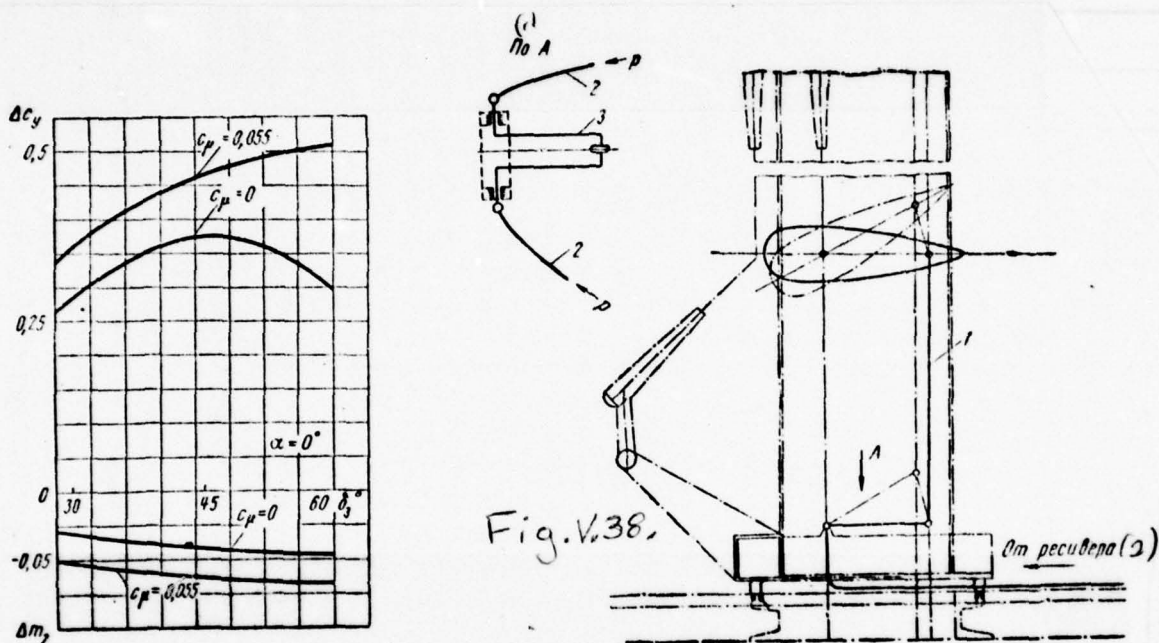


Fig. V.37. Effect of blowing on the lift increment and torque/moment.

Fig. V.38. The schematic of the supply of air to the model: 1 - feed of the compressed air into model; 2 - flexible hose; 3 - conduit/manifold, $d=38$ mm.

Key: (1). On. (2). From receiver.

Page 137.

The intensity of blowing is characterized by the coefficient of

momentum

$$c_{\mu} = \frac{Q_m v_m}{\rho_{\infty} \frac{v_{\infty}^2}{2} S},$$

where v_m - average over the section of slot velocity of blown out air; Q_m - mass flow rate of the blown out air; S - wing area, operated by blowing.

Figure V.37 depicts for the same model the effect of blowing on the lift increment and pitching moment during different flap deflection. The moderate lift increment is connected with relatively low value of the coefficient c_{μ} , which in real construction/designs due to the limitedness of possible air bleed from engines reaches values $c_{\mu} = 0,1-0,15$.

The experimental investigation of the effect of blowing on characteristics of wings and aircraft, conducted in wind tunnels, runs into some difficulties. The connected with the "earth/ground" system of the supply of the compressed air to models must not affect readings of the weights, which measure the lift and other aerodynamic characteristics. This requires the application/use of special construction/design, which joins air duct with model (for example, shown on Fig. V.38). The supply of air to model is realize/accomplished through the hinged parallelogram mechanism, establish/installed on the frame of balance. The front/leading hinge

joint of parallelogram is combined with the front/leading hinge line of model, and its rear part is the part of the rear suspension of model. This schematic of the feed of the compressed air does not disrupt the kinematics of weights during a change in the angle of attack and it does not affect on the values of forces and torque/moments, which act on model during experiments.

Another fact to which it is necessary to focus attention, is the simulation of slot, which in experiments must have the identical with respect to spread/scope width of 0.2-0.4 mm. And finally last/latter difficulty - this is the provision for uniform blowing all over length of slot, which requires the special chamber design of blowing.

§V:2. Boundary layer at high velocities.

Boundary layer and flow pattern in it have enormous effect on the flow around bodies not only with small ones, but also at high velocities (subsonic and supersonic), since due to the manifestation of compressibility sharply change all the aerodynamic characteristics of body. As is known, transition from supersonic flow to subsonic is accompanied by the education/formation of shock waves with an abrupt change in the velocity, pressure, density and temperature of gas. Form, character and intensity of shock waves depend not only on rate of flow, but also on the form of body and state of boundary layer on it.

Boundary layer on the body before the jump can be divided on two parts (Fig. V.39): lower - near wall with subsonic speed ($v/a < 1$) and upper - with supersonic speed ($M > 1$). In the supersonic region of boundary layer appear the shock waves which do not reach the surface of wall.

Page 138.

Pressure, caused by jump on the subsonic part of boundary layer, is spread upward on flow producing an increase in the boundary layer thickness, and subsequently and its breakaway. Due to boundary layer growth, which for laminar flow is considerably more than for turbulent, before the normal shock appear one or several oblique shock waves which are linked with straight line, and, thus, appears the double shock wave in the form of letter λ (Fig. V.40 and V.41).

The turbulent boundary layer, which has high kinetic energy, is less sensitive and to a change in the pressure, than laminar one. When, before the jump, turbulent layer is present, do not appear oblique and λ -shaped jumps (Fig. V.42), since here layer itself in subsonic part considerably thinner has smaller tendency toward breakaway.

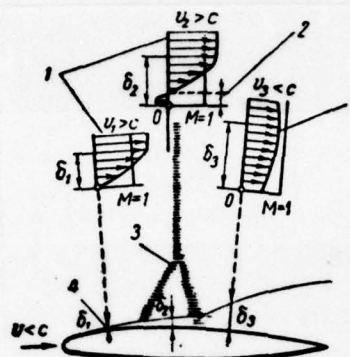
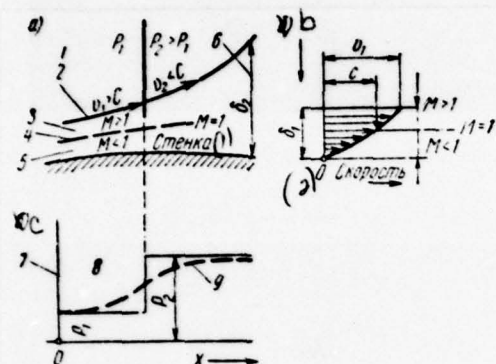


Fig. V.40.

Fig. V.39. Interaction of jump with the laminar boundary layer: a - the normal shock wave; b - high-speed/velocity boundary-layer profile before the jump; c - an abrupt change in the pressure above the boundary layer (in the supersonic part of boundary layer) 1 - free flow; 2 - boundary of the free flow; 3 - supersonic part of boundary layer; 4 - boundary line; 5 - subsonic part of boundary layer; 6 - boundary layer; 7 - the total pressure; 8 - wedge of pressure; 9 - steady change in the pressure in wall (in the subsonic part of boundary layer).

Key: (1). Wall. (2). Velocity.

Fig. V.40. λ-shaped wave on the case of the laminar boundary layer before the jump: 1 - high-speed/velocity profile; 2 - reverse flow; 3 - λ-shaped shock wave; 4 - laminar boundary layer.

Page 139.

But as a whole resistance (losses) in the direct/straight impact jump of turbulent layer is more than resistance in the λ -shaped jump of laminar layer, since in the first case jump more intense and passes nearer to wall.

To the state of the boundary layer before the jump, are exerted themselves the effect both of the Re number and surface condition. With the small Re numbers and smooth boundary layer surface, (in spite of the large Mach numbers) will be laminar, which will give rise to of the λ -shaped jumps which with an increase in Mach number (with $Re=const$) become more intense. With an increase in Re number and an increase in the degree of the roughness of boundary layer surface will pass into turbulent state and will arise the normal shock wave whose intensity with an increase in Mach number of the incident flow also will increase.

The separation point of flow behind shock waves (by straight lines and λ -shaped) with an increase in Mach number is moved from trailing edge to the basis of jump and with certain Mach number, which depends on the form of body, breakaway occurs from under jump, which causes the powerful eddying of flow, a change in the distribution of pressure on body, an increase in the resistance and a

lift breakdown (for an airfoil/profile).

At the hypersonic speeds of the phenomenon in boundary layer, substantially they become complicated. Braking hypersonic flow of gas in shock waves and boundary layer leads to the appearance of the regions with high temperature, physicochemical conversions in which have great effect on the course of gas.

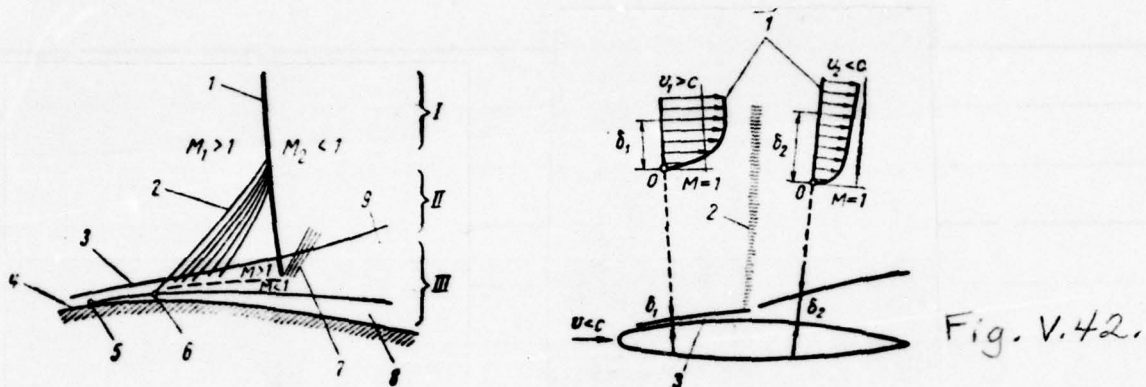


Fig. V.41. The analysis of the λ -shaped shock wave: I - large abrupt loss in the normal shock wave; II - small abrupt loss in oblique shock waves; III - large loss of separated flow and frictional resistance 1 - main normal shock wave; 2 - secondary oblique shock waves; 3 - laminar boundary layer; 4 - wall; 5 - separation point; 6 - transition point; 7 - small shock wave; 8 - stagnant air; 9 - boundary layer.

Fig. V.42. Normal shock wave with the turbulent boundary layer: 1 - high-speed/velocity airfoil/profiles; 2 - vertical shock wave; 3 - turbulent boundary layer.

Page 140.

Such processes, as dissociation, ionization, emission/radiation, not at all are exhibited or they have the low value at the low speeds of

the course of gas. Their account composes one of the important sides of the study of high-speed flows. For describing these processes, it is necessary to examine together with aerodynamic ones also the factors of chemistry and physics of high temperatures, what composes the object/subject of the investigations of the new region of aeromechanics - aerothermochemistry.

At the flow around plate of nitrogen N_2 and equilibrium dissociation the temperature in boundary layer at a low pressure of approximately $6000^\circ K$. Nitrogen in this case is half dissociated. If dissociation did not occur, then the temperature at the same pressure would be about $14000^\circ K$. The effect of this process on frictional resistance is insignificant (Fig. V.43). Effect on the coefficient of heat exchange for air is given in Fig. V.44.

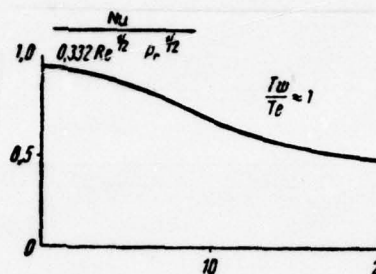
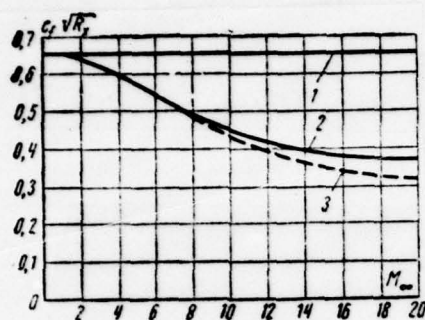


Fig. V.44.

Fig. V.43. Dissociation effect on frictional resistance: 1 - incompressible gas; 2 - course of gas taking into account dissociation; 3 - course of ideal gas without dissociation, $Pr=0.75$.

Fig. V.44. Dissociation effect on the coefficient of heat exchange for air T_e and T_s - temperature of wall and external flow.

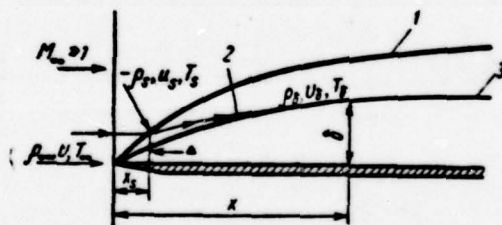


Fig. V.45. The schematic of the field of flow, induced with boundary layer on flat/plane plate at supersonic speeds: 1 - jump; 2 - flow line; 3 - boundary layer edge.

From purely aerodynamic special feature/peculiarities in

boundary layer at hypersonic speeds, one should first of all note the powerful inflation of boundary layer to the count of the decrease of density with a temperature rise. In this case, becomes essential the boundary layer effect on flow out of it, i.e., on external inviscid flow (Fig. V.45).

§V.3. Measurements in boundary layer.

The measurements, produced in boundary layer, pursue the target/purpose of the determination of the pattern of flow (laminar or turbulent), of distribution of the velocities and pressures in boundary layer, the positions of the transition point of layer from laminar into turbulent state, to positions of the separation point of layer, surface friction and other characteristics.

Determination of the profile of velocities. The velocity profile in the incompressible boundary layer is the fundamental characteristic, which makes it possible to determine virtually all parameters of layer (turbulence or laminarity, surface friction, breakaway, etc.). The determination of full speed is conducted by the small-diameter tubes, which contribute insignificant changes into the distribution of the velocities in boundary layer. Selection of the type of tubes and their calibrating are the basic cell/element, which are determining the accuracy of measurements. Some types of the

surface nozzles, used for measuring the total pressure in boundary layer, are given in Fig. V.46.

Static pressure on surface is measured with the aid of drainage narrow holes (on the order of 0.2-0.3 mm) on the very surface. Temperature on the body surface we can be measured by the thermocouple, installed into the body being investigated.

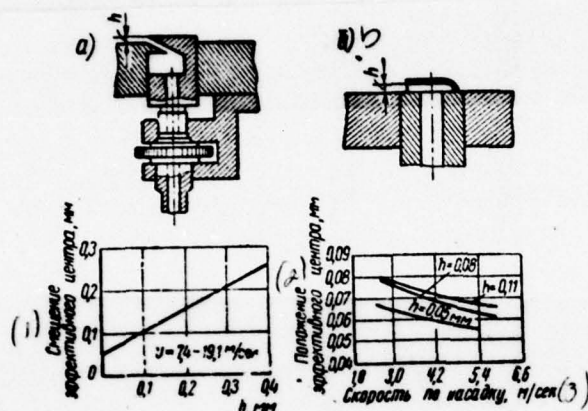


Fig. V.46. The surface cap/fillings of the total pressure: a - Stanton's nozzle; b - nozzle of Feydzh and Faulkner.

Key: (1). Displacement of effective center, mm. (2). Position of effective center, mm. (3). Velocity on cap/filling, m/s.

Page 142.

For measuring of tangents, that compose velocities into boundary layer at different distances from body, it is necessary to have the capability to move micronozzles along the normal to body. This displacement is conducted with the aid of coordinate spacer apparatus (Fig. V.47), which makes it possible to pass entire the velocity field in boundary layer.

The nozzle, fasten/strengthened to coordinate spacer apparatus, is made from medical needles by diameter - 0.9 mm, and intakes in static-pressure tube are drilled by usual needle. Together with the careful calibrating of nozzle, it is necessary to see to it that its opening/apertures would not be clogged by the condensed moisture.

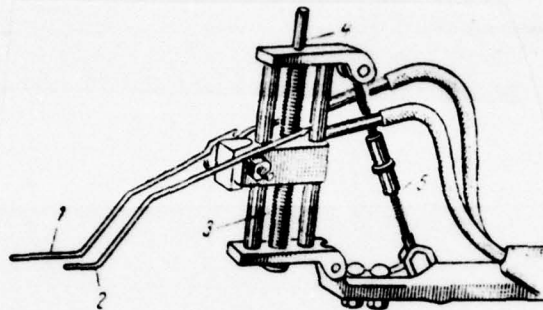


Fig. V.47. Coordinate spacer apparatus for the passage of field in the boundary layer: 1 - nozzle of static pressure; 2 - nozzle of the total pressure; 3 - micrometer screw/propeller, 40 threads/inch, course 25 mm; 4 - place of the attachment of flexible driving/homing cylinder; 5 - regulating turnbuckle.

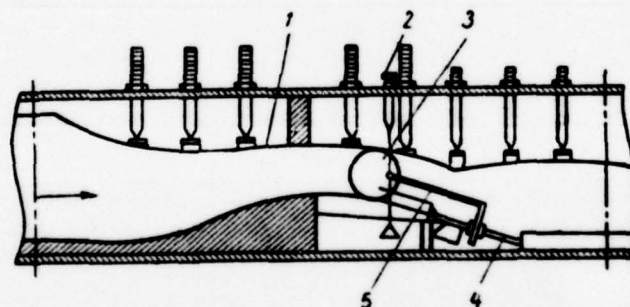


Fig. V.48. the installation of nozzle for studying the boundary layer at high velocities: 1 - adjustable wall; 2 - screw/propeller for displacing the wire; 3 - optical glass; 4 - screw/propeller for the axial displacement of nozzle; 5 - nozzle.

Measurements in boundary layer with large Mach numbers require special thoroughness and need of decreasing the disturbance/perturbations, introduced into flow by nozzle and bracket, and also the careful account of pitot losses for the leading shock wave, which appears before the nozzle in the supersonic part of boundary layer. Figure V.48 shows as example of one of the installations for studying the boundary layer with large velocities and investigation of interaction of boundary layer and shock waves.

If surface does not have noticeable curvature, i.e., it is close to flat/plane, either is absent considerable pressure gradient along chord, or finally boundary layer has small thickness, then it is possible to disregard a change in the static pressure along the normal to the surface and to measure it only on surface. When this change cannot be disregarded, it is necessary on the coordinate spacer apparatus, which moves the nozzle of the total pressure, to install additionally the nozzle of static pressure (Fig. V.49). In all cases special attention must be directed to the smallness of the disturbance/perturbations, introduced by tube:

- 1) to relative smallness of tube in comparison with boundary layer thickness - the diameter of tube it is desirable to have not

more than 100% of the predicted boundary layer thickness.

2) to the account of the mutual effect of the lower part of the tube and of the arranged/located about it surface, which lies in the fact that the effective center of tube, to which should relate the measured pressure, differs from the geometric (see Fig. V.49).

3) to the account of Reynolds number whose low value introduces the regular difference between readings of the micro-nozzles, which have of internalizations diameter to 0.1 mm and by readings of the nozzles of the same exterior form, but having inner diameter on the order of 1-2 mm.

To measure the velocity in boundary layer is possible with the aid of the hot-wire anemometers by which are recorded the oscillation/vibrations and velocity.

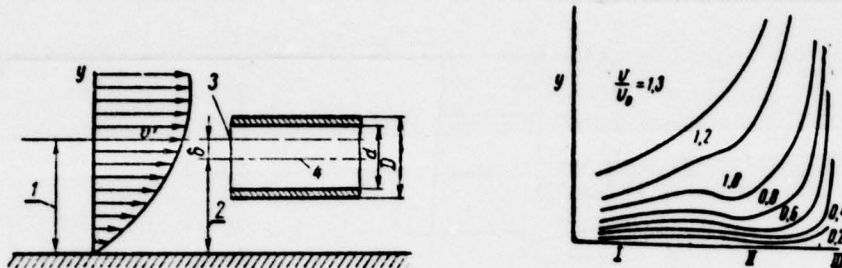


Fig. V.49. The displacement of the effective center of total pressure tube in the boundary layer: 1 - effective position; 2 - geometric position; 3 - effective center; 4 - centerline.

Fig. V.50. The duct/contours of the equal velocities in the boundary layer: I - laminar flow; II - transition; III - breakaway.

Page 144.

The results of measuring the distribution of the velocities in boundary layer usually are depicted in the form of curves $v=f\left(\frac{y}{\delta}\right)$, or of "duct/contours" of the equal velocities (Fig. V.50), that depict the family of curves, each of which is locus (S, y) , for which $\frac{v}{v_0}$ remains constant. On these curves it is possible to note the character of boundary-layer flow and to approximately determine the transition point of boundary layer from laminar into turbulent state.

Determination of local skin friction coefficient. In a series of

aeromechanical problems, are determined friction stress and local skin friction coefficient

$$c_f = \frac{\tau}{\rho_{\infty} \frac{v_{\infty}^2}{2}}.$$

The complexity of the experimental determination of values τ and c_f is connected with the difficulties of measuring of the velocities and pressures in boundary layer. For plane-parallel flow resistance of friction of cylindrical body with generatrix normal to direction of the flow

$$Q_{\tau} = \int_0^l c_f \frac{\rho_{\infty} v_{\infty}^2}{2} b dl,$$

where l - chord; b - width of body; c_f - local skin friction coefficient.

The immediate determination of frictional force by the weight possible method (Fig. V.51).

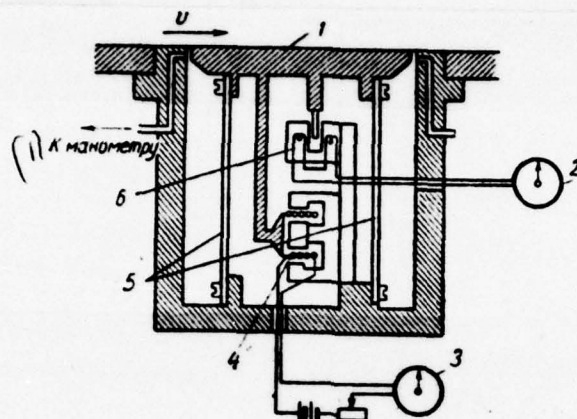


Fig. V.51. Weights for measuring the frictional force: 1 - disk; 2 - indicator of displacement; 3 - indicator of force; 4 - electromagnet; 5 - elastic plates; 6 - displacement pickup.

Key: (1) . To manometer.

Page 145.

Such measurements usually conduct on the chosen with a small clearance (0.1-0.15 mm) cell/element of surface ($d=50$ mm). In these experiments it is important so that the cell/element being investigated would not protrude from the surface of wall, but the sensitivity of weighing device was high, since the measured frictional force is very small.

Friction stress on wall can be found also with the aid of the measurements of boundary layer velocity profile. Such measurements, the produced by micronozzles total pressures and opening/apertures on wall, make it possible to determine values $\left(\frac{dv}{dy}\right)_{y=0}$ by the extrapolation of dependence $v = f(y) u_\infty$ into point $y=0$. Obtained values $\tau = \mu \left(\frac{dv}{dy}\right)_{y=0}$ prove to be insufficiently precise. More precise they are determined by the method, instituted with the account of a change of the momentum in boundary layer (with the known velocity profile). Thus, for instance, for the case of the flat-plate flow of the unrestricted flow in which velocity v does not depend on the longitudinal coordinate x , the equation of momentum takes the form

$$\tau = \frac{d}{dx} \int_0^\delta \rho (V - v) v dy,$$

where v - longitudinal component the velocities in boundary layer at a distance of y from wall.

Is possible also the determination of surface friction on the basis of velocity measurements with the aid of surface nozzles in point, very close to the surface of wall within the so-called laminar sublayer. It is here assumed that the velocity to zero on wall from the value, shown by nozzle, varies linearly, i.e.,

$$\tau = \mu \frac{v}{y},$$

where y - a distance of the effective center of the nozzle (see Fig. V.49).

It is necessary to bear in mind, that from experiments according to the indirect determination of the local coefficient of friction, i.e., its determination in boundary layer velocity profile, one ought not to expect high accuracy/precision. This is connected with the fact that the measurement of the distribution of the velocities in immediate proximity of wall even in the case of applying the special micro-nozzles ($d \approx 0.2-0.3$ mm), optical timing devices of coordinate y does not free from known arbitrariness in the determination of value $\left(\frac{\partial v}{\partial y}\right)_{y=0}$ and consequently also $\sqrt{\tau}$. The experiments indicated in the majority of the cases bear qualitative or comparative character and it is desirable their results to compare with the results of direct measurements (in a weight manner or on pitot loss for the case flow in duct).

Determination of the position of the transition point and boundary-layer separation.

Page 146.

The information about the position of the separation point and transition point gives the representation of physical character of flow and criteria for the evaluation of the airfoil characteristics of wings, fuselages, bodies of revolution and similar cell/elements,

and also they serve for checking the theoretical and calculated methods of their construction. By themselves the position of transition point and boundary-layer separation do not make it possible to unambiguously interpret the values of aerodynamic characteristics and into formulas for their calculation they do not enter, but it is sufficient reliably indicated, in what direction of these of characteristic they will change.

Determination of transition point. As was already said earlier, the transition of boundary layer from laminar state into turbulent is accompanied by more rapid increase of velocity in proportion to removing from surface and by more rapid thickening of quite boundary layer. These facts serve as basis for the following determinations of transition point:

1. Method of determining the transition point from the measurement of the velocity profile. If is known profile of the velocities in several sections along chord or surface, then the position of transition point is determined by the place of a change of the character of airfoil/profile to the side of the larger slope/transconductance of the growth/build-up of velocity on rigid surface. This method is sufficiently complex and laborious and usually it they use when the velocity profile must be determined, also, for other target/purposes.

2. Method, instituted on determination of turbulent ones of pulsation. Since transition in laminar boundary layer to turbulent flow conditions is accompanied by the beginning of the intense pulsations of velocity, the place of origin of the latter indicates the position of transition point. Turbulent pulsations comparatively simply are detected with the aid of the nozzle of total pressure connected to low-inertia manometer or with the aid of the hot-wire anemometer, connected to oscillograph. Nozzle in these experiments it is necessary to move along wall from front/leading to trailing edge and always to follow the readings (manometer or oscillograph).

3. Method of measuring total pressures. The nozzle of the total pressure (or the sensor of hot-wire anemometer), moved directly along wall over surface in the direction of the flow, which flows around body, falling into the region of transition, it will show a noticeable increase in the total pressure. This they will be explained by the fact that in the transient and turbulent regions of boundary layer during removing from surface the velocity grow/rises faster than in laminar boundary layer. In a series of cases the total pressure is determined not by displacement of one and the same nozzle (which is complicatedly - it is necessary coordinate spacer apparatus and other devices), but by the establishment of certain quantity of

nozzles ("houses"), of the total pressure, placed on body after each other in the direction of flow. So that the nozzles would not affect each other they are placed not into "back", but with displacement.

4. Visual and optical methods. These methods are described in §VII.6.

AD-A066 280

FOREIGN TECHNOLOGY DIV WRIGHT-PATTERSON AFB OHIO
EXPERIMENTAL AEROMECHANICS (SELECTED CHAPTERS), (U)
JAN 79 S M GORLIN

F/G 20/4

UNCLASSIFIED

FTD-ID(RS)T-2011-78

NL

2 OF 4
ADA
066280



Page 294.

Chapter VIII.

Aerodynamic characteristics of different bodies.

§ VIII.1. Flat/plane plate. Sphere. ^Cylinder.

In the overwhelming majority of the cases, aeromechanical investigations are conducted for obtaining one or the other characteristics in connection with the varied conditions of flow or motion of bodies. To these characteristics first of all they are related aerodynamic force coefficients, values of overpressures in different points of body, the coefficients of friction, the ^{Distribution} temperature ~~physicochemical~~ parameters of the gas, which flows around body, etc. In many instances it is required on the basis of aeromechanical measurements to determine the losses of pressure or the resistance and the parameters of gas during its motion in conduit/manifolds or channels of diverse form, characteristic of the aeromechanical devices and machines as, for example, the pressure recovery coefficient of the diffusion, efficiency of the propeller, and flow rate of fan, compression ratio of compressor, etc.

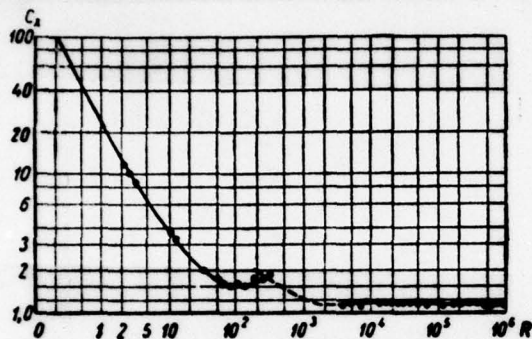


Fig. VIII.1. Dependence of the drag coefficient of flat/plane plate, establish/installed across flow, on Re number.

Page 295.

Flat/plane plate. The aerodynamic investigations of flat/plane thin plate occupy the considerable place in aeromechanics. This is explained by the fact that similar flow is encountered in many aeromechanical devices (fine/thin airfoil/profiles, wall of channel, etc.). Special place occupy the investigations on the flat/plane plate of boundary layer, which are supporting/reference ones for many theoretical investigations.

The drag coefficient of the flat/plane plate, establish/installed across flow, is graphically depicted in Fig.

VIII.1. Distribution of pressure according to plate depending on angle of attack is given on Fig. VIII.2, and the obtained on basis distributions of pressure the value of coefficients c_x and c_y — in Fig. VIII.3. As can be seen from figures, c_x plate with $Re > 1000$ is virtually constant and composes 1.12 (or 1.06). With $Re < 1000$ for the circular plate

$$c_x = \frac{64}{\pi Re} \quad \text{или} \quad c_x = \frac{64}{\pi Re} \left(1 + \frac{Re}{2\pi}\right).$$

Key: (1) . or.

In the presence of opening/aperture with a diameter of d in circular plate c_x it varies approximately parabolically from 1.16 (with $d=0.2D$) to 1.78 (with $d=0.8D$).

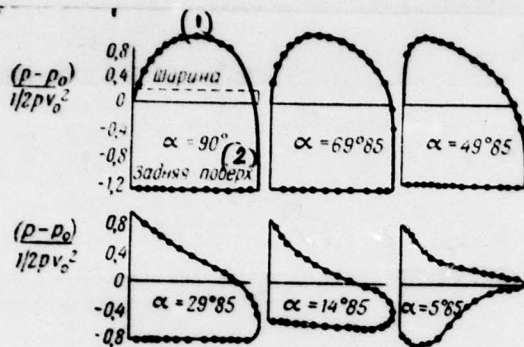


Fig. VIII.2. Distribution of pressure according to plate depending on angle of attack.

Key: (1). Width. (2). Rear Surface.

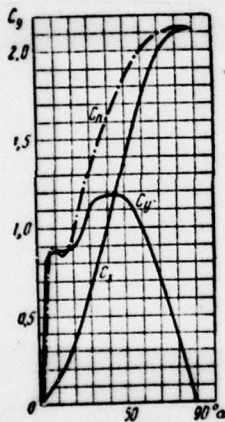


Fig. VIII.3. Dependence of coefficients c_y , $c_n = f(\alpha)$ and $c_x = f(\alpha)$ for a flat/plane plate.

Page 296.

For a square plate the drag coefficient c_x is conditionally taken as the equal to 1.28 (with $Re = 6.2 \cdot 10^5$ $c_x = 1.15$).

FOOTNOTE 1. Square flat/plane plate in aviation calculations is applied sometimes as standard for bringing to it the resistance of compounds, for example aircraft. In these cases they tell about "equivalent flat/plane plate", i.e., the plate of this area, which $c_x = 1.28$ has the same resistance as the compared with it aircraft.

ENDFOOTNOTE.

For a rectangular plate the coefficient c_x depends on the relationship/ratio of sides (Fig. VIII.4).

Fine/thin cup- hemisphere in flow direction inside it has $c_x = 1.43$ ($Re = 4.5 \cdot 10^5$), and during its flow from spherical side $c_x = 0.35$ (for $Re = 4.5 \cdot 10^5$).

The coefficient of friction drag of the longitudinally streamlined fine/thin flat/plane plate depends on the state of its surface and Re numbers and M .

In laminar zone of flow, according to Blasius's law (i.e. for Re numbers $< 5 \cdot 10^5 - 5 \cdot 10^6$), the coefficient of friction drag of the plate, moistened on the one hand:

$$c_f = \frac{1.328}{\sqrt{Re}}.$$

where

$$Re = \frac{v_{\infty} l}{\nu},$$

here l — longitudinal size/dimension of plate.

Boundary layer thickness at a distance x from leading edge can be found from the expression

$$\delta \sim 5 \sqrt{\frac{\nu x}{v_{\infty}}}.$$

The displacement thickness of the boundary layer

$$\delta^* = \int_0^{\delta} \left(1 - \frac{v}{v_{\infty}}\right) dy$$

is the physically more specific measure. This is average distance, up to which they are moved aside from body along the normal to it of the flow line of external flow as a result of the education/formation of boundary layer. For a plate $\delta^* = 1/3\delta$ or

$$\delta^* = 1.73 \sqrt{\frac{\nu x}{v_{\infty}}}.$$

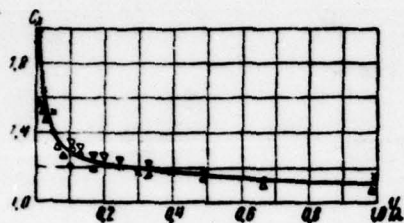


Fig. VIII.4. Dependence of the coefficient C_x of flat/plane plate on the ratio/relation of sides.

Page 297.

The momentum thickness, which occurs as a result of boundary-layer friction

$$\delta^{**} = \int_0^{\delta} \frac{v}{v_{\infty}} \left(1 - \frac{v}{v_{\infty}}\right) dy,$$

composes $0.664 \sqrt{\frac{v x}{v_{\infty}}}$.

The distribution of the velocities in laminar layer on the longitudinally streamlined flat/plane plate is represented in Fig. VIII.5. During an increase in Re number, the boundary layer on plate transfer/converts from laminar into turbulent state. This transition is completed with numbers $Re=0.5 \cdot 10^6$. In this case, is observed the

more intense increase of the velocity in boundary layer

(approximately according to the law of the root of the seventh degree

$$v = v_{\infty} \left(\frac{y}{\delta} \right)^{\frac{1}{7}}.$$

$$c_f = 0,74 \cdot Re^{-\frac{1}{2}} (2 \cdot 10^5 < Re < 10^7),$$

$$\delta = 0,37x \left(\frac{v_{\infty} x}{\nu} \right)^{-\frac{1}{5}},$$

$$\delta^* = \frac{\delta}{8},$$

$$\delta^{**} = \frac{7}{72} \delta = 0,036x \left(\frac{v_{\infty} x}{\nu} \right)^{-\frac{1}{5}}.$$

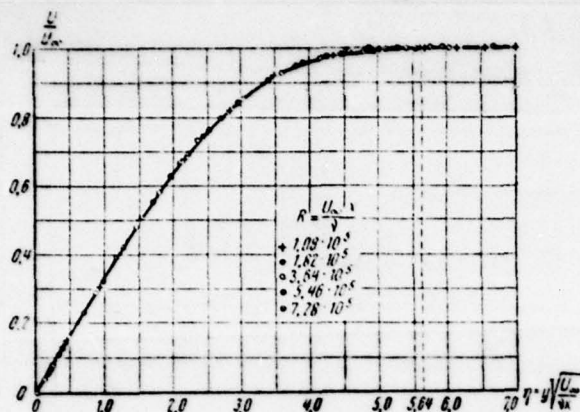


Fig. VIII.5. Distribution of the velocities in laminar boundary layer on the flat/plane plate, streamlined lengthwise (on measurements of Pikuradze).

Page 298.

Formula for c_f is valid, if boundary layer on an entire plate, beginning with leading edge, turbulent. However, in actuality on the part of the plate, boundary layer will be laminar, that to decrease the frictional resistance. Under these conditions for a boundary layer, the frictional resistance

$$c_{f_{\text{en}}} = \frac{0.074}{\sqrt{Re}} - \frac{A^*}{Re},$$

where by A^* is determined by the position of transition point and depends on Re number, with which in boundary layer is completed the changing over from laminar to turbulent flow Re_{sp} :

$Re_{\text{sp}} = 3 \cdot 10^5;$	$5 \cdot 10^5;$	$10^6;$	$3 \cdot 10^6$
$A^* = 1050;$	1700;	3300;	8700

The dependence of the coefficient of friction on Re numbers is represented in Fig. VIII.6.

The resistance of rough plate is greater than resistance of smooth, and it depends on relative roughness, i.e., on the ratio of the height/altitude of the prominence/protruberances of roughness K to boundary layer thickness. For technology has high value as the called permissible degree of roughness, i.e., that ceiling of roughness elements, which during the flow around wall does not yet produce an increase in the resistance in comparison with the resistance of smooth plate. For determination $K_{\text{доп}}$ (Fig. VIII.7) it is possible to use the expression

$$\frac{\sigma_{\text{доп}} K_{\text{доп}}}{\nu} = 100 \quad (1) \quad \text{или} \quad K_{\text{доп}} \leq \frac{100}{\text{Re}}.$$

Key: (1) . or .

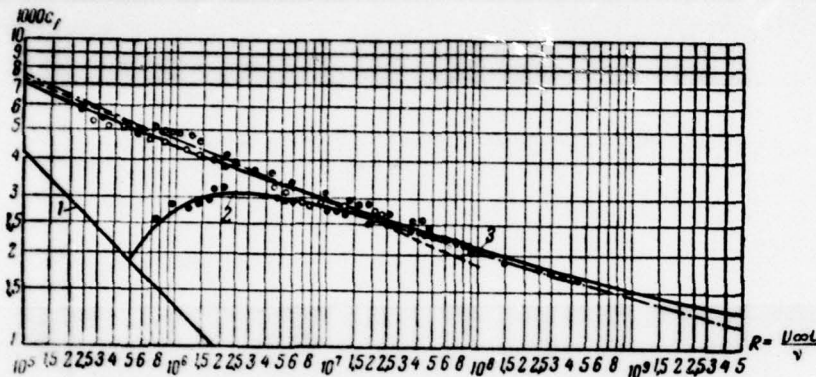


Fig. VIII.6. The dependence of the coefficient of friction for the smooth flat/plane plate: 1 - on Blasius for laminar flow; 2 - for transition conditions/mode; 3 - for turbulent flow (Prandtl Schlichting).

Page 299.

In the flow around plate of the flow high velocity essential effect on boundary layer exerts temperature field, or temperature boundary layer (Fig. VIII.8). If at the low speeds of flow heat from hot body is spread into the environment virtually evenly in all directions, then at high velocities the zone of flow, which undergoes heating, forms narrow zone around body and long trace of the heated liquid of behind of it, in which changes of the temperature cause substantial changes in the viscosity¹.

FOOTNOTE 1. $\frac{\mu}{\mu_0} = \left(\frac{T}{T_0}\right)^{\omega}$, $1/2 < \omega < 1$; for 0°C $\omega = 0.8$. For low temperatures $\omega \approx 1$, for high ones - $\omega = 0.5$. ENDFOOTNOTE.

Furthermore, appears the need for considering the effect of Mach number (Fig. VIII. 9), which characterizes in this case increase temperature, caused by adiabatic compression, and number of Prandtl

$$\text{Pr} = \frac{\mu g c_p}{\lambda}.$$

The temperature of the wall itself T_w .

$$T_w = T_{\infty} \left(1 + \sqrt{\text{Pr} \cdot \frac{\gamma-1}{2}} M^2 \right).$$

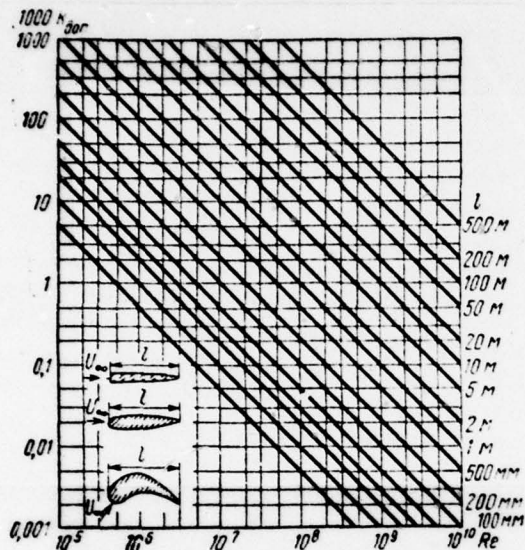


Fig. VIII.7. Permissible height/altitude of roughness.

Page 300.

For air ($\kappa=1.4$ $Pr = 0.716$)

$$T_e = T_\infty (1 + 0.169 M^2).$$

If flow occurs with so high a velocity, that in the vicinity of body are formed the regions in which the local velocity of flow exceeds the speed of sound, then in the places of the transition supersonic velocity into subsonic appear shock waves. Their emergence, as was shown in §V.3, strongly affects the character of

boundary-layer flow. In turn, the shock waves affect the flow pattern. The part of boundary layer, most close to wall, moves in any event with subsonic speed. Jumps appear in area of supersonic speeds: in external flow they cannot "reach" the wall and is formed the system of λ -shaped jumps. In this case, pressure gradient along wall in the zone of jump is considerably weaker than in external flow (Fig. VIII.10).

After jump the boundary layer thickness increases, moreover for a laminar layer this build-up considerable, than for turbulent. In the zone of jump, there are considerable pressure gradients in the direction, normal to wall, namely: to jump in proportion to removal/distance from wall, the pressure falls, and after jump, on the contrary, it is powerful it increases.

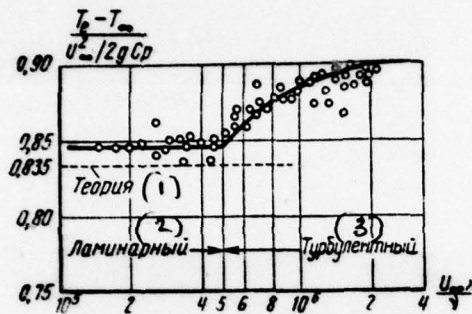


Fig. VIII.8. Results of measuring its own temperature of the flat/plane plate, streamlined lengthwise and turbulent boundary layer.

Key: (1). Theory. (2). Laminar. (3). Turbulent.

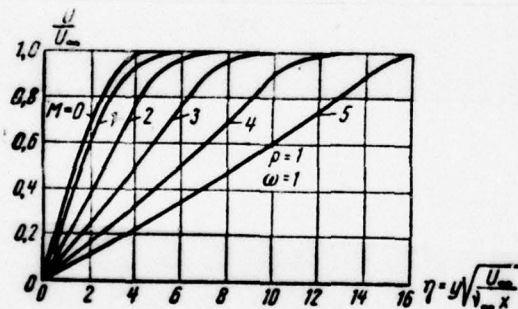


Fig. VIII.9. The distribution of the velocities in the compressed laminar boundary layer on the flat/plane plate (heat transfer is absent).

Thereby is disrupted the main assumption, which lies at the basis of the calculation of the boundary layer, namely the assumption of the extreme smallness of pressure gradient in the direction, normal to wall. Furthermore, in the zone of jump the gradients of velocity dv/dx and dv/dy along plate and along the normal to it are identical with respect to the orders of their magnitudes, what into its turn leads to nonobservance and another important assumption of boundary-layer theory - about the possibility of neglect in equations of motion by the square of the gradient of tangential velocity as by low value in comparison with the square of the gradient of normal velocity. On these reasons the theoretical analysis of interaction of jump with boundary layer meets the unsurmounted, until now, difficulties and here widely are utilized different experimental methods of study.

Characteristics of sphere (sphere). To determining the characteristics of sphere are devoted many experimental and theoretical studies, moreover considerable place they occupy the measurement of the distribution of pressure and of frontal resistance of sphere under the varied conditions of its flow (Re numbers and α) (for example, see Fig. V.19). Figure V.17 depicts data according to the distribution of pressure for a sphere during different conditions/modes of flow. The values of the drag coefficient of sphere depending on Re number are shown on Fig. (VIII.11, and to

dependence on Re numbers and M - in Fig. VIII. 12. Example of the distribution of pressure according to sphere when $M=0.7$ - in Fig. VIII.13.

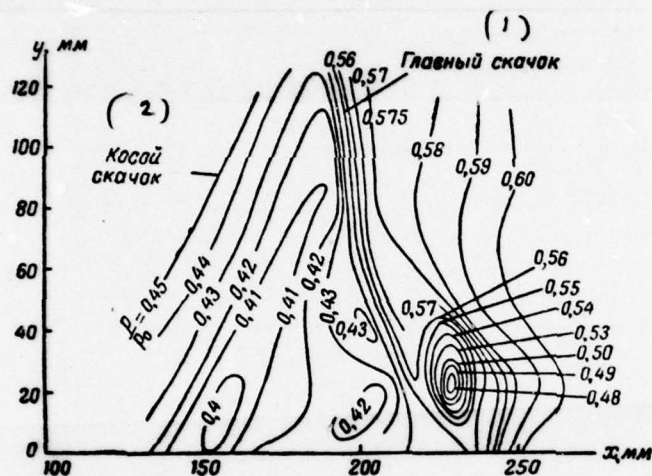


Fig. VIII.10. Isobars of shock wave with laminar boundary layer (λ -jump).

Key: (1). Main jump. (2). Oblique shock.

Page 302.

As can be seen from Fig. VIII.13, with number $M=0.7$ on sphere, appear the shock waves (at 80 and 280°), which leads to an increase in the coefficient c_x (Fig. VIII.12).

Given data served in essence for comparison and evaluation of the stream conditions and turbulence in wind tunnels, and also

comparison of the conclusions of the theory of an ideal liquid with results of experiment. In recent years, in connection with development of jet technology and space flights, determining the aerodynamic characteristics of sphere at supersonic and hypersonic speeds began to occupy the extremely large place in aerodynamic investigations.

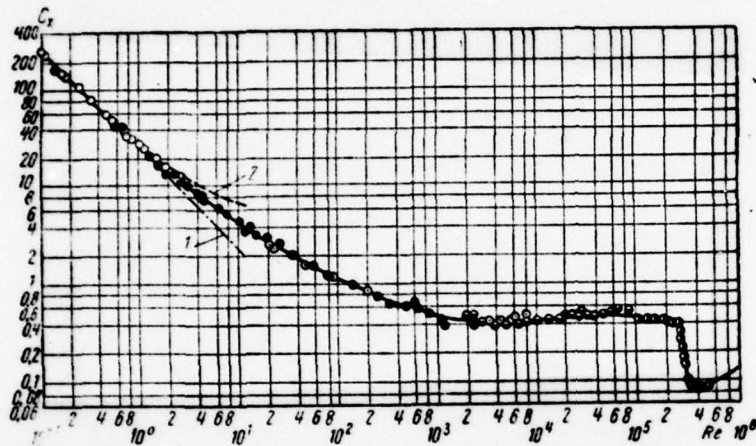


Fig. VIII.11. The dependence of the drag coefficient of sphere on Re number: 1 - according to Stokes's theory; 2 - according to the theory of Ozin.

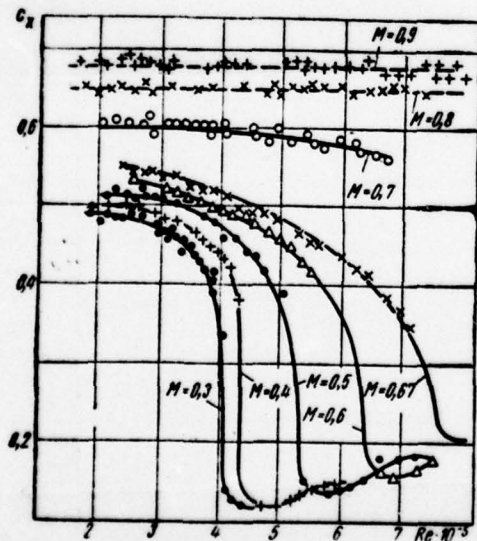


Fig. VIII.12.

Fig. VIII.12. Dependence of the drag coefficient of sphere on Re numbers and M.

Page 303.

This is explained by the fact that in a series of cases the space objects are sphere. Furthermore, the aerodynamic and physico chemical processes, which occur on sphere, especially in the vicinity of front/leading critical point, are similar to the phenomena, taking place on the nose sections of rocket and other bodies, which fly with high supersonic velocities. On by these to reasons to the investigation of frontal resistance of spheres, position (departure/withdrawal) of shock wave, to the distribution of the temperatures and pressures and other characteristics in dependence on Mach numbers, Re, Pr, α and the like devoted considerable number both of theoretical and experimental works.

In recent years receive increasing propagation the spherical construction/designs of different designation/purpose, calculation for strength of which requires the knowledge of the distribution of pressure and drag with the large Re numbers ($Re > 10^7 - 10^8$). Figure VIII.14 depicts to the photograph of shock waves during the flow around hemisphere of the supersonic flow. Theoretical distribution of pressure and value of the departure/withdrawal of shock wave on sphere and blunted bodies with different Mach numbers of the incident flow is given in Fig. VIII.15 and VIII.16, where is also given the comparison of calculations (solid line) with experiment (point).

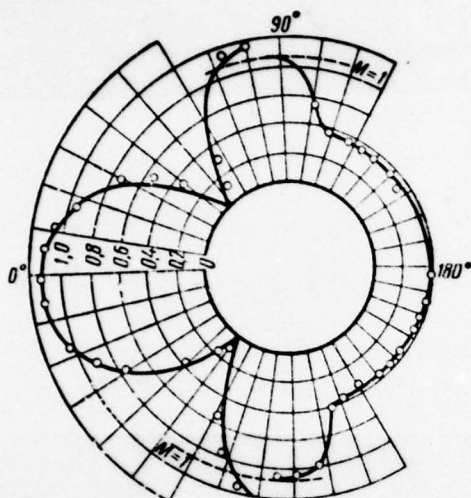


Fig. VIII.13. Distribution of pressure according to sphere with $M=0.7$
($Re=7 \cdot 10^5$) .



Fig. VIII.14. Flow around hemisphere of the supersonic flow.

Page 804.

The character of the dependence of the drag coefficient on Mach number of large Reynolds numbers, obtained in the hypersonic tunnel of low density LDH (center of Fig. in Arnold, USA) is shown on Fig. VIII.17.

Characteristics of cylinder. To determining the characteristics of cylinder, just as sphere, are devoted many different investigations. Cylindrical cell/elements widely are encountered in various flight vehicles, and also constructions and construction/designs, streamlined with the flow of gas or liquid.

The distribution of pressure according to the surface of round cylinder is represented in Fig. VIII.18, and dependence its drag coefficient on Re number is given in Fig. VIII.19. The critical Re number for cylinder is equal approximately $3 \cdot 10^5$, after this boundary-layer flow from laminar transfer/converts into turbulent state and occurs (by analogy with sphere) the sharp decrease of drag coefficient.

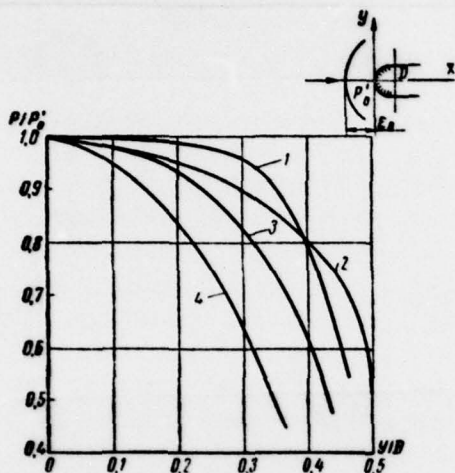


Fig. VIII. 15. The distribution of pressure in the forward section of the sphere and other bodies: 1 - end/face with rounding; 2 - segment $\alpha = 30^\circ$; 3 - ellipsoid $\delta=2$; 4 - sphere.

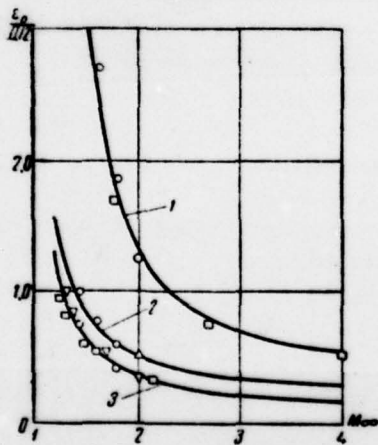


Fig. VIII. 16. The departure/withdrawal of shock wave in dependence from Mach number: 1 - circular cylinder, 2 - ellipsoid $\delta=2$; 3 -

sphere.

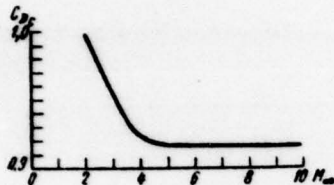


Fig. VIII.17. Resistance of sphere with the large Re numbers and M (Re=0.4-2·10⁶).

Page 305.

As can be seen from Fig. VIII.20, at the initial moment of acceleration/dispersal (Fig. VIII.20a) the picture of flow is close to potential (irrotational). Subsequently begins the breakaway at rear critical point (Fig. VIII.20b). Point is moved back/ago against the current (Fig. VIII.20c) and are formed two concentrated eddy/vortices (Fig. VIII.20d, e) which as a result of instability decompose and are taken away by external flow. After cylinder is formed the fluctuating flow, which creates the distribution of pressure, different from theoretical (Fig. VIII.21). The same character of the flow around cylinder occurs, also, at high velocities.

Presented facts have high value for determining of loads and fluctuations of cylinder in flow.

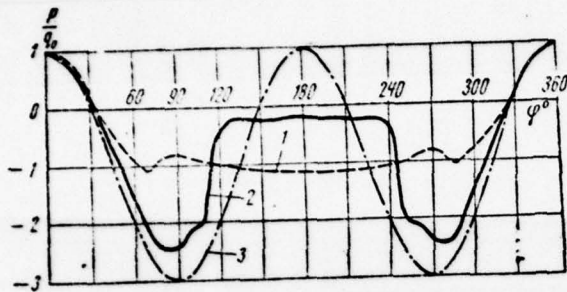


Fig. VIII.18. The distribution of pressure on the surface of round cylinder with subcritical ($Re_{\text{эксп}} = 1.86 \cdot 10^5$) and supercritical ($Re_{\text{эксп кр}} = 6.7 \cdot 10^5$) Reynolds numbers: 1 - subcritical; 2 - supercritical; 3 - theoretical.

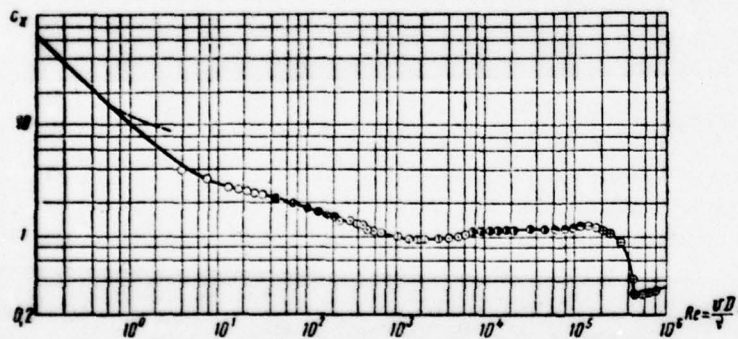


Fig. VIII.19. Dependence of the drag coefficient of the round cylinder on Reynolds number.

Page 306.

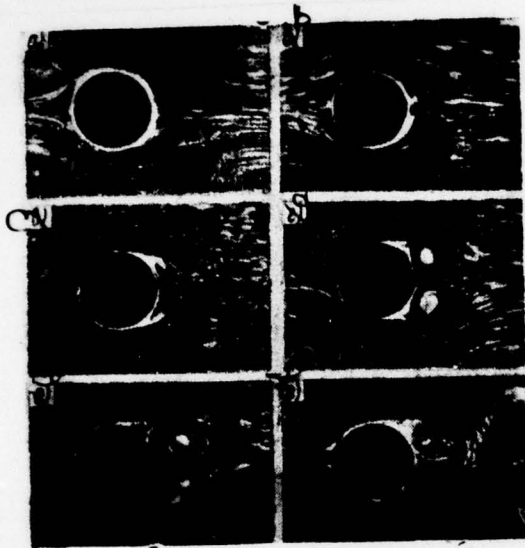


Fig. VIII.20. Education/formation of eddy/vortex during the flow around of cylinder, novice from state of rest.

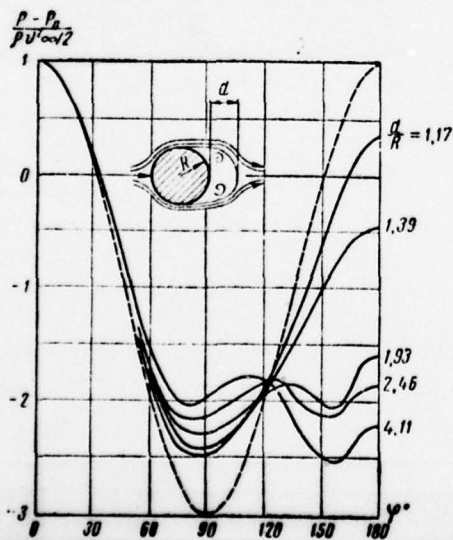
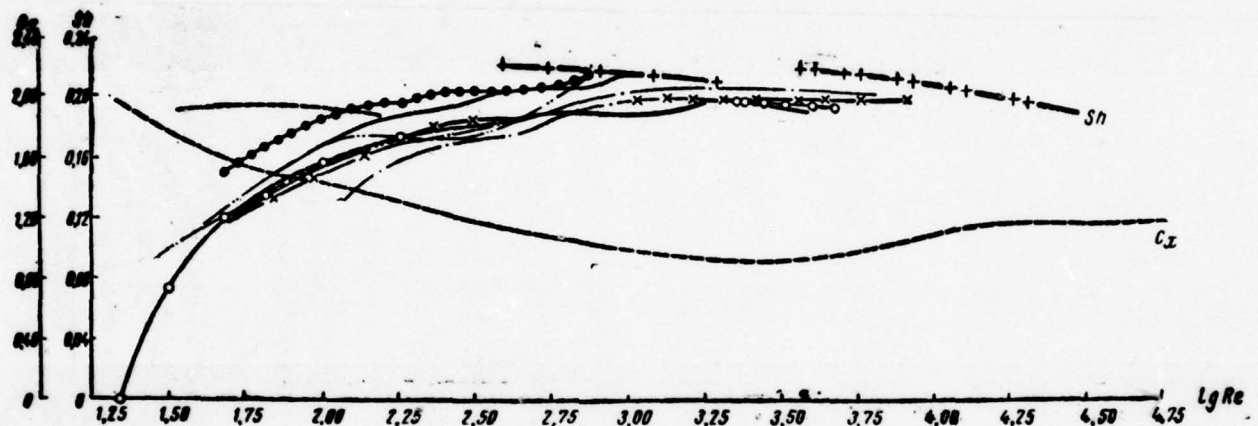


Fig. VIII.21. Measurement of the distribution of pressure about cylinder upon acceleration/dispersal. To dash of lines shown theoretical distribution of pressure for steady flow.

Page 307.

Fig. VIII. 22. Dependence $Sh=f(Re)$ for a cylinder.

Page 308.

For the purpose of the reduction of frequency and amplitude of the pulsations of pressure, is accepted the number of measures for change the character of the flows around cylinder, main target/purpose of which is the prevention of the resonance of the frequency of exciting force and the natural frequencies of oscillation of construction/design. As showed different investigations, pulsations of pressure after cylinder they correspond over a wide range of Re numbers to Strouhal number $Sh = \frac{nf}{v_{\infty}} \approx 0.2$ (Fig. VIII.22 and VIII.23).

As can be seen from Fig. VIII.23 because of superstructures it is possible to change Strouhal number and to leave from the dangerous for construction/design zone of the ripple frequencies of pressure.

With the character of the flow around cylinder, is connected the temperature field around it (Fig. VIII.24).

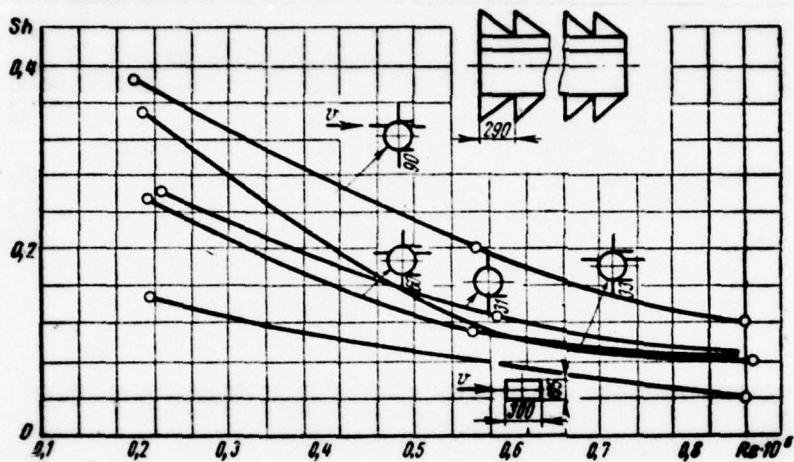


Fig. VIII.23. Effect of different superstructures on number Sh for a cylinder.

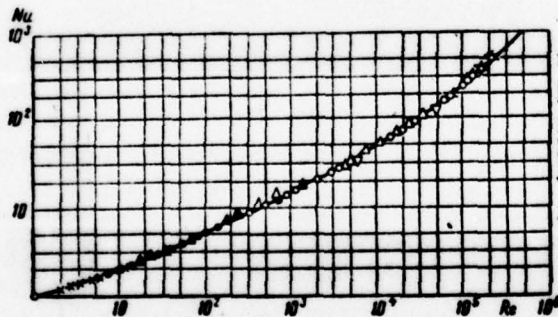


Fig. VIII.24. Dependence of Nusselt number for a round cylinder on Re number Re ($t_{cr} = 100^\circ C$)

Page 309.

This character, temperature distributions is retained to high subsonic speeds. The average value of the local its own temperature T , at transverse flow for an unheated cylinder can be determined according to the empirical dependence

$$(T_e - T_\infty) \frac{2gc_p}{v_\infty^2} \approx 0.7.$$

On the resistance of cylinders essential effect exerts the degree of the roughness of its surface (Fig. VIII.25).

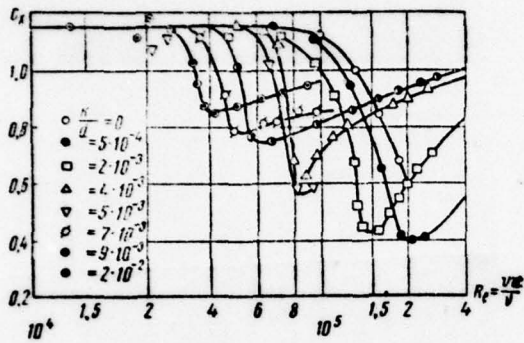


Fig. VIII.25. Resistance of round cylinder with different roughness of its surface.

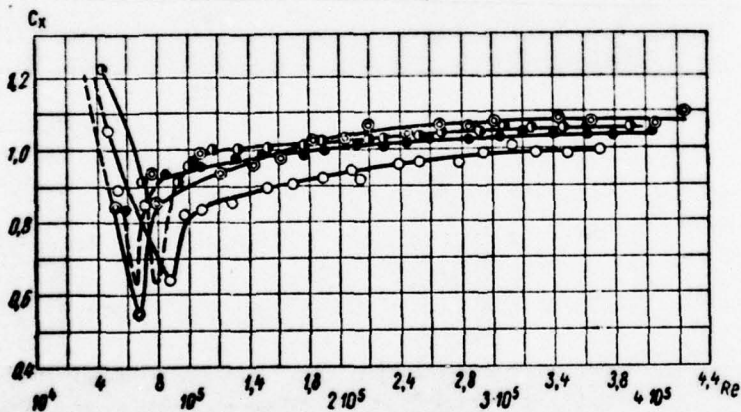


Fig. VIII.26. $c_x = f(Re)$ cylinders with different superstructures (racks).

In the practice of the construction of the various kinds of construction/designs, for example conduit/manifolds, the cylindrical cell/elements used are smooth, but have various kinds projections (roughness on surface). To a number of such cell/elements can be referred the superstructures and the combs, which are one of the resources of the reduction of the amplitudes of the oscillating body, and also the lining racks, employees for a preservation from the damages to insulation/isolation of the conduit/manifolds, placed on the bottom of rivers. The drag coefficients of this type of cylinders differ significantly from values c_x for smooth cylinders.

Figure VIII.26 depicts to dependence $c_x = f(Re)$ of very rough of cylinders $k/D = 3 \cdot 10^{-2}$. As can be seen from diagrams, c_x the very rough cylinders of more than value c_x for smooth cylinders; the transition of laminar layer into turbulent and independence c_x from Re number begins in rough cylinders with $Re > 3 \cdot 10^5$, but in smooth ones - with $Re > 6 \cdot 10^5$. The device of vertical combs on cylinders leads to an increase c_x to 1.35 in comparison with $c_x = 0.6$ for cylinders with horizontal cell/elements (Fig. VIII.27). The characteristics of cylinders with overloads are given in Fig. VIII.28. The effect of different superstructures on cylinder on lift coefficient is shown on Fig. VIII.29.

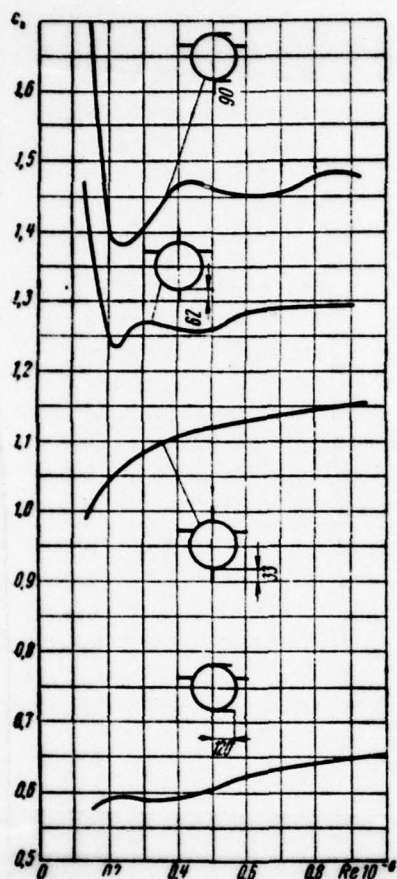


Fig. VIII.27. $c_x = f(Re)$ of cylinders with combs.

Page 311.

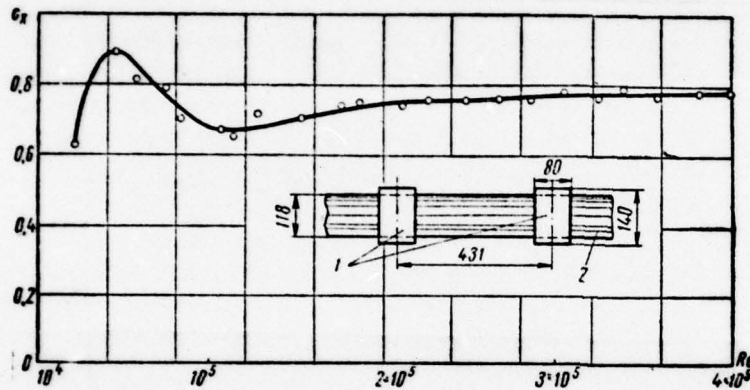


Fig. VIII.28. $c_x = f(Re)$ cylinders with overloads: 1 - smooth overloads; 2 - rack rough, $b = 6$ mm, $h = 3$ mm, the distance between racks 1 - 0.33 λ .

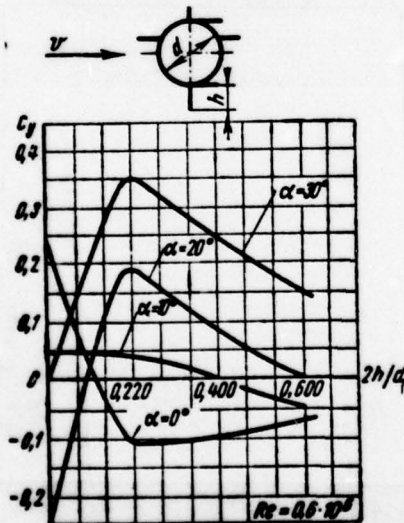


Fig. VIII.29. $c_y = f(\alpha)$ for cylinders with superstructures.

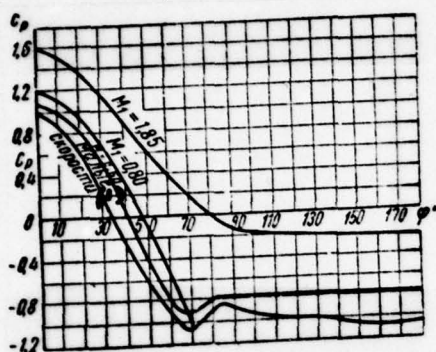


Fig. VIII.30. $c_p = f(M, \varphi)$ for circular cylinders ($Re = 12 \cdot 10^5$).

Key: (1). Low speeds.

Page 312.

The flow around cylinder at supersonic speeds, just as sphere, it is connected with considerable changes of distributing the pressure, the temperatures and other parameters. In Fig. VIII.30 and VIII.31 represented experimental distribution of pressure and the drag coefficients of different supersonic velocities of the flow, which encounters to cylinder.

§VIII.2. Bodies of revolution.

Fuselages of aircraft and projectiles, dirigibles and torpedoes, rockets and artificial satellites of the Earth are actually the bodies of revolution of various forms. For bodies of revolution depending on the velocity of their motion the dominant role play these or other the characteristics. At comparatively low speeds the form of body of revolution must possess the smallest possible resistance. At high supersonic and hypersonic speeds the value which is not smaller acquire the thermal phenomena and the connected with them physico-chemical processes, which occur in the vicinity of body and its surface.

At small subsonic velocities the resistance of bodies of revolution with the smoothly outlined forms in essence connected with friction depends on the thickness (completeness) of body. The typical distribution of pressure on body of revolution is represented in Fig. II.26. Figure VIII.32 shows the aerodynamic characteristics of the fuselage of aircraft at low speeds.

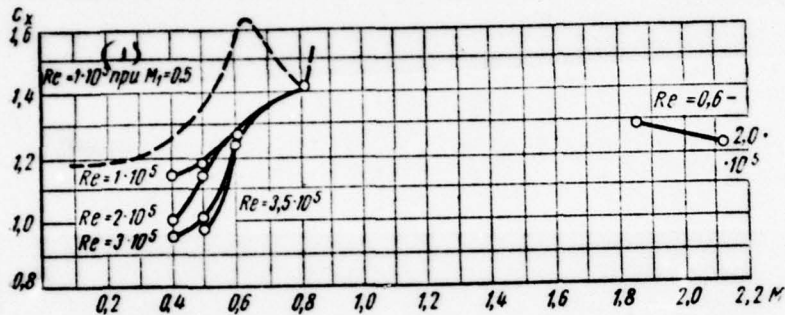


Fig. VIII.31. Resistance of circular cylinders with large Mach numbers.

Key: (1). with.

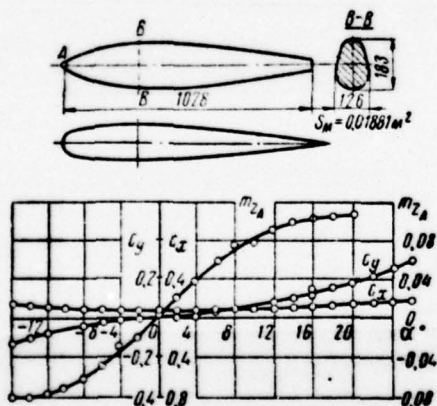


Fig. VIII.32. Aerodynamic characteristics of fuselage.

The compressibility effect of the compressibility of air at subsonic velocities in essence depends on the aspect ratio of the nose part of the body and can be described by the coefficient (Fig. VIII.33),

$$\eta_n = f(\lambda_n, \alpha, M).$$

Of these conditions the drag coefficient of bodies of revolution (fuselages) ¹

$$c_X = c_f \frac{S_{\text{ноз}}}{S_{\text{max}}} \eta_n \eta_c,$$

where c_f — coefficient of the friction of flat/plane plate, depending on Re number (Fig. VIII.34);

$S_{\text{ноз}}$ — body surface of rotation;

S_{max} — area of maximum cross section;

η_c — the correction factor, which considers the difference for the resistance of body of revolution from the frictional resistance of flat/plane plate (Fig. VIII.35).

FOOTNOTE 1. The majority of the given below expressions for determining the resistance and other characteristics of bodies of revolution is obtained on the basis of processing experimental data.
ENDFOOTNOTE.

In the presence of different form of superstructures on body of revolution, increases the drag coefficient

$$c_x = c_f \frac{S_{\text{DOP}}}{S_{\text{DHA}}} \eta_c \eta_m + \frac{\Sigma c_{x_{\text{DHA}}} S_{\text{DHA. DHA}}}{S_{\text{DHA}}} + \Delta c_x.$$

where Δc_x — a drag coefficient of those cell/elements of the superstructures which it is difficult to isolate from maximum cross section of the fuselage.

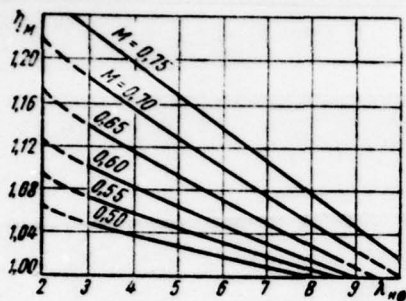


Fig. VIII.33. Dependence of coefficient $\eta_M = f(\lambda_M \phi)$

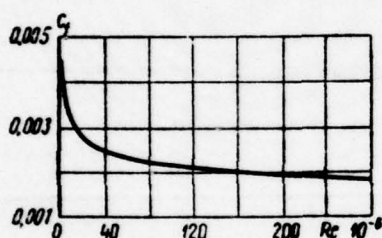


Fig. VIII.34. $c_f = f(Re)$ for a flat/plate plate.

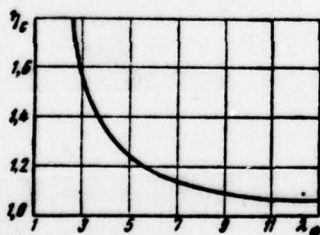


Fig. VIII.35. Dependence of coefficient $\eta_c = f(\lambda_\phi)$

Value $\sum_{C_{X_{n+1}}} S_{n+1}$ varies within considerable limits, for example for antenna ones fighter it composes 0.01, for the motionless machine gun of bomber - 0.03 for the canopy of cockpit $\frac{\Delta C_X}{S_{n+1}} \approx 0,001 - 0,004$ and the like.

The dependence of the coefficient of frontal resistance of the bodies of revolution of different elongation on Mach number is given in Fig. VIII.36. A reduction in this resistance at high velocities is possible by an increase in the elongation and imparting to the forward section of this form that would not appear the peaks of evacuation/rarefaction, leading to the education/formation of shock waves. In this case, considerably increases M_{kp} (Fig. VIII.36), which for the slim fuselages can achieve almost $M_{kp} = 1$ (with $c = 150/o$, $M_{kp} = 0.95$).

By others the method of decreasing the resistance of bodies of revolution is imparting to them the laminar form, with which maximum thickness is displaced back/ago to $40 - \frac{5}{100}$ of length of body, and the decrease of the surface roughness. The transition point of laminar boundary layer into turbulent in similar type fuselages with the large Re numbers lie/rests at a distance of 70-80% of length of fuselage. Comparison $C_X = f(M)$ for the usual and laminated fuselages is given in Fig. VIII.37, where is also shown the effect of the

sucking action of plume exhaust of the engine, placed in the rear portion of the fuselage. It should be noted that very low resistance have the bodies of revolution of the parabolic form, formed, for example, by rotation around the axle/axis of the curve of form $r=2t(x-x^2)$ (Fig. VIII.38).

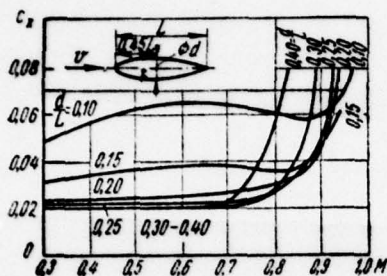


Fig. VIII.36. Dependence of the drag coefficient of body of revolution on its elongation and Mach number

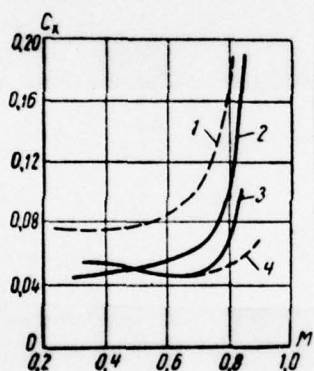


Fig. VIII.37. The comparison of the drag coefficients of the usual and laminarized fuselages: 1 - classical fuselage without jet engine; 2 - the same, with jet engine; 3 - laminar fuselage without jet engine; 4 - the same, with jet engine.

Page 315.

With an increase in the velocity to small supersonic the resistance of the streamlined bodies of revolution depends mainly on losses in bow shocks. These losses depend on velocity and form of nose section. As a whole resistance will be composed of wave impedance, frictional resistance and of the bottom, caused by evacuation/rarefaction after the bottom body (fuselage, projectile, etc.).

Experiments show that the resistance of bodies of revolution at supersonic speeds in high degree depends on the angle of taper of nose section. Table VIII.1 depicts the values of the coefficient of pressure \bar{p} depending on Mach number on projectiles with different conical knob/cap of numbers $M=1.1-3.5$. As can be seen from these data, the lesser the angle of taper, the lesser the resistance.

As can be seen from Table VIII.1 during the flow around projectile of the supersonic flow, pressure on the bottom falls, which causes the supplementary resistance, called bottom. The

resistance of tail section can be decreased because of imparting to it of conicity.

Re number is the very important parameter, which characterizes resistance at high velocities.

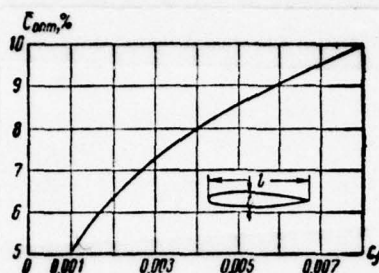


Fig. VIII.38. Optimum value of the thickness ratio of fuselage taking into account surface friction.

Table VIII.1. Ratio of pressure on the surface of projectile and pressure in the incident flow depending on the angle β of the dissolution of the cone of the nose section and Mach number

β	M	(1) Конусная часть	(2) Цилиндриче- ская часть	(3) Дно
20°	1,11	0,64	0,64	0,48
	1,6	1,18	0,72	0,51
	2,0	1,28	0,75	0,49
	3,5	1,74	0,74	0,37
40°	1,6	1,67	0,62	0,45
	2,0	1,92	0,65	0,43
	3,5	3,45	0,69	0,73
60°	2,0	2,8	0,64	0,44
	3,5	5,9	0,70	0,40

Key: (1). Conical part. (2). Cylindrical part. (3). Bottom.

Page 316.

Despite the fact that with an increase in the Mach number due to slope deviation of bow shock total coefficient c_x falls, resistance

from an increase in the Mach number sharply grow/rises due to an increase of velocity head.

Wave impedance and frictional resistance body of revolution are called head resistance. Coefficient of total drag c_x :

$$c_x = c_{x_s} + c_{x_{fp}} + c_{x_{res}}$$

The coefficient of wave impedance depends both on the Mach number and form and elongation of body of revolution. For the body of revolution, comprised of conical cell/elements (Fig. VIII.39), value c_x can be found from the approximate dependence

$$c_{x_s} = 0,02 (0,8 + M_{\infty}^{-2}) \left[(\beta_{01})^{1,7} + (\beta_{02})^{1,7} \cdot \left(1 - \frac{S_{002}}{S_{001}} \right) \right].$$

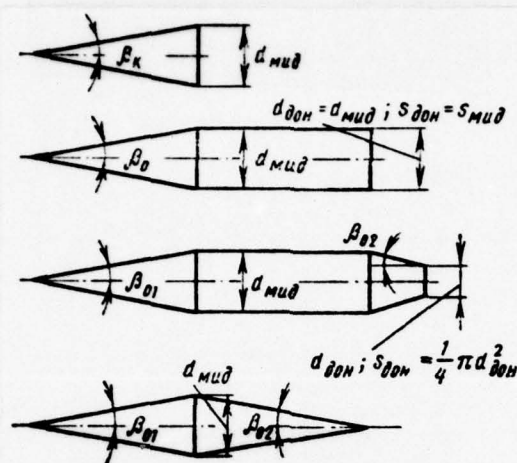


Fig. VIII.39. Forms of the bodies of revolution, comprised of conical cell/elements.

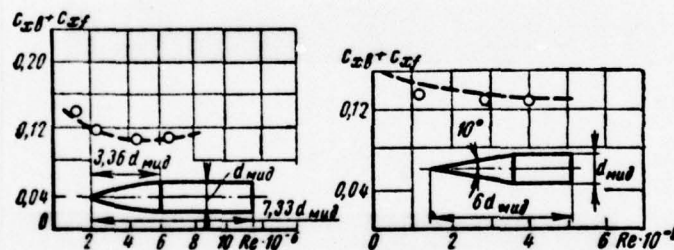


Fig. VIII.40. Change of the coefficient of head resistance in dependence on Re number.

Page 317.

For fine/thin bodies of revolution with arbitrary generatrix

$$c_{x_0} = 0,415\varphi P_{\infty}$$

where

$$\varphi \approx 0,8.$$

If body of revolution is very fine/thin, then

$$c_{x_0} = 1,17\lambda^{-2}.$$

From last/latter expression it is evident that in this case the wave impedance depends only on the value of elongation.

The coefficient of friction drag of bodies of revolution depends on the character of boundary-layer flow, surface condition of Re number and of form of body (Fig. VIII.40). Experiments show that head resistance $(c_{x_0} + c_{x_{tp}})$ with turbulent boundary layer approximately to 200/o is more than resistance with laminar. It must be noted that for the bodies of revolution (of type of projectiles) the frictional resistance composes $\approx 200/o$ of total resistance.

Base drag. This resistance is the consequence of the evacuation/rarefaction, which is formed after model (on the bottom), and depends mainly on surface condition of body, its length and of contraction, i.e., on the factors, which are determining the properties of boundary layer in bottom section/shear. Observations show that the flow after the bottom of model has a character, depicted in Fig. VIII.41. The distribution of pressure in the trace

with of $M=1.3$ for model $d=7.62$ mm ($\lambda=4$) is shown on Fig. VIII.42.

Great effect on the value of the pressure (are more precise, evacuation/rarefactions) on the bottom of model, exerts the boundary layer which separates the external flow from internal cavity after the bottom.

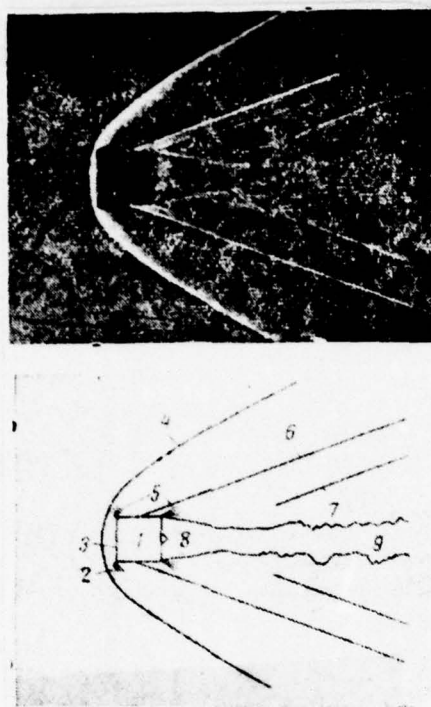


Fig. VIII.41. Shallow photograph and schematic of the flow around blunted body ($M=3$): 1 - body; 2 - sonic line; 3 - deceleration point; 4 - the leading shock wave; 5 - fans of rarefaction; 6 - jump of secondary compression; 7 - tailed jump; 8 - stagnation zone; 9 - turbulent feed trace.

Page 318.

The thicker the boundary layer, the greater the frictional resistance and the less the sucking action of external flow and, consequently, also evacuation/rarefaction on the bottom. Base drag in this case

descends. On these reasons during the investigation of base drag, sometimes they are utilized as the parameter the coefficient of friction $c_{f_{\text{дон}}} = c_f \left(\frac{\dot{S}_6}{S_{\text{дон}}} \right)$, referred to base area. Experimental data showed:

$$\bar{P}_{\text{дон}} = - \frac{0,029}{\sqrt{c_{Xf_{\text{дон}}}}},$$

and

$$c_{X_{\text{дон}}} = \frac{0,029}{\sqrt{c_{Xf}}} \left(\frac{d_{\text{дон}}}{d_{\text{мнл}}} \right)^2,$$

where c_{Xf} - the coefficient of friction, in reference to lateral surface, equal to $\bar{c}_{Xf} \left(\frac{S_6}{S_{\text{мнл}}} \right)$; c_{Xf} it is calculated from lateral surface.

The dependence of the ratio of pressure on the bottom to static pressure in the incident flow is shown on Fig. VIII.43.

It is sometimes more convenient the coefficient of base drag to determine directly through the coefficient of base pressure. In this case

$$c_{X_{\text{дон}}} = - \frac{\bar{P}_{\text{дон}} S_{\text{дон}}}{S_{\text{мнл}}}.$$

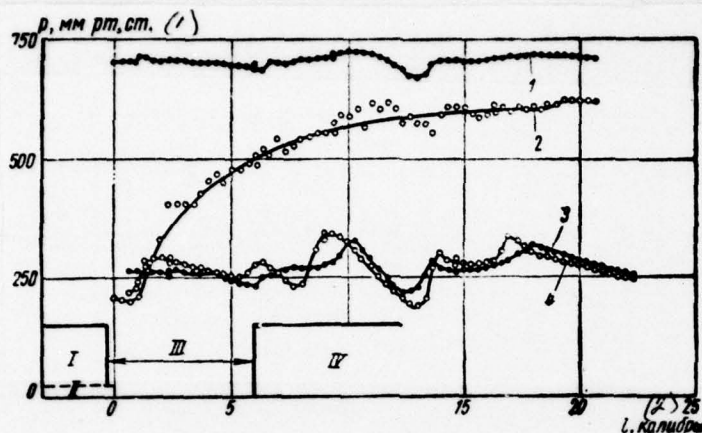


Fig. VIII.42. The distribution of pressure in the trace: I - nozzle; II - model; III - clearance; IV - exit cone/diffuser 1 - total pressure in empty duct; 2 - total pressure trace after model; 3 - static pressure in empty duct; 4 - static pressure in trace after model.

Key: (1). mm Hg. (2). bores.

Page 319.

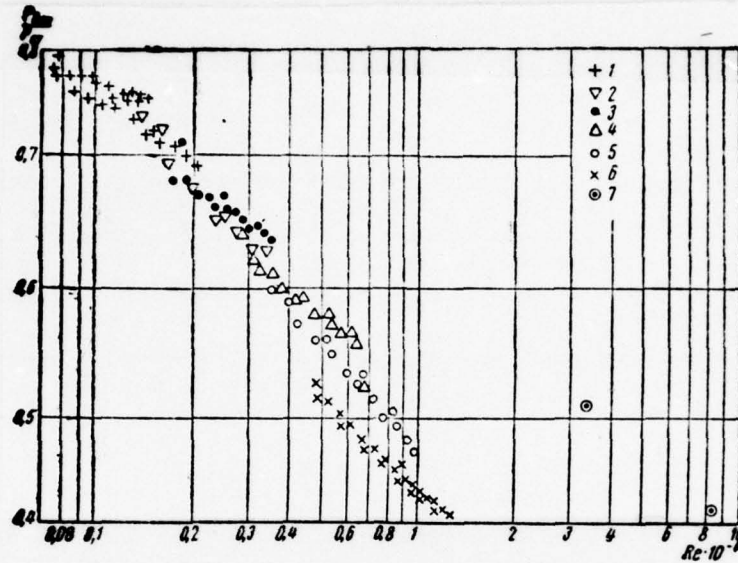


Fig. VIII.43. The ratio of pressure in trace to static: it is squashed in the incident flow depending on Re number: the diameters of the model: 1 - 7.62 mm; 2 - 12.7 mm (normal position); 3 - 12.7 mm (50.8 after the bottom); 4 - 25.4 mm; 5 - 34.9 mm; 6 - 44.4 mm; 7 - rifle tests.

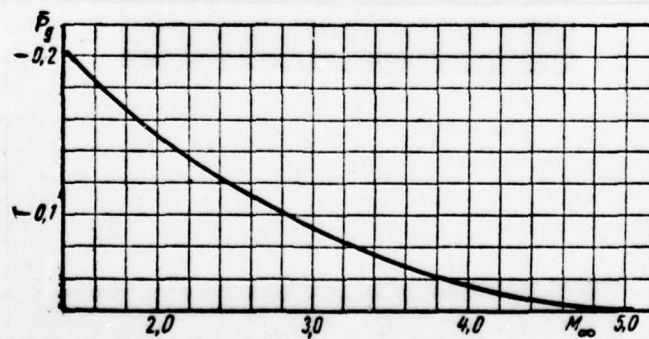


Fig. VIII.44.

Fig. VIII.44. Dependence of base pressure on Mach number

Page 320.

As showed the results of processing numerous experiments, value P_{zon} can be determined depending on Mach number ($M \geq 1.5$) according to the equation, proposed by G. E. Khudyakov (Fig. VIII.44),

$$P_{\text{zon}} = -\frac{1.43}{M^{4.7}} (M^{2.7} - 0.92 M^2 - 0.03).$$

In the extreme case with $M \rightarrow \infty$ this formula gives known value for $P_{\text{zon}} = -\frac{1.43}{M^2}$, which corresponds to vacuum in bottom region.

Total drag of body of revolution at zero or low angle of attack depends on form of body, Mach numbers and Re and state of boundary layer (Fig. VIII.45). The comparison of the drag coefficients of the various forms of the bodies of revolution, and also disk and sphere of Mach number is represented in Fig. VIII.46, but the effect of angle of attack is shown on Fig. VIII.47.

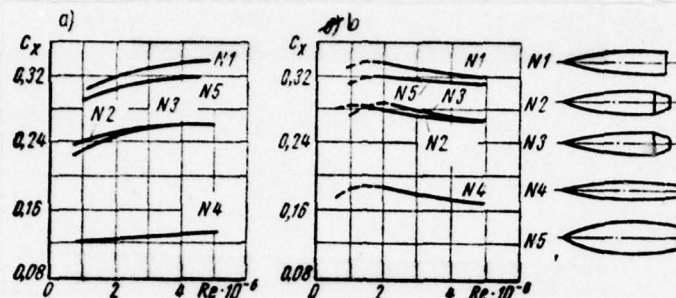


Fig. VIII.45. Dependence of complete drag coefficient on Re number ($M=1.5$): a) laminar flow, b) turbulent flow.

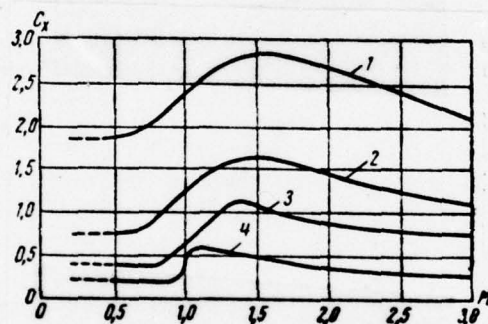


Fig. VIII.46. The comparison of the drag coefficients of different bodies: 1 - disk; 2 - sphere; 3 - the flat-headed shell; 4 - pointed projectile.

Page 321.

For bodies of revolution high value have not only resistance characteristics, but also the lift and the connected with it moment characteristics. In practice in the majority of the cases, the flow

around bodies of revolution occurs asymmetrically, in consequence of which changes the distribution of pressure, appears lift and turning moment (Fig. VIII.48). It is possible to count dependence c_N on α close to form $c_N = 2\alpha$. The same value c_N gives the linearized theory for very fine/thin bodies of revolution. This dependence can be applied also for large Mach numbers.

In a widespread manner of determining the moment coefficient is its calculation:

$$c_m = c_N c_{n,1}$$

where $c_{n,1}$ - a center-of-pressure coefficient.

$$c_{n,1} = \frac{x_{n,1}}{x_b}$$

$x_{n,1}$ - coordinate of point of intersection with resultant of aerodynamic forces with the axle/axis of body.

x_b - length of body.

In the majority of the practical cases, coefficients c_N , c_m and $c_{n,1}$ find on the basis of experimental investigations in wind tunnels or during ballistic installations. The shortened bodies of revolution have more rear center-of-pressure location (to $c_{n,1} = \frac{2}{3}$). If to the nose section of the body of revolution is connected supplementary long section, then center of pressure is displaced to the bottom. During the contraction of cylindrical section, it is shift/sheared

less, while during expansion - it is more. The center-of-pressure location bodies of revolution has high value for the evaluation of their stabilization and especially nose sections of the rockets. Static stability occurs only in such a case, when center of pressure is arranged/located after the center of gravity, i.e., it is nearer to bottom ($x_{n.p.} - x_{n.g.} > 0$).

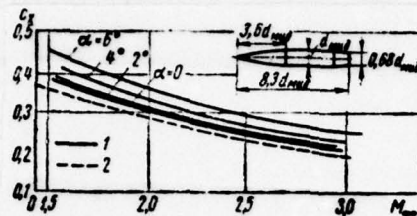


Fig. VIII.47. A change in the complete coefficient c_x body of revolution in dependence on Mach number and angle of attack (turbulent boundary layer): 1 - experimental data; 2 - calculation data.

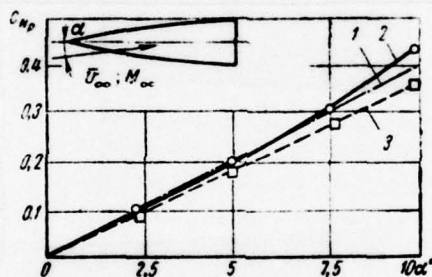


Fig. VIII.48. A change of the coefficient of normal force in dependence on the angle of attack of of $M=5.05$: 1 - calculated curve; 2 - experimental curve when $\lambda_{max}=0$; 3 - the same, when $\lambda_{max}=3$

Page 322.

The stability factor is quantitatively determined by the relationship/ratio

$$Y = \frac{x_{H, R} - x_{H, T}}{x_{H, R}} 100.$$

Usually $Y=8-10\%$.

With the impossibility to attain the necessary stability factor because of the displacement of the center of gravity and nose section, are utilized different aerodynamic methods of stabilization. They include the stabilization with the aid of the tail assembly of body of revolution and the stabilizing "skirts" (Fig. VIII.49). Solid cone, for example static, is unstable, since

$$x_{n,r} = \frac{3}{4}, \text{ a } x_{n,l} = \frac{2}{3}$$

$$Y = \left(\frac{2}{3} - \frac{3}{4} \right) 100 = -$$

$$= -8,34\%.$$

If we extend cone to height/altitude h , then with the insignificant weight of the skirt

$$x_{n,r} = \frac{x_{n,r}}{h} = \frac{3}{4} \cdot \frac{h}{h_1}.$$

If center of pressure is arranged/located at a distance $2/3h$ from point, and the center-of-pressure coefficient is equal to $2/3$, then

$$Y = \frac{2}{3} \left[1 - \frac{9}{8} \left(\frac{h}{h_1} \right) \right] 100.$$

Being assigned $Y=10\%$, we will obtain

$$\frac{h}{h_1} = \frac{8}{9} \left(1 - \frac{3}{2} \cdot \frac{10}{100} \right) = 0,76,$$

i.e. the addition of skirt with size/dimension to $1/4$ cones provides the required stability factor.

Bodies of revolution at hypersonic speeds. The characteristics of friction at hypersonic speeds differ significantly from characteristics with the moderate supersonic ones. This difference is

connected with the properties of the hypersonic flows whose first special feature/peculiarity is caused by large Mach numbers of motion, the second - by high energy of flow.

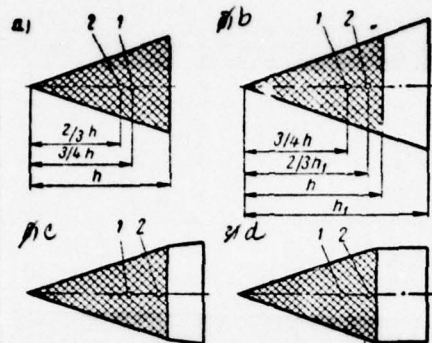


Fig. VIII.49. The diagram of the mutual layout of the center of pressure and center of gravity in conical body with the stabilizing skirt and without it: 1 - center of gravity; 2 - center of pressure.

Page 323.

Large flow mach numbers (or flight) lead to essential slope/inclination and bending of intense shock waves, emergence of the considerable gradients of the parameters of flow (entropy, etc.). Boundary layer on body due to the decrease of density with a temperature rise inflates and is caused the disturbance/perturbation of external (inviscid) flow.

With the high temperatures, caused by braking flow in powerful shock waves, are connected the physicochemical processes at hypersonic speeds. In this case, can be excited the vibrational

degrees of freedom of the molecules, which then dissociate to atoms; can take place the ionization of molecules or free atoms and the education/formation of such molecular or ionic components whose role at low temperatures is insignificant.

At the sufficiently high temperatures of gas, entire the increasing role plays the emission/radiation, calling of energy transfer. Due to the high concentration gradients of different molecular and ionic components essential become the processes of diffusion. Furthermore, during hypersonic flows they can take the place of the phenomenon of interaction of the particles of the gas with body surface. However, the effect of the physicochemical processes indicated usually bears local character (for example, for flow in the nose section of the body) and therefore in many instances the hydrodynamic characteristics of flow they are sufficient ones for evaluating interaction of body and hypersonic flow.

In the examination of the flow around bodies by hypersonic flow one should distinguish flow about the blunted bodies and the pointed bodies. Common/general/total for these types of bodies is the ne-perturbation of flow to certain boundary at very small distance from nose section. Such boundary is the shock wave, which envelopes body and which stretches downstream in the form of the weakly expanded surface.

If body has sufficiently large positive slope/inclination relative to direction of undisturbed flow, then the envelope jump is arranged/located very closely to the surface of body (Fig. VIII.50). The narrow region between this jump and body is called shock layer. In shock layer the temperature, pressure and density of dissociated and ionized gas is considerably more than in the undisturbed flow. If the temperature of the body of the same order as the temperature of the undisturbed flow, then proceeds considerable heat emission from gas to body.

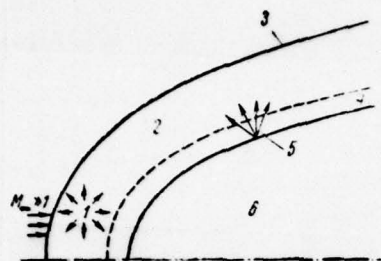


Fig. VIII.50. The hypersonic flow around the blunted nose section of the body: 1 - emission/radiation of the heated gas; 2 - shock layer; 3 - front of the bent shock wave; 4 - boundary layer of gas; 5 - emission/radiation from surface; 6 - body.

Page 324.

In flow behind the bent shock wave, occur the high transverse gradients of entropy.

For slender bodies in hypersonic flow, the velocity in the disturbed region (after jump) changes barely in comparison with the velocity of the undisturbed flow despite the fact that other parameters of flow (pressure, density, temperature, speed of sound ¹ undergo considerable changes ¹.

FOOTNOTE ¹. The speed of sound in the disturbed region about slender

body remains sufficiently small and entire field of flow will be hypersonic. ENDFOOTNOTE.

Especially important in hypersonic flow are conditions near the leading edge/nose of slender body. In practice almost it is not possible to carry out a forward section of the body in the form of ideal point. Moreover localized heating in nose section at hypersonic speeds is so great, that the fine/thin point will be rapidly fused and near this body will appear the same local flow, such as is observed before that blunted, with the which is inherent in it powerful shock wave and the large increase of entropy. Shadow photograph and schematic of the flow around blunted body ($M=3$) are given in Fig. VIII.41.

Numerous theoretical studies of hypersonic flow, which appeared in recent years, consider the flow of nonviscous gas as the flow of continuous medium, and is considered the effect of rarefaction when mean free path of molecules is commensurable with the size/dimensions of body. In the investigations, dedicated to hypersonic flow of nonviscous gas, is assumed number $M_\infty > 1$, body is considered fine/thin, $\sin \theta \ll 1$, here θ - local angle of the surface' slope of body to the direction of the incident flow. The ratio/relation to density to jump ρ_∞ to density after jump ρ_s is accepted as very small - $\epsilon = \frac{\rho_\infty}{\rho_s} < 1$, and jump itself is assumed to be powerful - $M_\infty \sin \theta > 1$.

One of the initial theories of hypersonic flows is called of Newton's theory. It is based on a small density ratio and assumption about the absence of the forces of interaction between the particles of gas, moreover the force of impact of particle about body is accepted as the proportional to the sine of angle of incidence and is directed along the normal to body. Component of this force, which is exhibited in the form of resistance, is proportional to the square of the sine of angle of incidence.

Formula for the pressure, which acts on body under the assumptions indicated, takes the form²

$$p - p_{\infty} = \rho_{\infty} v_{\infty}^2 \sin^2 \theta.$$

FOOTNOTE ². In practice for a comparison with experiment, they frequently use the instituted on experiments "modified formula of Newton"

$$c_p = c_p^* \frac{\sin^2 \theta}{\sin^2 \theta_0}.$$

ENDFOOTNOTE.

Page 325.

This approximation formula gives the possibility to calculate

pressure directly after jump and, strictly speaking, it is valid in the extreme case of the zero density ratio and if we take the form of shock wave will coincide with the form of body. Moreover pressure after jump will be equal to pressure on body, if in the shock layer of particle they will move without acceleration, which occurs for a cone or a wedge at zero angle of attack. During the flow around body with curvilinear duct/contour, must be accepted in attention the fact that in shock layer the particle will move over curved path, and due to the effect of centrifugal forces pressure on body decreases. This correction, introduced by Busemann for pressure taking into account centrifugal forces, leads to Newton - Busemann's formula

$$c_p = \frac{c_p^*}{\sin^2 \theta_0} \left(\sin^2 \theta + \sin \theta \frac{d\theta}{dF} \int_{F_0}^F \cos \theta dF \right),$$

where c_p^* - the value of pressure coefficient at the tip of body which is located in accordance with the theory of the supersonic courses of perfect gas;

θ - angle between the tangent to the duct/contour of body at this point and the direction of the incident flow (for the blunted bodies $\sin \theta_0 = 1$);

F - sectional area of the streamlined body by the plane, normal to the direction of the incident flow.

Especially important value for the bodies, which move with hypersonic speed, have the processes of heat exchange. For the possibility of the successful landing/fitting of spacecraft, rockets and other bodies, which return in the atmosphere, it is necessary their enormous kinetic energy (for example, upon the return of satellite to the earth its kinetic energy per unit mass of equivalent 84000 kcal/kg) to scatter in the form of heat. Since there are not no such materials, which without damages could absorb the significant part of this heat, investigations were directed toward that so that the large part of the energy would go for heating of the surrounding body gas. On these reasons for the problem of heat transfer at hypersonic speeds, they began to occupy the recently prevailing place in theoretical and experimental studies in this region of aeromechanics.

Thermal energy is transferred to body as by the way of thermal conductivity and diffusion in the boundary layer (see Fig. VIII.50), so also by the way of the emission/radiation of the heated gas, which is located in shock layer near the nose section of the body. In turn, the heated surface also emits energy. In the majority of the cases, thermal energy, received by body surface, is absorbed either by sublimation or by of melting and, possibly, evaporating the material of surface, which is accompanied by combustion or dissociation of the particles of the material in the boundary layer of gas.

Page 326.

On these reasons for providing the successful descent of space objects in the atmosphere very important and are the processes both of convective and radiation heat exchange.

The velocity of heat exchange on rigid surface depends in essence on common/general/total enthalpy drop across flow (boundary layer). With inactive surface the velocity of the convective heat exchange in the critical point of the blunted body

$$(q_w) \sqrt{R_0} = A \sqrt{\rho_\infty} v_\infty \left(1 - \frac{h_w}{h_s}\right),$$

where q_w - heat flux to wall;

R_0 - radius of blunting;

v_∞, ρ_∞ - velocity and density of the incident flow;

h_w - value of enthalpy on wall;

h_s - stagnation enthalpy of flow;

A - constant, which depends on the chemical composition of the

incident flow (atmosphere); for earth's atmosphere $A=4710$.

If surface is active, then due to the diffusion of the atoms, which are formed during dissociation to the body surface and their subsequent recombination, which is accompanied by heat liberation, heat fluxes to surface can substantially grow/rise. With an increase in altitude of flight, this special feature/peculiarity is exhibited the more sharply (due to less density diffusion becomes more intense, and recombination in gas phase occur/flow/lasts more slowly). To decrease the heat flux to wall is possible by introduction (injection) to the boundary layer of the chemically active substances which, entering into reaction with gas in boundary layer, absorb the part of the heat.

At the high temperatures, corresponding to the high flight velocities in the sufficiently dense layers of the atmosphere (with descent along abrupt/steep trajectories), important becomes the emission/radiation of the gas, heated in transit through the shock wave. Heat fluxes to body in this case in certain cases can be considerably more than convective ones. Then it is possible to determine in the kilocalories, divided into of 1 m² per second, by the expression

$$\frac{q_{\text{max}}}{R_0} = 12 \left(\frac{p_{\infty}}{p_0} \right)^{1.2} \left(\frac{v_{\infty}}{3250} \right)^{12.5}.$$

Are recently developed various theoretical methods of

determining the parameters of flow near the bodies of various forms, streamlined with hypersonic flow. They give the possibility, in combination with experimental measurements, to determine the aerodynamic characteristics of these bodies under the diverse conditions of motion.

Page 327.

Cone. Pressure on the cone (pressure p_r , referred to static pressure in undisturbed flow p_∞) equal to coefficient wave impedance can be found from approximations (M. F. Krasnova)

$$\bar{P}_r = \frac{p_r}{p_\infty} = \left(\frac{2}{x M_\infty^2} \right) \left(\frac{p_r}{p_\infty} - 1 \right),$$

$$\bar{P}_r M_\infty^2 = c_{x_r} M_\infty^2 = \frac{2(x+1)(x+7)}{(x+3)^2} K^2 \left(1 + \frac{1}{5x} K^{-\frac{2}{3}} \right),$$

when $x=1,4$ $c_{x_r} M_\infty^2 = 2,09 K^2 \left(1 + 0,143 K^{-\frac{2}{3}} \right)$, where $K = M_\infty \beta_r$, here β_r - one-half angle of the solution/opening of cone.

Of infinite Mach numbers the limiting value of pressure coefficient on the cone

$$\bar{P}_r = \frac{2(x+1)(x+7)}{(x+3)^2} K^2,$$

which when $x=1,4$ gives $\bar{P}_r = 2,09 K^2$.

Dependence $\bar{P}_r = c_{x_r} = f(M, \beta_r)$, calculated on the formula indicated, is graphically expressed in Fig. VIII.51.

Newton's theory allows with sufficient for a series of the practical problems accuracy/precision to rate/estimate the aerodynamic characteristics of bodies at hypersonic speeds. So, the excess pressure on cone, which appears as a result of the loss of that part of the momentum which is determined normal component of undisturbed velocity $v_{\infty} \beta_1$:

$$p - p_{\infty} = \rho_{\infty} v_{\infty}^2 \beta_1^2,$$

whence

$$P_1 = 2\beta_1^2,$$

which corresponds to the case when shock wave fits closely to surface. However, in actuality this condition is not satisfied and particles behind shock wave move over the bent trajectories, which leads to the emergence of the centrifugal forces, which decrease the pressure. On the other hand, pressure rise behind shock wave, which occurs during real flow, compensates for the effect of centrifugal forces, and total pressure on body proves to be sufficiently close to that which can be obtained according to Newton's refined theory.

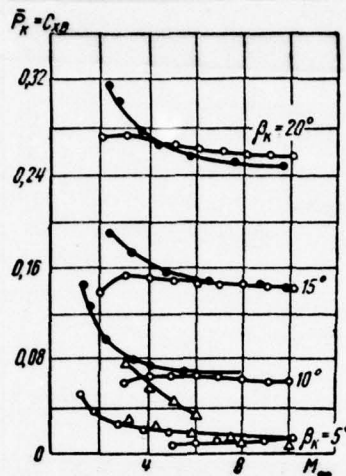


Fig. VIII.51. Curves $c_{x2} = f(M)$ for cones.

Page 328.

Blunted bodies of revolution. The wide application of blunting of bodies during their motion in the atmosphere with high velocities is connected with the fact that these bodies in comparison with those sharpened less are heated and, consequently, also less they are destroyed. In the vicinity of forepart/nose point, the jump is close to straight line, and transition through this jump of the particles of the gas is accompanied by the considerable losses of complete pressure head and an increase in the entropy. At the same time after velocity discontinuity, (but sometimes also density) substantially decreases, grow/rises the extent of laminar boundary layer, decreases

friction, and as a whole heat fluxes from the heated gas to body decrease. On these reasons, investigations of the blunted bodies of various forms devoted considerable number both of theoretical and experimental works.

Figure VIII.52 shows the position of shock waves for a sphere. Figure VIII.53 gives distributing the pressure according to hemispherical leading edge/nose with number $M_\infty = 5.8$. Values $c_x = f(M)$ are given in Fig. VIII.54, and the corresponding characteristics for a flat/plane end/face - in Fig. VIII.55 and VIII.56. The effect of the aperture angle and form of the blunting of cone on the distribution of pressure with $M=6$ on the character of the distribution of pressure is represented in Fig. VII.57, but the comparison of drag coefficients is produced in Fig. VIII.58.

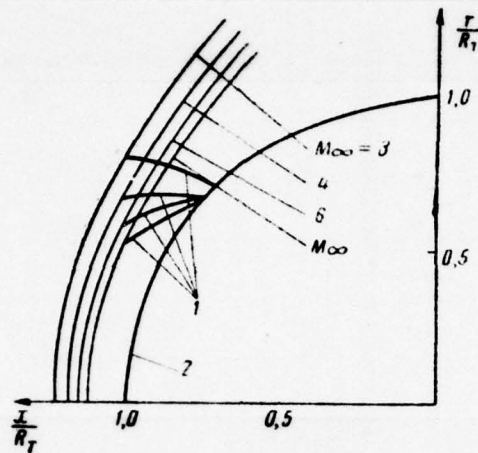


Fig. VIII.52. The shock waves before the sphere: 1 - sonic lines; 2 - sphere.

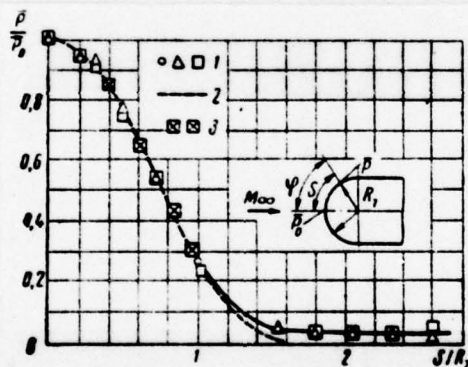


Fig. VIII.53. The distribution of pressure according to surface of hemisphere and adjacent it cylinder: 1 - experimental data; 2 - formula $\frac{p}{p_\infty} = \cos^2 \alpha$; 3 - according to the method of integral relationship/ratios.

Important characteristic during the flow around the blunted bodies is the departure/withdrawal of shock wave. In Fig. VIII.59 is compared the position of shock wave during the flow around bodies with the various forms of blunting. The distribution of pressure for bodies of the type of ellipsoids of revolution is represented in Fig. VIII.60. The blunting of the nose section of the body affects shaping of the boundary layer whose increasing along the length of body thickness has its effect on external inviscid flow. As a result of this interaction, which depends on the number

$$Re = \frac{v_{\infty} \mu_{\infty} D_1}{\mu_{\infty}}$$

and a thermal condition, the pressure on body increases. This effect it is possible to represent to itself as the inviscid flow around the body, increased to the displacement thickness of boundary layer.

The blunting of bodies of revolution has great effect on the physicochemical processes and the thermal phenomena in the vicinity of body, especially in nose section, which in turn, affects the position of the shock wave whose distance from body is changed depending on nonequilibrium.

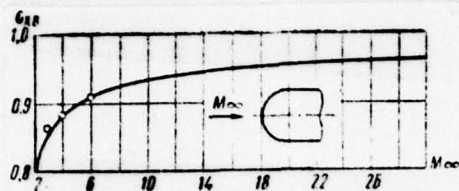


Fig. VIII.54. Values $c_{x0} = f(M)$ for the hemisphere (small circle showed the data of experiment).

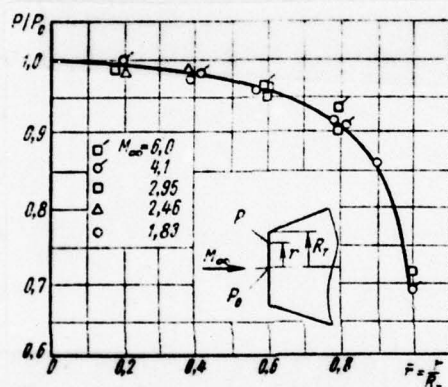


Fig. VIII.55. The distribution of pressure according to the flat/plane end/face (points showed the data of experiment).

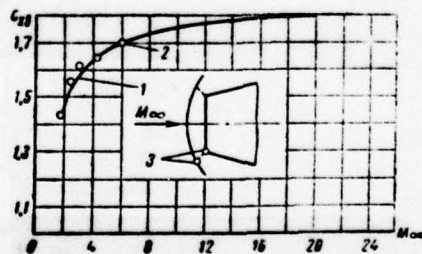


Fig. VIII.56. The coefficient of the wave impedance of the flat/plane end/face: 1 - theoretical calculation; 2 - data of experiment; 3 - sonic points.

Page 330.

Thus, for instance, with the ne-had time to dissociate ("frozen") flow this distance two times more in comparison with that case when chemical reactions behind wave occur rapidly, and dissociation covers entire region between the wave and the body. The temperature in the case of the "frozen" flow in comparison with is equilibrium below approximately to 200/o.

Special importance for the blunted bodies of revolution has friction heat transfer. This is connected with the fact that the pressures and the aerodynamic forces (with exception of stability characteristics) of such bodies play smaller role in connection with the large margins of thrust, required for imparting high velocity the motion. The preservation/retention/maintaining of bodies (for example, spacecraft or Earth satellite) depends in essence on its heat shielding.

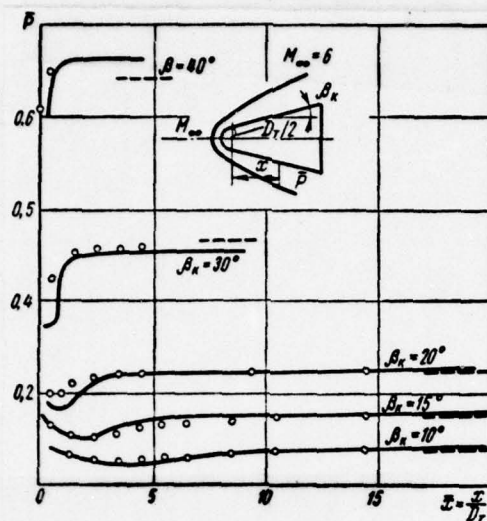


Fig. VIII.57. The distribution of pressure on the blunted according to sphere cone: \circ - experimental data; ---- - according to the theory of acute cone; — - calculation p of "universal" curve.

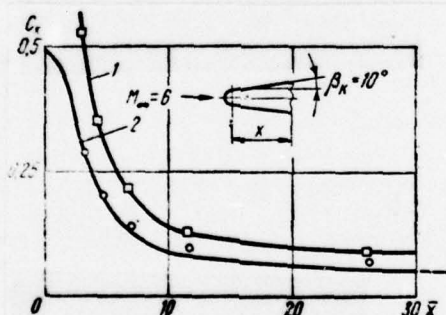


Fig. VIII.58. The coefficient of the wave resistance of blunt-nosed cone and end/face: 1 - end/face; 2 - cone.

Page 331.

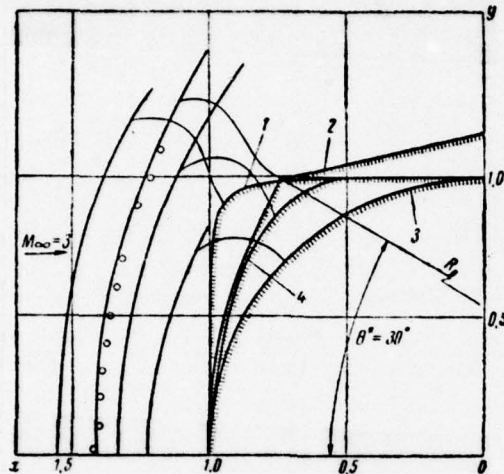


Fig. VIII.59. The departure/withdrawal of shock wave for different bodies (points showed the data of experiment): 1 - end/face with rounding; 2 - segment; 3 - sphere; 4 - ellipsoid $\delta=2$.

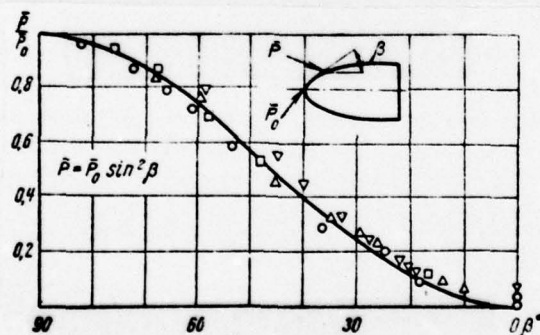


Fig. VIII.60. Distribution of pressure according to the symmetrically streamlined ellipsoid.

Page 332.

The value of heat transfer rates at the critical point of the blunted leading edge/nose can be determined from approximate dependence

$$q_0 = \frac{31500}{\sqrt{R_r}} \sqrt{\frac{\rho_n}{\rho_{\text{sen}}} \left(\frac{v_{\infty}}{7.93} \right)^{3.26}} \left(1 - \frac{i_{cr}}{i_r} \right),$$

where R_r - a radius of sphere, m;

i_r - enthalpy of restoration/reduction ($i_r \approx 0.5v_{\infty}^2$);

i_{cr} - the enthalpy, which corresponds to the temperature of wall ($i_r - i_{cr} = c_{p,cr} (T_r - T_e)$).

Heat fluxes in the forward section of the bodies reach the significant magnitudes. Thus, for instance, for spherical leading edge/nose $R_r = 0.25 \text{ m}$, $H = 30 \text{ km}$, $M_{\infty} = 15$, $T_{cr} = 1000^\circ \text{K}$, $q_0 = 1200 \text{ kcal/m}^2\text{s}$. For end/face ($R_r = 0.5 D_r = 0.25 \text{ m}$, $q_0 = 506 \text{ kcal/m}^2\text{s}$) heat flux is less due to the more intense braking of flow in end/face in comparison with sphere.

Heat-flow distribution in the vicinity of critical point for a sphere is shown on Fig. VIII.61, and the comparison of total heat fluxes for spherical and conical leading edge/noses is given in Fig. VIII.62. It must be noted that the value of heat fluxes affects a

series of supplementary factors. The effect of eddying in the layer, which adjoins the wall, leads to certain increase in the heat fluxes at high altitudes (approximately to 200/o). Radiation flux to surface from the overheated shock layer because air ceases to be transparent, also leads to certain increase in the heat fluxes, which can be estimated in the kilocalories to of 1 m^2 per second according to the empirical expression

$$q_{\text{rad}} = 2,12 \cdot 10^7 R_r \left(\frac{v_\infty}{10^4} \right)^{8,6} \left(\frac{p_{\text{st}}}{p_{\text{seu}}} \right)^{1,6}.$$

For low altitudes this value reaches ~30o/o of aerodynamic heat flux. The diffusion of generatrices as a result of dissociating of atoms and ions in region with their smaller concentration is accompanied by recombination and liberation of supplementary heat.

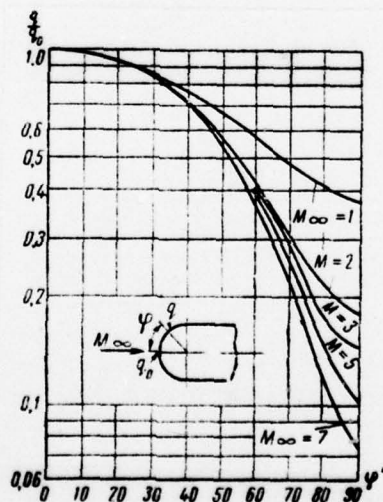


Fig. VIII. 61.

Fig. VIII.61- Distribution of laminar heat flux on sphere with different Mach numbers.

Page 333.

This heat depends, in turn, on a number of circumstances: the flight speed, which decreases the diffusion heat flow, the temperature of the wall whose smallness on the whole impedes the liberation of a large quantity of chemical energy, the chemical activity of surface (catalytic or noncatalytic), of form of nose section, etc.

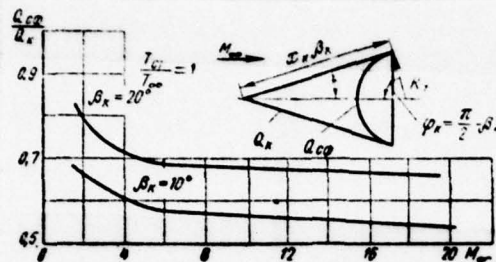


Fig. VIII.62. Comparison of laminar heat fluxes for spherical and conical leading edge/noses.

§VIII.3. Characteristics bluff bodies.

The determination of the wind loads on different industrial and technical constructions, the powers, required for the advance of ground-based transport, and similar problems require the knowledge of the aerodynamic characteristics of the diverse, so-called, bluff bodies.

Autos. In connection with an increase in the velocities of the motion of autos, the power, spent on overcoming by them air resistance, grow/rises proportional to the cube of the velocity:

$$N = \frac{c_x \rho S_{\text{max}} v^3}{2.75}.$$

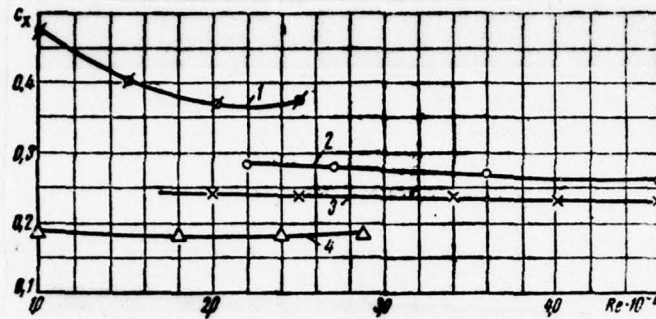


Fig. VIII.63. The drag coefficient of the autos: 1 - bus PAZ-6; 2 - "Moskvich -407"; 3 - "Moskvich-van"; 4 - "Volga- M-21".

Page 834.

The drag coefficient of autos, depending on their form, attains the significant magnitudes (Fig. V.III.63). The distribution of pressure according to the housing of auto is important for the regular arrangement of the air-inlet, cooling and ventilation units and it is also connected with form. In Fig. VIII.64 and VIII.65 given typical distribution of pressure according to the housing of passenger auto and bus.

Trains. In recent years of the velocity of the motion of trains, they reach 200 km/h, and is observed tendency toward their further increase. At such velocities the aerodynamic drag of train comprises more than 50o/o of total resistance. On these reasons the vital importance has a selection of optimum ones, from the point of the view of resistance, aerodynamic shapes.

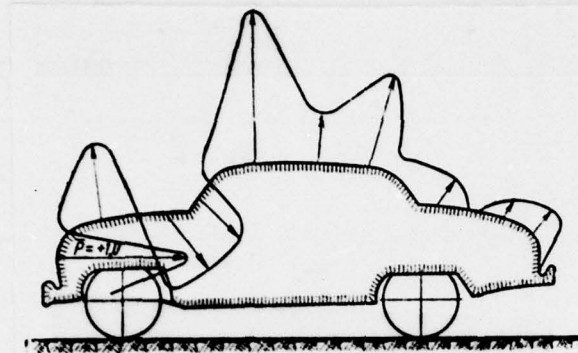


Fig. VIII.64. Distribution of pressure according to the housing of auto.

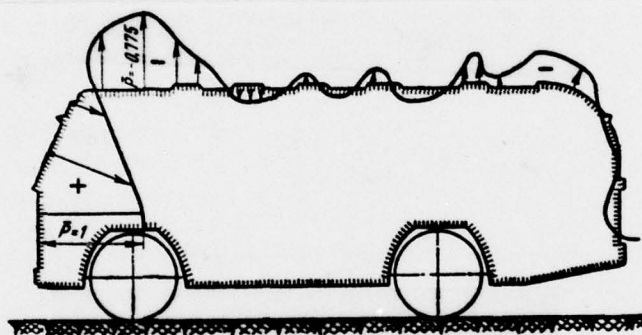


Fig. VIII.65. Distributions of pressure according to the housing of bus.

Page 335.

This selection can be to a considerable degree produced on the basis of experiments in wind tunnels. Figure VIII.66 depicts the dependence of drag coefficient C_x on Re number for the model of car from by

various forms nose section¹.

FOOTNOTE ¹. The given below experimental materials due to aerodynamics of trains are obtained in MGU G. A. Romanenko.

ENDFOOTNOTE.

As can be seen from diagrams, the form of nose section exerts a substantial influence on resistance at high velocities. During transition from one to several cars, the effect of the form of nose section logically decreases, but it remains sufficiently perceived (Fig. VIII.67).

From the point of view of experiment, very important and at the same time complex is the separation of the drag of car into its components, namely: for the resistance of nose, average and tailed section.

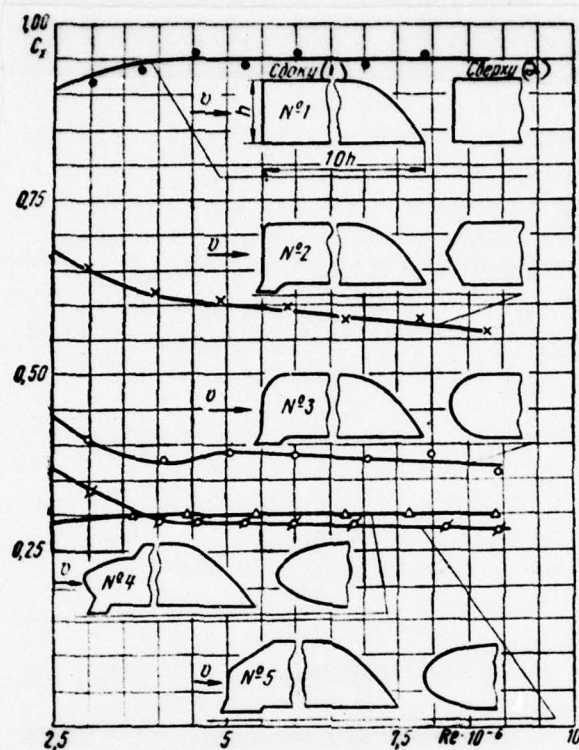


Fig. VIII.66. Dependence $c_x = f(Re)$ for the model of car with various forms of nose section.

Key: (1). On the side. (2). On top.

Page 336.

If we cut car and hang up on weights only nose section and measure its resistance in the presence of the remaining part of the car, then obtained resistance in such a case it only corresponds to true, if is

taken into account pressure in section plane. On these reasons the experiments with the separation of resistance require special thoroughness. In particular, the drainage of section plane must be produced in several radial directions, and the averaging of the measured pressure is carried out on small equivalent area/sites. Furthermore, the necessary condition is convergence of the sum of the divided resistances and total drag with error not more than $\pm 3-5\%$.

Another special feature/peculiarity of experiments with trains - nonobservance of similarity in connection with pentrite, that the screen, which imitates the earth/ground as train in duct, they are motionless, while in nature the earth/ground relative to train "movable". Furthermore, in duct to model usually attacks uniform (on the height/altitude of train) flow, and in nature train is virtually located in surface boundary layer. The carried out by us experiments showed that the effect of the profile of velocity and turbulence of the incident flow on resistance (in particular train) is very considerable.

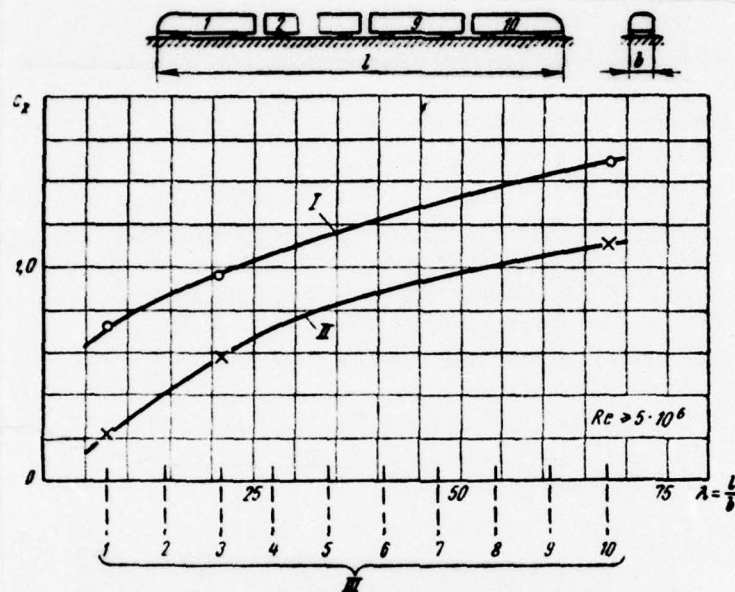


Fig. VIII.67. The effect of a number of cars (elongation) and of form of nose section on the resistance of the model of the train: I - bluff form; II - streamlined shape; III - number of cars.

Page 337.

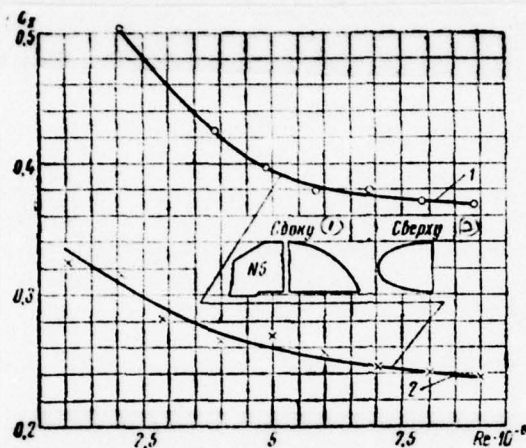


Fig. VIII.68. The effect of superstructures on drag coefficient for the model of single car; 1 - with all superstructures; 2 - without superstructures.

Key: (1). On the side. (2). On top.

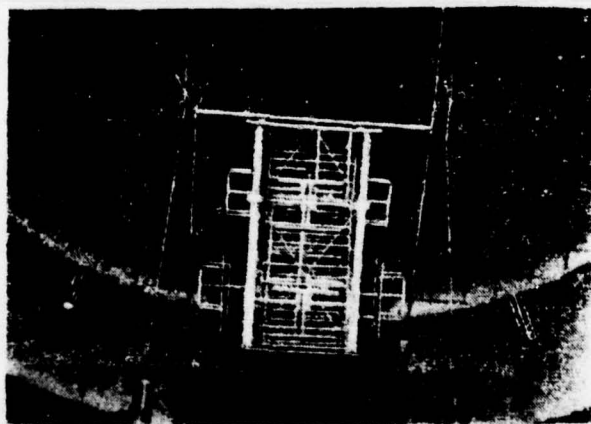


Fig. VIII.69. Antenna in wind tunnel.

Page 338.

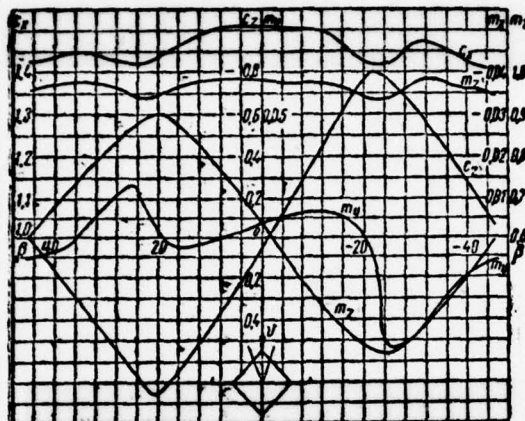


Fig. VIII.70. Aerodynamic characteristics of antenna, shown on Fig. VIII.69.

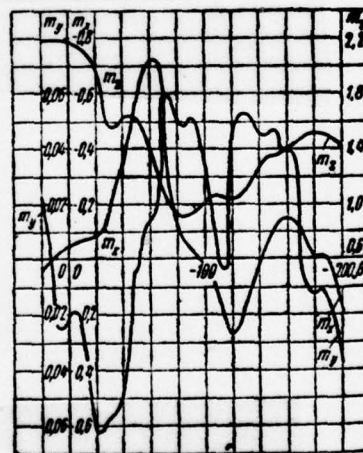
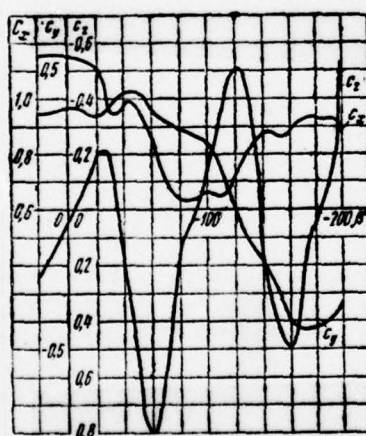


Fig. VIII.71. Aerodynamic characteristics of the antennas of triangular form.

Page 339.

During the investigation of the models of trains, it is necessary to thoroughly simulate fine details (handrails, pantographs, roof superstructures, etc.), which substantially affect aerodynamic drag. As show experiments (Fig. VIII.68), the resistance of different car superstructures composes ~30-40o/o of common/general/total.

Antennas. The widespread introduction of radio, television and radio astronomy led to the appearance of different form of the antenna systems whose size/dimensions they reach enormous values. As can be seen from Fig. VIII.69-VIII.71, on antenna systems act not only considerable forces, but also high torque/moments.

Prismatic beams and shaped airfoil/profiles. Prismatic beams and shaped airfoil/profiles widely are applied in industrial constructions. Dependence $c_x = f(\alpha)$ for the prismatic beam of square section is given in Fig. VIII.72. Greatest values of the drag coefficient of different shaped airfoil/profiles (Fig. VIII.73) following:

Номер про- филя	1	2	3	4	5	6	7
$c_{x \max}$	2,76	2,68	2,08	2,66	1,66	1,76	2,20
$\alpha_{c_{x \max}}$	90°	260°	10°	150°	30°	0°	180°

Key: (1). Number of airfoil/profile.

AD-A066 280

FOREIGN TECHNOLOGY DIV WRIGHT-PATTERSON AFB OHIO
EXPERIMENTAL AEROMECHANICS (SELECTED CHAPTERS), (U)
JAN 79 S M GORLIN

F/G 20/4

UNCLASSIFIED

FTD-ID(RS)T-2011-78

NL

3 OF 4
ADA
066280



The values of the aerodynamic coefficients of some bodies are given below in Table VIII.2. For the comparison of the drag coefficients bluff bodies and bodies with the aerodynamic ideal shapes, let us point out that the coefficients c_x are equal: for fine/thin wings ($\bar{c} = 0,09$), $c_{x_p} = 0,0088$; for streamlined fuselages $c_x = 0,065$; for high-speed aircraft $c_x = 0,016-0,02$.

Construction constructions. The distribution of wind loads on ground-based ones strength can be obtained on the basis of experiments in wind tunnels. Figure VIII.74 shows an example of the distribution of pressure according to building.

In recent years received wide acceptance of various kinds the cylindrical large-size ones capacitance/capacities. Figures VIII.75 and VIII.76 give the photographs of the models, tested in wind tunnel for the distribution of pressure all over surface under the varied conditions of their flow. The results of these experiments are given in Table VIII.3 and VIII.4.

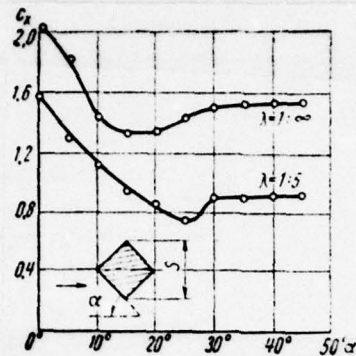


Fig. VIII.72. dependence $c_x = f(\alpha)$ for prismatic beams.

Page 340.

As can be seen from Fig. VIII.77, for such cylinders of the value of numbers Sh , calculated according to diameter, they differ from numbers Sh of the cylinders of the infinite span. For the calculation of pulsations after short cylinders with $Re \geq 1 \cdot 10^4$, it is possible to accept Strouhal numbers, calculated on height/altitude $Sh_h = 0.2$. With the decrease of Re number, a number Sh_h grow/rises to 0.5.

The characteristics of different bodies near screen ("the Earth") differ significantly from their characteristics in the free flow.

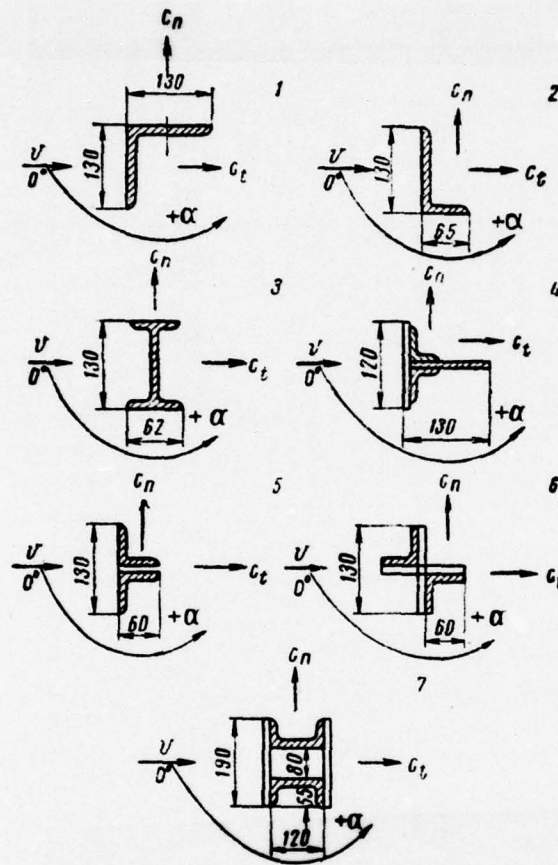


Fig. VIII.73. The shaped airfoil/profiles (number of airfoil/profile is shown by numeral).

Page 341.

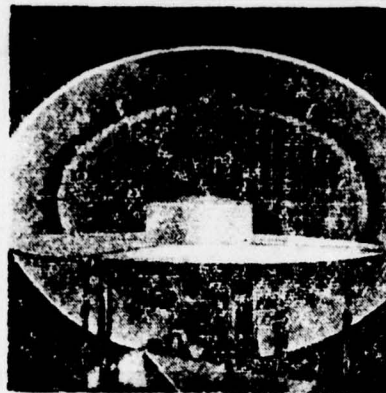
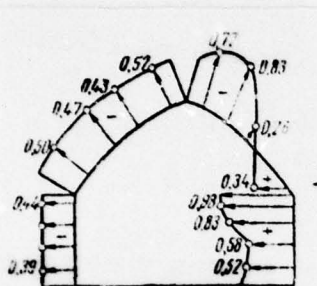


Fig. VIII.74. Distribution of pressure according to building.

Fig. VIII.75. Cylinder testing on screen in duct.



Fig. VIII.76. Group testing of cylinders in duct.

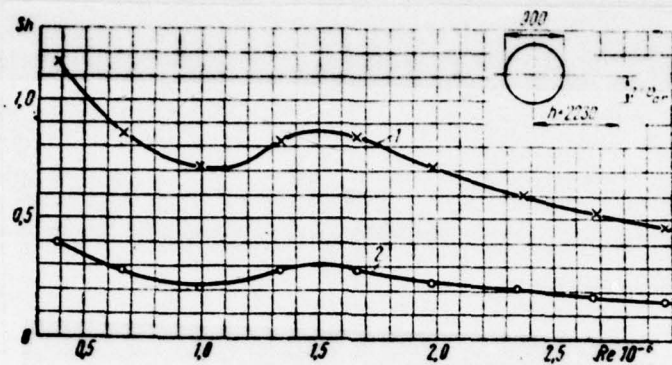
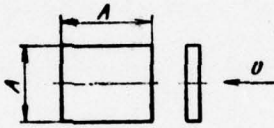
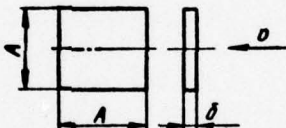
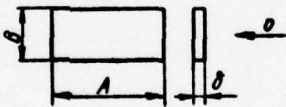


Fig. VIII.77. Dependence $Sh=f(Re)$ for the "short" cylinder, establish/installed on the screen: 1 - Sh is calculated according to the diameter of cylinder; 2 - Sh are calculated on the height/altitude of cylinder.

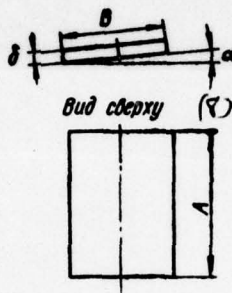
Pages 342-353.

Table VIII.2. Values of aerodynamic coefficients.

(1) Модель	(2) Размеры тела	ϵ_x	Re
(3) Условная плоская пластинка (квадратная)		1,28 (условно) (4)	
(5) Плоская квадратная пластинка		1,15	$6,2 \cdot 10^5$
(6) Плоская прямоугольная пластинка	 $\frac{A}{B} = 2$ $\delta = 5$ $\delta = 10$ $\delta = 30$	1,16 1,20 1,22 1,62	$6 \cdot 10^5$

Continuation table VIII.2.

(1)
Плоская прямоугольная пластинка,
расположенная под углом к напращ-
влению потока



$$\frac{A}{B} = 5$$

$\alpha = 5^\circ$
 $\alpha = 10^\circ$
 $\alpha = 20^\circ$
 $\alpha = 30^\circ$
 $\alpha = 40^\circ$
 $\alpha = 50^\circ$
 $\alpha = 60^\circ$



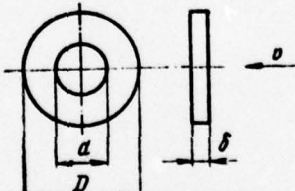

0,05
 0,14
 0,30
 0,50
 0,64
 0,80
 0,90

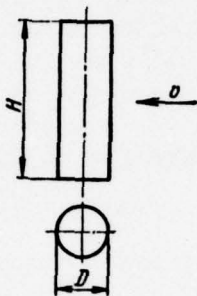
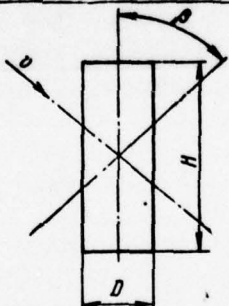
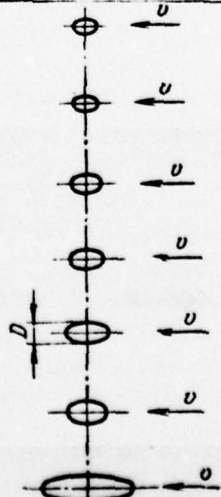
$$\frac{A}{B} = 1$$


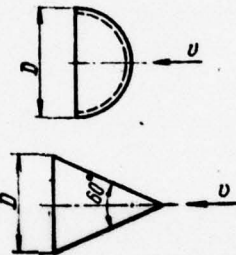
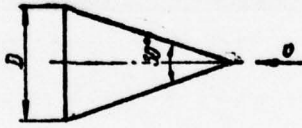
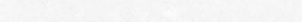


$\alpha = 5^\circ$
 $\alpha = 10^\circ$
 $\alpha = 20^\circ$
 $\alpha = 30^\circ$
 $\alpha = 40^\circ$
 $\alpha = 50^\circ$
 $\alpha = 60^\circ$

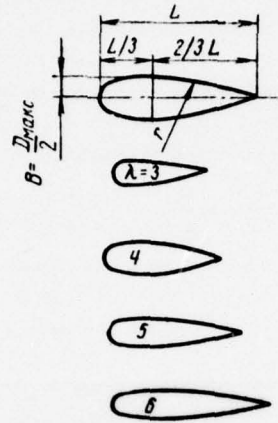
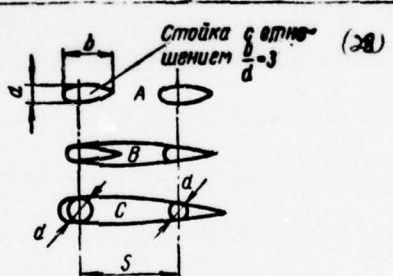
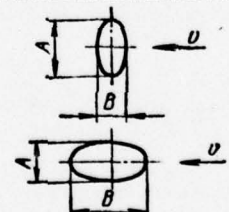
0,04
 0,09
 0,30
 0,70
 1,10
 0,84
 0,98

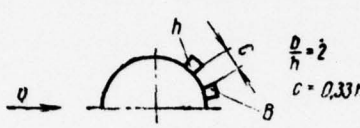
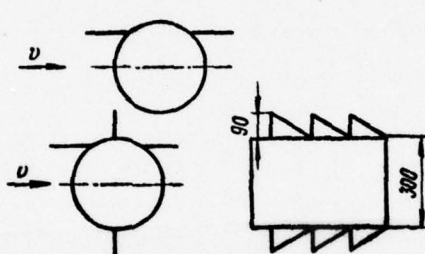
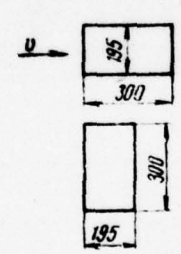
(4)
От $4 \cdot 10^3$ до
 $6 \cdot 10^3$

① Модель	② Размеры тела	ϵ_A	Re
	$\frac{A}{B} = \frac{1}{5}$ $\alpha = 5^\circ$ $\alpha = 10^\circ$ $\alpha = 20^\circ$ $\alpha = 30^\circ$ $\alpha = 40^\circ$ $\alpha = 50^\circ$ $\alpha = 60^\circ$	0,02 0,03 0,17 0,44 0,76 1,04 1,08	
(10) Плоский круглый диск, расположенный нормально к направлению потока	$\frac{\delta}{D} = \frac{1}{100}$ 	1,16	$6,2 \cdot 10^4$
(11) Два плоских круглых диска, расположенных нормально к направлению потока один за другим		(12) Оба вместе 1,16	
	$\frac{L}{D} = 0,5$ $> = 1,0$ $> = 1,5$ $> = 2,0$ $> = 3,0$ $> = 4,5$	$0,97 \cdot 1,16$ $0,84 \cdot 1,16$ $0,73 \cdot 1,16$ $0,96 \cdot 1,16$ $1,40 \cdot 1,16$ $1,90 \cdot 1,16$	
(13) Плоское кольцо, расположенное нормально к направлению потока	 $\frac{d}{D} = 0,2$ $> = 0,4$ $> = 0,6$ $> = 0,8$	1,16 1,20 1,22 1,78	$3,6 \cdot 10^4$
(14) Цилиндр круглый, поставленный осью параллельно скорости потока	 $\frac{H}{D} = 0,5$	1,00	

Модель (1)	(2) Размеры тела	c_x	Re
	$\frac{H}{D} = 0,5$ $\gg = 1,0$ $\gg = 2,0$ $\gg = 4,0$ $\gg = 5,0$ $\gg = 7,0$	1,00 0,84 0,76 0,78 0,80 0,88	
(15) Цилиндр круглый с осью, расположенной перпендикулярно к направлению потока	 $H = D$ $H = 2D$ $H = 5D$ $H = 10D$ $H = 20D$ $H = 40D$	0,64 0,68 0,76 0,80 0,92 0,98	$0,9 \cdot 10^6$
(16) Цилиндр круглый, ось которого направлена под углом к потоку		(17) $c_{x\beta} = c_{x0} \sin 1,225\beta$ c_{x0} — коэффициент сопротивления цилиндра при $(\beta = 0)$ Формула применяется для углов β от 0 до 60°	
(19) Основание эллиптического цилиндра представляет собой сечение круглого цилиндра под углом β_k образующей: $\beta_k = 80^\circ$ $\beta_k = 70^\circ$ $\beta_k = 60^\circ$ $\beta_k = 50^\circ$ $\beta_k = 40^\circ$ $\beta_k = 30^\circ$ $\beta_k = 20^\circ$		0,98 0,96 0,92 0,74 0,62 0,48 0,26	

① Модель	② Размеры тела	c_x	Re
Шар (20)		0,48 0,2	$1 \cdot 10^5$ $5 \cdot 10^6$
Полусфера-чашка (21)		1,44 1,42	$4 \cdot 10^5$ $5 \cdot 10^6$
Полусфера-чашка (27)		0,36 0,34	$4 \cdot 10^5$ $5 \cdot 10^6$
Конус (23)		0,51	$2,7 \cdot 10^5$
То же (23)		0,328	$2,7 \cdot 10^5$
Конус-полусфера (24)		0,16	$1,35 \cdot 10^5$
Полусфера-конус (25)		0,068	$1,35 \cdot 10^5$

Модель (1)	Размеры тела (2)	c_x	Re
Тела вращения (2b)		$0,05-0,1 (\alpha = 0^\circ \div \div 20^\circ)$ $0,05-0,12$ $(\alpha = 0^\circ \div 20^\circ)$ $0,06-0,15$ $(\alpha = 0^\circ \div 20^\circ)$ $0,075-0,18$ $(\alpha = 0^\circ \div 20^\circ)$	4 от $5 \cdot 10^4$ до $6 \cdot 10^5$
Стойка (2a)		$A = 0,16-0,18$ $B = 0,12-0,18$ (для $s/d = 3-12$) $C = 0,08-0,18$	
Проволочка (3b)	$d = 0,23 \div 5,55 \text{ мм}$	$1,1-1,20$	
Эллипсоид (3a)	 $\frac{A}{B} = \frac{1}{0,75}$ $\frac{A}{B} = \frac{1}{0,33}$ $\frac{A}{B} = \frac{1}{1,8}$ $\frac{A}{B} = \frac{1}{3}$	$\begin{cases} 0,60 \\ 0,60 \\ 0,58 \end{cases}$ $\begin{cases} 0,26 \\ 0,10 \\ 0,12 \end{cases}$ $\begin{cases} 0,10 \\ 0,06 \\ 0,08 \end{cases}$ $\begin{cases} 0,07 \\ 0,05 \\ 0,05 \end{cases}$	$\begin{cases} 1 \cdot 10^4 \\ 2 \cdot 10^4 \\ 4 \cdot 10^4 \end{cases}$ $\begin{cases} 1 \cdot 10^4 \\ 2 \cdot 10^4 \\ 4 \cdot 10^4 \end{cases}$ $\begin{cases} 1 \cdot 10^4 \\ 2 \cdot 10^4 \\ 4 \cdot 10^4 \end{cases}$ $\begin{cases} 1 \cdot 10^4 \\ 2 \cdot 10^4 \\ 4 \cdot 10^4 \end{cases}$

Модель (1)	Размеры тела (2)	c_x	Re
(33) Цилиндры ($\lambda = 18$), покрытые шкуркой № 20 ($k/d = 8,25 \cdot 10^{-4}$) № 50 ($k/d = 5,25 \cdot 10^{-4}$) № 80 ($k/d = 1,5 \cdot 10^{-3}$)		1,05 0,95 0,9	$5 \cdot 10^5$ $5 \cdot 10^5$ $5 \cdot 10^5$
(33) Цилиндры, обклеенные рейками		1,05	$5 \cdot 10^5$
(34) Цилиндры с ребрами		0,45 1,35	$0,8 \cdot 10^6$ $0,8 \cdot 10^6$
Балки ($\lambda = 7$) (35)		0,9 1,8	$0,5 \cdot 10^6$ $0,5 \cdot 10^6$
Куб ($\lambda = 1$) (36)		1,05	$8 \cdot 10^5$
Призматическое тело квадратного сечения (37) $\lambda = 3$ $\lambda = 5$		1,2 1,26	$5 \cdot 10^5$ $5 \cdot 10^5$
(38) Автомобиль типа «Москвич-407» Автомобиль типа «Москвич-407», фургон (39) Автомобиль типа «Волга-М-21» (40) Автобус типа ПАЗ-6 (41) Одиночный вагон поезда со всеми надстройками (42) Одиночный вагон поезда без надстроек (43) Одиночный плохо обтекаемый вагон (плоская головная часть) (44) Одиночный хорошо обтекаемый вагон (45) Поезд из десяти вагонов (плоская головная часть) (46) Поезд из десяти вагонов (обтекаемая головная часть) (47)		0,27 0,24 0,17 0,37 0,37 0,24 0,86 0,28 1,5 1,1	$4 \cdot 10^5$ $4 \cdot 10^5$ $3 \cdot 10^5$ $2 \cdot 10^5$ $8 \cdot 10^5$ $8 \cdot 10^5$ $8 \cdot 10^5$ $8 \cdot 10^5$ $5 \cdot 10^5$ $5 \cdot 10^5$

Key: (1). Model. (2). Size/dimensions of body. (3). Conditional flat/plane plate (square). (4). conditionally. (5). Flat/plane square plate. (6). Flat/plane rectangular plate. (7). Flat/plane rectangular plate, arrange/located at angle to flow direction. (8). Top view. (9). From $4 \cdot 10^5$ to $6 \cdot 10^5$. (10). Flat/plane circular disk, arrange/located normal to flow direction. (11). Two flat/plane circular disks, arrange/located it is normal to flow direction one after another. (12). Both instead of. (13). Flat/plane ring, arrange/located normal to flow direction. (14). Cylinder circular, placed by axle/axis in parallel to velocity of flow. (15). Cylinder circular with axle/axis, arrange/located perpendicular to flow direction. (16). Cylinder circular whose axle/axis is directed at angle toward flow. (17). drag coefficient of cylinder of ($\beta=0$). (18). Formula is applied for angles β from 0 to 60° . (19). Basis of elliptical cylinder is section of round cylinder at angle β_k of generatrix. (20). Sphere. (21). hemisphere-cup. (22). housing. (23). The same. (24). cone- hemisphere. (25). hemisphere-cone. (26). Bodies of revolution. (27). Strut. (28). Strut with ratio. (29). for. (30). Thin wire. (31). Ellipsoid. (32). Cylinders ($\lambda=18$), covered with sandpaper. (33). Cylinders, glued round by racks. (34). Cylinders with fin/edges. (35). Beams. (36). Cube. (37). Prismatic body of square section. (38). Auto of type "Moskvich-407". (39). Auto of type "Moskvich-407", van. (40). Auto of type "Volga- M-21". (41). Bus of

type PAZ-6. (42). Single car of train with all superstructures. (43). Single (44). Single bluff car (flat/plane nose section). (45). Single well streamlined car. (46). Train of ten cars (flat/plane nose section). (47). Train of ten cars (streamlined nose section).

Page 354.

Table VIII.3. Greatest values of the coefficients of pressure p of of the flows around short cylinders with the various forms of coating.

(1) Измерение		(2) Сферическое покрытие	(3) Коническое покрытие	(4) Плоское верхнее покрытие	(5) Плоское покрытие, утопленное до середины	(6) Плоское покрытие, утопленное до низа
$\frac{h}{d} = \frac{1}{6}$	На покрытии (7) . . .	-1,5	-1,08	-0,91	-0,57	-0,59
	На боковой поверхности (8) . . .	$\sim +0,92$			+0,96	-0,96
	На внутренней поверхности (9) . . .	—			-0,53	-0,61
$\frac{h}{d} = \frac{1}{3}$	На покрытии (7) . . .	-2,07	-0,93	-0,91	-0,69	-0,69
	На боковой поверхности (8) . . .	$\sim -1,38$			-1,3	-1,3
	На внутренней поверхности (9) . . .	—			-0,76	-0,76

Key: (1). Measurement. (2). Spherical coating. (3). Conical coating. (4). Flat/plane top coat. (5). Flat/plane coating, embedded to middle. (6). Flat/plane coating, embedded to bottom. (7). During coating. (8). On lateral surface. (9). On internal surface.

Table VIII.4. The maximum values of coefficient (\bar{p}) for the models of cylinders, arranged/located on corners of a square (distance between cylinders is equal to their diameter).

(1) Измерение	(2) Передний левый по потоку цилиндр			(3) Задний левый по потоку цилиндр			(4) Задний правый по потоку цилиндр		
	Сечения (5)			Сечения (5)			Сечения (5)		
	I-I	II-II	III-III	I-I	II-II	III-III	I-I	II-II	III-III
(6) Верх $\beta = 7.5^\circ$	-1.39	-0.74	-0.66	-0.53	-0.51	-0.56	-0.52	-0.61	-0.56
Боковая поверхность (7)									
(6) $\beta = 7.5^\circ$	+0.84	-0.59	-0.38	+0.74	-0.65	-0.45	+0.80	-0.82	-0.66
Верх $\beta = 22.5^\circ$	-0.75	-0.52	-0.67	-0.56	-0.60	-0.55	-0.56	-0.53	-0.58
Боковая поверхность (7)									
(6) $\beta = 22.5^\circ$	± 0.58	-0.8	+0.25	± 0.75	-0.72	± 0.27	+0.60	-0.75	± 0.36
Верх $\beta = 37.5^\circ$	-0.88	-0.58	-1.13	-0.55	-0.57	-0.82	-0.55	-0.53	-0.54
Боковая поверхность (7)									
(6) $\beta = 37.5^\circ$	± 0.39	-0.75	+0.75	± 0.33	-0.74	+0.73	-0.25	-0.42	+0.43
Верх $\beta = 52.5^\circ$	-0.64	-0.65	-1.23	-0.58	-0.69	-1.24	-0.54	-0.56	-0.59
Боковая поверхность (7)									
(6) $\beta = 52.5^\circ$	-0.30	-0.50	+0.88	-0.45	-0.60	+0.81	-0.57	-0.62	0.77

Note. Sections I-I, II-II and III-III are arranged/located with $\beta=0$ under angles to flow direction, with respect to the equal ones to 7.5° , by 67.5° and 127.5° .

Key: (1). Measurement. (2). Front/leading left along flow cylinder. (3). Rear left along flow cylinder. (4). Rear right along flow cylinder. (5). Sections. (6). Top. (7). Lateral surface.

Page 355.

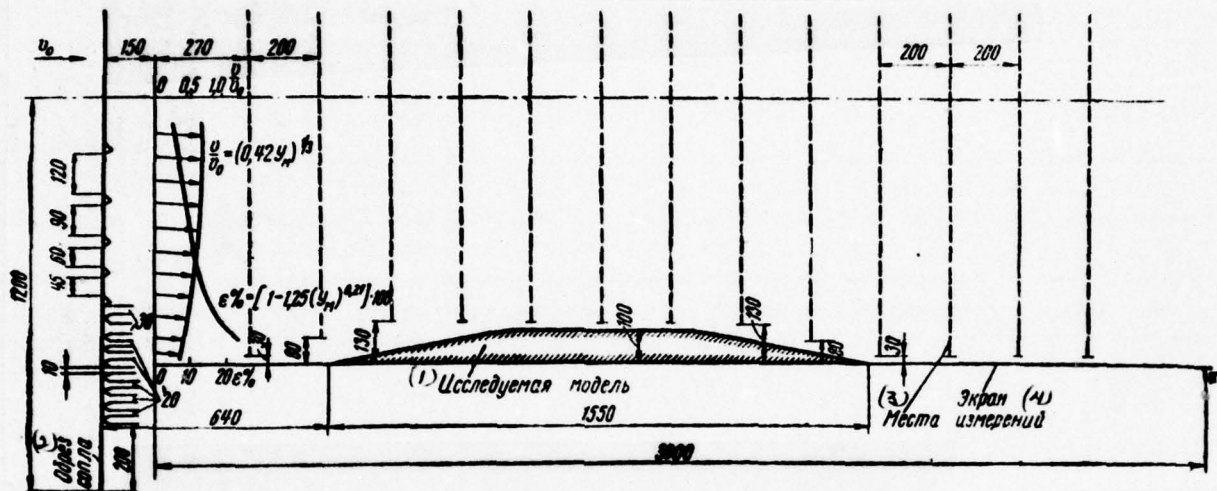


Fig. VIII.78. Diagram of layout of "parasitic" drag for changing in the velocity fields.

Key: (1). The model being investigated. (2). Edge of nozzle. (3). Places. (4). Screen of measurements.

Page 356.

It is especially important to consider this difference for the above-ground structures about which flow in actuality not steady flow, but they are located in surface boundary layer, where the field of velocities and turbulence

$$\frac{du}{dy} \neq 0, \quad \frac{dv}{dy} \neq 0$$

differs significantly from the velocity field in the test section of the duct. However, in wind tunnels for the reconstruction of the variable (on vertical line) field of velocities and turbulence, it is necessary to apply special methods. One of them is installation during nozzle exit section of the specially selected distributed "parasitic" drag (Fig. VIII.78). Figure VIII.79 shows the distribution of the velocities, downwashes and degree of its turbulence in the flat/plane flow around the schematized model of single hill in the wind tunnel of subsonic speeds in the nonuniform incident flow. The characteristics of flow for the case of the uniform and variable velocity field are dissimilar. This fact must be considered during the evaluation of the similarity in of this type investigations.

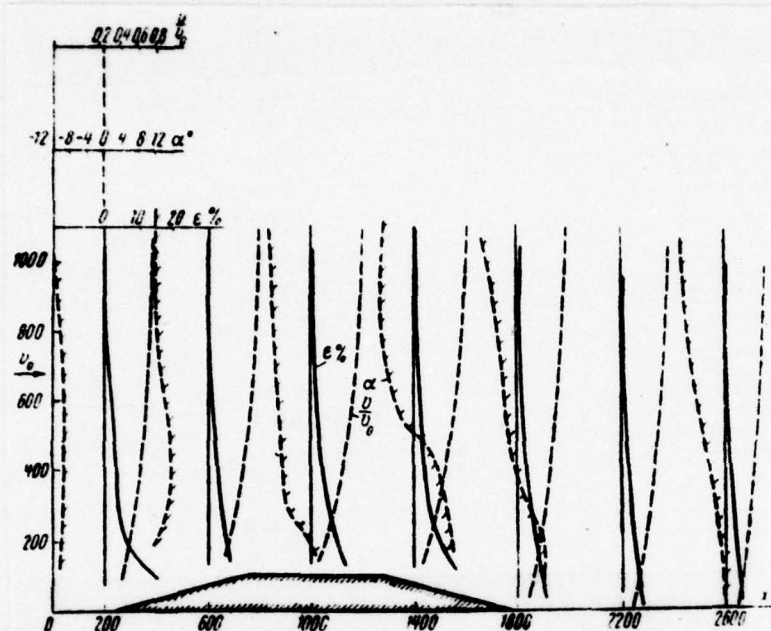


Fig. VIII.79. Stream conditions above of model single hill.

Page 357.

For obtaining different degree of the initial turbulence of flow in test section, it is possible to use Table VIII.5.

Table VIII.5. Dependence of turbulence level on the type of grids.

(1) Устройство на выходном обрезе сопла	(2) Степень турбулентности потока в рабочей части (в %)
(3) Сетка 13 × 13 мм ² (панцирная); δ = 1,9 мм	0,5
(4) Две сетки, наложенные друг на друга, размером 20 × 20 мм ² ; δ = 2 мм	0,85
(5) Две сетки 20 × 20 мм ² ; δ = 2 мм и уголки 12 × 12 мм, установленные через 80—100 мм	5,6
(6) Сетка 13 × 13 мм ² ; δ = 1,9 и уголки 12 × 12 мм, установленные через 35 мм	10

Key: (1). Device on the exit edge of nozzle. (2). Turbulence level of flow in worker they are frequent. (3). Grid 13x13 mm² (armored); δ=1.9 mm. (4). Two grids, superimposed to each other, by size/dimension. (5). Two grids 20x20 mm²; δ=2 mm and angle irons 12x12 mm, establish/installed through 80-100 mm. (6). Grid 13x13 mm²; δ=1.9 and angle irons 12x12 mm, establish/installed through 35 mm.

Page 325.

Chapter IX.

Characteristics of profiles and wings.

IX.1. Characteristics of profiles.

Profile is called the geometric configuration of wing sections. Airfoil/profiles are the basic most widely used cell/elements not only wings, but also all possible flight vehicles, aeromechanical machines and equipment/devices. For this reason to the investigation and creation of the airfoil/profiles of different designation/purpose and for the varied conditions of motion (flow) is devoted the majority of theoretical and experimental works on aerohydrodynamics.

Geometric contours of profile are characterized by the following parameters:

1. Chord. This is the line, connecting two outermost points of

airfoil/profile (internal chord), or lines, drawn tangentially to pressure side of profile and which connects tailed point with the perpendicular, omitted from the tip of airfoil/profile (external chord).

2. Thickness ratio (\bar{c}). Thickness ratio is called the ratio of maximum profile thickness c to chord b . This value usually expresses in the percentages:

$$c\% = \frac{c}{b} \cdot 100.$$

For the contemporary airfoil/profiles \bar{c} , it changes over wide limits (4-200/o) in dependence on designation/purpose and conditions of the flow around airfoil/profile. Thickness distance relative to the leading edge of an airfoil profile

$$x_c\% = \frac{x_c}{b} 100$$

substantially affects aerodynamic characteristics and for contemporary airfoil/profiles oscillates within limits by 30-600/o.

3. Center-line camber of airfoil/profile. If we connect the middles of profile thicknesses in each section (along the normal to chord) then will be obtained the line whose curvature depends on the curvature of upper and pressure sides of profile.

Page 359.

It is called the line of average/mean concavity, or camber line. Center-line camber, or camber, is called the ratio of the maximum bending deflection of center line to the chord:

$$\bar{f}\% = \frac{f}{b} \cdot 100.$$

The position of the maximum center-line camber of airfoil/profile in the portions of chord

$$x_f\% = \frac{x_f}{b} \cdot 100$$

oscillates for contemporary airfoil/profiles within limits of 15-40o/o, and $\bar{f}=0-2-30/o$. For many airfoil/profiles center line is the circular arc or parabola.

4. Completeness of nose section of airfoil/profile. This value is conditionally characterized by the ratio of thickness at a distance to 10/o of chord to maximum profile thickness or by radius of a circle, in which is outlined the leading edge of an airfoil profile.

5. Upper and pressure sides of profile. Upper and lower surfaces are obtained by construction according to a certain law of ordinates of upper and lower surface from the selected middle line of

airfoil/profile $\bar{y}_{cp} = f(\bar{x})$. Usually first is constructed the diagram airfoil/profile of this series (Fig. IX.1) for $\bar{c}=100\%$. the ordinates of this airfoil/profile find from the expressions

$$g_{a, on} = g_{cp} + g_{cnn} \text{ and } g_{a, on} = g_{cp} - g_{cnn}.$$

The coordinates of the airfoil/profile of this series, but another thickness ratio $c\%$ find by the formulas

$$g_a = g_{a, on} \frac{c\%}{100}; \quad g_n = g_{n, on} \frac{c\%}{100}.$$

The various forms of airfoil/profiles for small ones (subsonic speeds) flight are given in Fig. IX.2.

Under aerodynamic characteristics are understood the characteristics of all infinite on spread/scope and identical in profile cross sections virtually of this type of characteristic they obtain by testing either the wing, supported to the walls of duct or testing the rectangular finite-span wing and further recalculation of the obtained results.

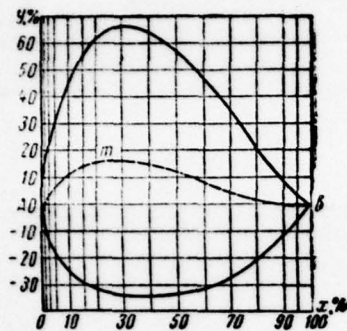


Fig. IX.1. Diagram airfoil/profile.

Page 360.

The dependence of the fundamental aerodynamic characteristics (coefficients) of airfoil/profile on its attitude (angles of attack) is shown on Fig. IX.3 (for a symmetrical airfoil/profile). The angle of attack, of which the lift coefficient attains its maximum value $c_{y_{max}}$ is called critical, while the angle at which $c_y = 0$ (for curved profiles) - zero-lift angle. Under the quality of airfoil/profile (wing) is understood the ratio of lift to drag

$$K = \frac{Y}{Q} = \frac{c_y}{c_x}.$$

The angle of attack, at which the quality is maximal, is called the angle of maximum quality or, in the case of aircraft, by the optimum angle of attack.

Dependences $c_x = f(\alpha)$ and $c_y = f(\alpha)$ can be changed in the form $c_y = f(c_x)$, after locating on this curve the value of angles of attack. This curve, constructed on equal scales, is the locus of the terminuses of the vector of total aerodynamic force c_R or polar diagram with coordinates c_R and $\varphi = \text{arctg} \frac{c_y}{c_x}$.

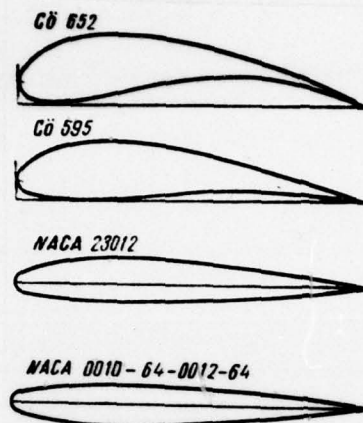


Fig. IX.2. Forms of different airfoil/profiles for subsonic speeds.

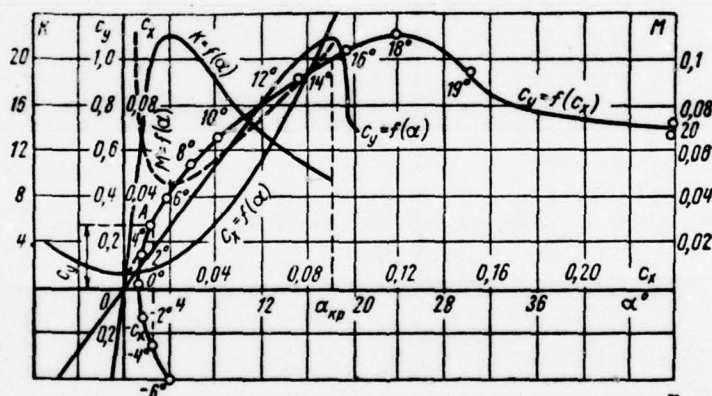


Fig. IX.3. Aerodynamic characteristics of symmetric airfoil/profile.

Page 361.

Angular coordinate ϕ is counted off from polar axis c_x , coinciding with direction velocity of incident flow. Curve $c_y = f(c_x)$ is called by

polar of I kind ¹, or polar (, also, when c_x and c_y they are constructed on different scales).

FOOTNOTE ¹. In contrast to polar of II kind, representing curve $c_y = f(c_x)$, where c_y and c_x - coefficients in body coordinate system. The polar coordinates of this curve will be c_R and $\varphi = \arctg \frac{c_y}{c_x}$. Angular coordinate ϕ is counted off from the polar axis c_x , which coincides with airfoil chord (wing). ENDFOOTNOTE.

During the flow around airfoil/profile, it is possible to disregard the lateral layer Z and torque/moments M_x and M_y and to examine only flat/plane system which is reduced in this case to one total aerodynamic force, which lies at the plane of symmetry. The point of intersection of this force with airfoil chord (wing) is called center of pressure aerodynamic force (Fig. IX.4). Center-of-pressure location in dependence on angle of attack shown on Fig. IX.5. The aerodynamic moment, which acts on airfoil/profile, can be found, calculating the moment of the total aerodynamic force of the relatively selected point (usually the leading edge of an airfoil profile or point, arrange/located from leading edge/nose to $1/4$ chords).

The center-of-pressure location can be determined from the diagram of the forces, which act on airfoil/profile (Fig. IX.6).

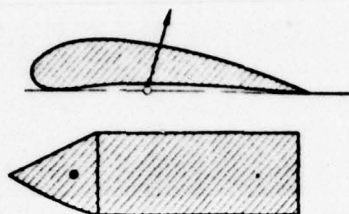


Fig. IX.4. Center of pressure.

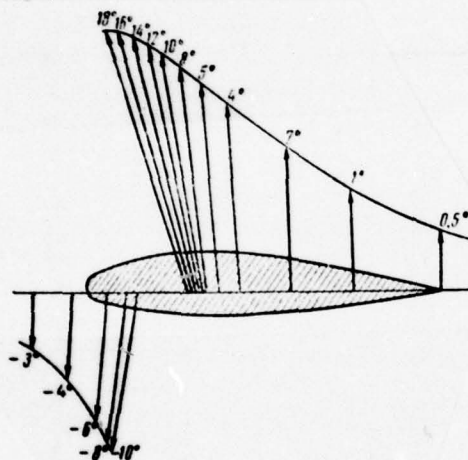


Fig. IX.5. Center-of-pressure location at different angles of attack.

Page 362.

The torque/moment of the normal force Y relative to tip

$$M = -Yc_{pb}$$

where c_{pb} - distance from the point of the application/appendix of

resultant to the moment point O (c_x - center-of-pressure location in chord).

Let us note that component X of total aerodynamic force R of moment with respect to point O does not give. Then moment coefficient

$$m_z = c_m = - \frac{Y c_x b}{\rho \frac{v^2}{2} S b} = - c_y c_x.$$

Torque/moment has negative sign, since it is directed toward dive. The dependence of moment coefficient on the coefficient of lift is represented in Fig. IX.7.

For the linear range of characteristics $c_y = f(\alpha)$ expression for a moment coefficient can be written analytically:

$$c_m = c_{m_0} - m c_y,$$

where m - a slope tangent straight line c_m to axle/axis c_y (it is usually equal to 0.23-0.25).

If we take the moment with respect to of certain point, which lies at a distance x from leading edge, then is moment coefficient

$$c_m = c_{m_0} - m c_y + \frac{x}{b} c_y = c_{m_0} - c_y \left(m - \frac{x}{b} \right).$$

With

$$\frac{x}{b} = m, \quad c_m = c_{m_0}$$

this is correct for all angles of attack, if occurs the even flow of airfoil/profile (wing).

The point, which lies on chord at a distance $x = \bar{x}$ from leading edge, is called focus or aerodynamic center of airfoil/profile (wing) moment coefficient relative to focus is constant and equal to the moment coefficient when $c_y = 0$.

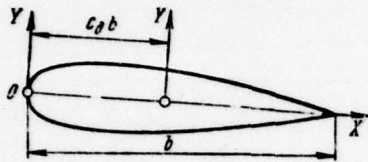


Fig. IX.6.

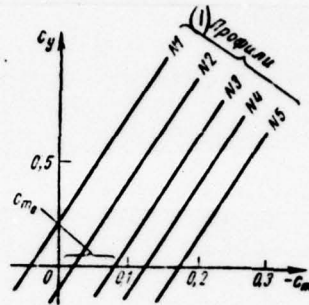


Fig. IX.7.

Fig. IX.6. To the determination of the center-of-pressure location.

Fig. IX.7. Dependence of moment coefficient on lift coefficient.

Key: (1). Airfoil/profiles.

Page 363.

The position of focus can be found by aerodynamic characteristics

$c_l = f(\alpha)$ and $m_z = f(\alpha)$. Regarding we have

$$M\left(\frac{x}{b}\right) = -M_z + Y_x = \text{const}$$

or, having divided by $\frac{\rho v^2}{2} Sb$, we will obtain

$$-m_z + c_l \frac{x}{b} = \text{const.}$$

Having differentiated on α , we find

$$\frac{dm_z}{d\alpha} + \frac{x}{b} \cdot \frac{dc_y}{d\alpha} = 0,$$

whence

$$\frac{x}{b} = x_F = - \frac{\frac{dm_z}{d\alpha}}{\frac{dc_y}{d\alpha}},$$

where the derivatives $\frac{dc_y}{d\alpha}$ and $\frac{dm_z}{d\alpha}$ - rates of change to curves $c_y=f(\alpha)$ and $m_z=f(\alpha)$. Value x_F - is negative, since $dm_z/d\alpha$ - negative, and $dc_y/d\alpha$ - positive. Hence it follows that the mean aerodynamic center of wing is arranged/located on certain distance from leading edge (on the negative part of axle/axis Ox in body coordinate system).

At the low speeds of flight (flow) are favorable the classical airfoil/profiles, which remind the airfoil/profiles of the classical wings (see Fig. IX.2), which possess large lift, considerable negative zero-lift angle, although comparatively high resistance. To air foil data at these speeds substantially affects Re number, since the flow around airfoil/profile in this case depends on the state of boundary layer, and resistance, in essence, from friction. Under these conditions small resistance have airfoil/profiles with the greatest section of laminar boundary layer, whose transition points and also the minimum of pressure are displaced back/aft. However, in such airfoil/profiles value $c_{y_{max}}$ is somewhat less, but their polars

and character curved $c_Y = f(\alpha)$ change in dependence on number Re. Slope/inclination with curve $c_Y = f(\alpha)$ in linear range with change Re it does not virtually change; also does not change zero-lift angle.

With an increase in Re number to numbers $M \sim 0.6$, when compressibility effect yet is not exhibited, are more favorable airfoil/profiles of the type NACA-230 (see Fig. IX.2). They have convexo-convex form with small maximum curvature ($\sim 20^\circ$), arrange/located in the first quarter-chord, smaller resistance and minimum center-of-pressure travel, which makes it possible to more completely control aircraft with this airfoil/profile.

Page 364.

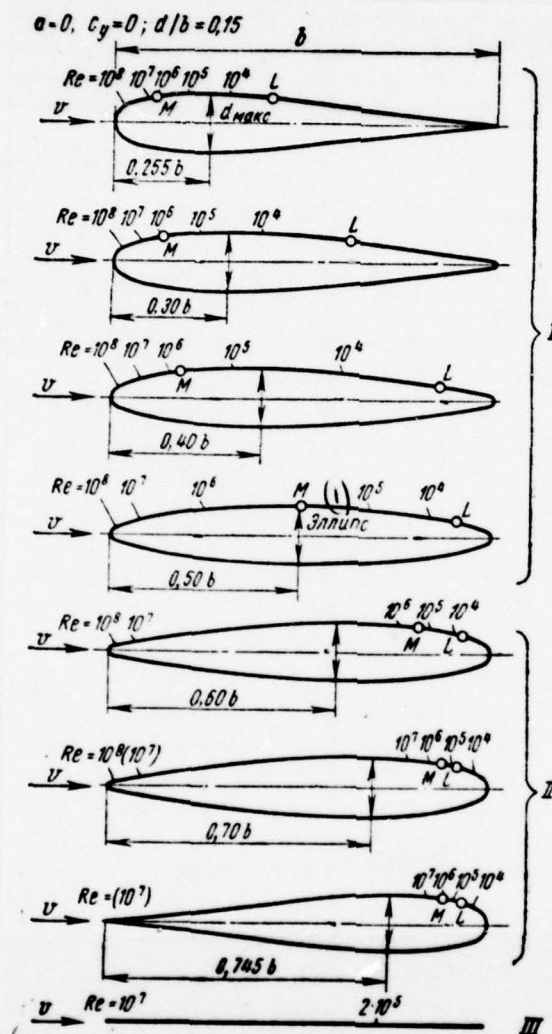


Fig. IX.8. The dependence of the position of transition point from thickness distance for symmetrical airfoil/profiles; I - Zhukovskiy profiles; II - laminar-flows profile; III - smooth plate L- the

separation point of laminar flow (independent of Re); M - maximum speed of irrotational flow.

Key: (1). Ellipse.

Page 365.

At these speeds found use and so-called laminar-flows profile (Fig. IX.8), having as a result of the propagation of the region of laminar flow to the large part of the surface displaced separation point and smaller resistance (Fig. IX.9).

It is necessary to keep in mind that with $M < 0.6$ on high angles of attack the compressibility effect all the same is exhibited. This is connected with a considerable increase in the velocity (by pressure drop) on the nose and upper sections of the airfoil/profile. An example of the combined effect of Re numbers and M on air foil data is shown on Fig. VII.20. With further increase in the velocity even more greatly begins to manifest itself the compressibility effect. Especially sharply it is exhibited during education/formation on the airfoil/profile of regions with supersonic speeds.

When $M < M_{cr}$, resistance remains in effect constant, since it in essence is determined by the frictional resistance which to

insignificant degree depends on compressibility, i.e., on Mach number (friction - function of ductility/toughness/viscosity, but not the compressibility of gas). Lift and connected with it torque/moment somewhat grow/rise since local evacuation/rarefactions by the upper surface of airfoil/profile they increase. During the approach/approximation of Mach number to M_{sp} and the flow pattern of airfoil/profile significantly changes. The number M_{sp} , with which on airfoil/profile appears the speed, equal to the local velocity of sound, it is connected with the form of airfoil/profile, its angle of attack and is virtually unambiguously determined by the value of minimum evacuation/rarefaction on its surface. This is connected with the fact that due to compressibility effect the local velocities on airfoil/profile increase faster than velocity of incident flow.

For the compressible gas $\rho_2 < \rho_1$ (see Fig. IV.33) the velocities in section II are more than in section I. With an increase in the velocity of incident flow, the velocity in section II grow/rises more intensely than in section I. The incidence/drop in the density in section II, which depends on absolute velocity, is more than in section I. From the condition of the preservation/retention/maintaining of the constancy of expenditure/consumption along the streams of the velocity in section II, they must increase even additionally in order to compensate for a larger incidence/drop in the density in this section.

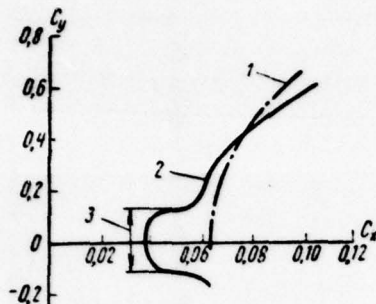


Fig. IX.9. The polar of laminar-flow profile: 1 - airfoil/profile NACA 0010; 2 - laminar-flow profile; 3 - region of laminar flow.

Page 366.

At the subcritical velocities (to numbers $M < M_{kp}$) aerodynamic forces at constant angle of attack grow/rise, according to Prandtl and Glauert, with an increase in the velocity (Mach number) is approximately proportional $\frac{1}{\sqrt{1-M^2}}$:

$$P_M = \frac{P_{\text{неск}}}{\sqrt{1-M^2}} \quad \nearrow 1$$

$$C_{Y_M} = \frac{C_{Y_{\text{неск}}}}{\sqrt{1-M^2}} \quad \nearrow 2$$

$$C_{m_M} = \frac{C_{m_{\text{неск}}}}{\sqrt{1-M^2}}.$$

FOOTNOTE 1. Somewhat more precise dependence gives Karman - Tzyan formula

$$P_M = \frac{P_{\text{неск}}}{\sqrt{1-M^2} + \frac{M^2}{1+\sqrt{1-M^2}} \frac{P_{\text{неск}}}{2}}.$$

2. More precise value gives S. A. Khristianovich theory, according to whom

$$c_{YM} = \frac{c_{Y \text{ неск}}}{\sqrt{1-M^2}} K; \left(\frac{\partial c_Y}{\partial \alpha} \right)_M = \left(\frac{\partial c_Y}{\partial \alpha} \right)_{\text{неск}} \cdot \frac{K}{\sqrt{1-M^2}},$$

where $K = 1 + \frac{0,05}{M_{\text{кр}}^2} M^2$ - function of angle of attack, thickness ratio of velocity of flow (Fig. IX.10, in which parameter $\bar{c}_x = \bar{c} + 0,17 P$).

ENDFOOTNOTE.

Drag coefficient does not virtually change.

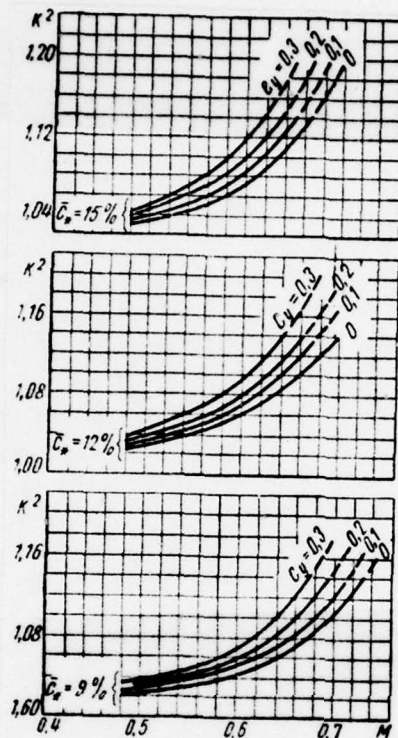
The degree of approximation of these dependences lies in the fact that they assume change \bar{P} on all airfoil/profile into an identical number once $\left(\frac{1}{\sqrt{1-M^2}} \right)$. In reality large evacuation/rarefactions (corresponding high velocities on airfoil/profile) will increase with an increase in the number of incident flow more rapid than it is smaller.

For the contemporary theory of the flow around winged airfoil/profile at high subsonic speeds it makes it possible to more accurately determine an increase in local rarefactions \bar{P} depending on

DOC = 78201107

PAGE ~~26~~ 228

Mach number, and to also refine calculation M_{sp} .

Fig. IX.10. Curve/graph for determining value K .

Page 367.

The latter is especially important, since the beginning of a sharp adverse change in all aerodynamic characteristics occurs directly on achievement $M_{кр}$. On these reasons during the creation of airfoil/profiles for high subsonic speeds, they attempt because of the form of airfoil/profile to obtain at low speeds such distribution of pressure, by which there would not be the local peaks of

evacuation/rarefaction (usually on upper surface), exceeding critical pressure. Value p_{kp} can be found from the expressions

$$\frac{p_1}{p} = \left(\frac{1 + \frac{\kappa-1}{2} M^2}{\frac{\kappa+1}{2}} \right)^{\frac{\kappa}{\kappa-1}},$$

$$q = \frac{1}{2} \rho v^2 = \frac{\kappa p}{2} \frac{\kappa^2}{\kappa p} = \frac{\kappa p}{2} M^2,$$

whence

$$p = \frac{p_1 - p}{q} = \frac{p_1 - p}{p} \cdot \frac{2}{\kappa M^2}$$

or

$$p_{krit} = \frac{2}{\kappa M_{kp}^2} \left[\left(\frac{2}{\kappa+1} + \frac{\kappa-1}{\kappa+1} M_{kp}^2 \right)^{\frac{\kappa}{\kappa-1}} - 1 \right].$$

Here M_{kp} - Mach number of the incident flow, with which on airfoil/profile is reached the local velocity of sound. Value M_{kp} depending on $p_{несж, min}$ can be found from expression for p_{kp} and dependence $p_n = f(p_{несж})$. The dependence M_{kp} on minimum evacuation/rarefaction on airfoil/profile is given in Fig. IV.36. The character of the distribution of pressure on the contemporary airfoil/profile, intended for high subsonic speeds, it is shown on Fig. IV.32.

As can be seen from Fig. IX.11, with an increase in the thickness ratio, decreases M_{kp} and increases resistance both on small ones and, especially, at the velocities of appropriate $M > M_{kp}$.

moreover small resistance have airfoil/profiles with the location of maximum thickness approximately to 40% of chord ¹.

FOOTNOTE ¹. For determining the increase in resistance at subcritical velocities, it is convenient to use the method of A. A. Drodnitsin and L. G. Loytsyanskiy, namely by the expressions:

$$c_{X_{p. n}} = c_{X_{несж}} \eta_n; \quad c_{X_{p. несж}} = 0.9252 c_t \eta_c,$$

where $c_t = f(Re, \bar{x}_t)$ and $\eta_c = f(c, \bar{x}_t)$. Value η_n depends on Mach number, thickness ratio and position of transition point. ENDFOOTNOTE.

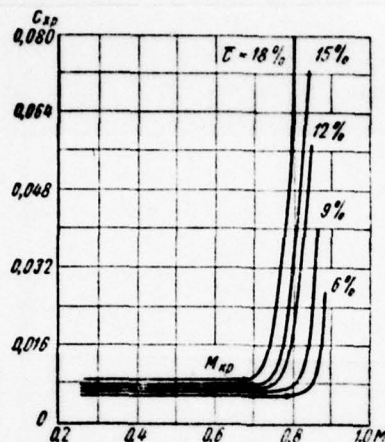


Fig. IX.11. Effect of thickness ratio on dependence $c_{xp} = f(M)$ when $c_y = 0$

Page 368.

The curve/graph, given in Fig. IX.12, shows that when $c_y = 0$ least resistance have the symmetrical airfoil/profiles (curvature 0), and with $c_y > 0$ the best is the curvature of order 20/o.

Compressibility exerts a substantial influence on lift coefficient and slope/inclination curve $c_y = f(\alpha)$ (Fig. IX.13) and a change in the moment coefficients. A change in the torque/moment due to compressibility effect can be found from the expression

$$C_{mZM} = \frac{C_{mZ\text{нечк}}}{\sqrt{1-M^2}} K^2;$$

$$\left(\frac{dc_m}{d\alpha}\right)_M = \left(\frac{dc_m}{d\alpha}\right)_{\text{нечк}} \frac{K}{\sqrt{1-M^2}}.$$

A change of position of center of pressure in compressible flow

$$x_{\text{ц.п. чк}} = x_{\text{ц.п. нечк}} K \quad \text{or}$$

$$x_{\text{ц.п. чк}} = \left(\frac{m_z}{c_y} + x_p\right) K,$$

shows that in the range of Mach numbers in question the center of pressure is displaced back/ago.

The amount of center-of-pressure travel (Fig. IX.14) can be rate/estimated from relationship/ratio Ya. M. Serebriyskiy

$$\Delta x_{\text{ц.п.}} = \frac{m_z}{c_y} \cdot \frac{(1 + 0.2 M^2)^2}{\sqrt{1-M^2}} - 1 = \frac{m_z}{c_y} B.$$

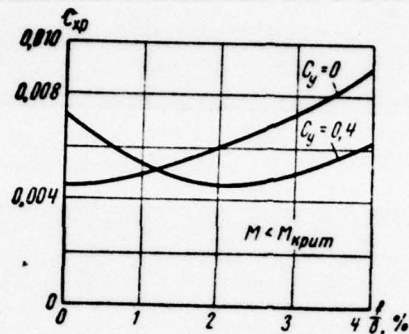


Fig. IX.12. Dependence of the drag coefficient on camber when $M < M_{krup}$

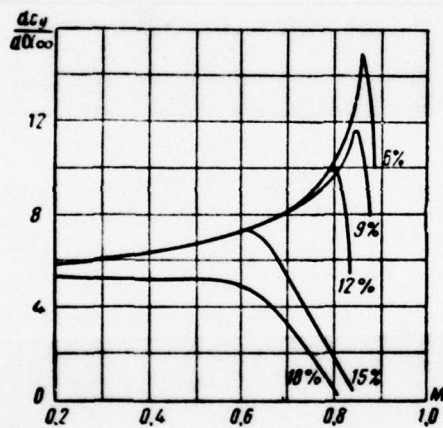


Fig. IX.13.

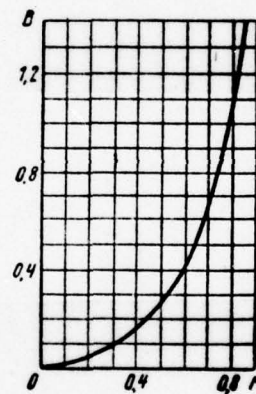


Fig. IX.14.

Fig. IX.13. Effect of thickness ratio on $\left(\frac{\partial C_y}{\partial \alpha}\right)_\infty$ when $C_y = 0$

Fig. IX.14. To the determination of center-of-pressure travel.

Surface condition of airfoil/profile, especially in its forward section, affects the resistance and at high velocities (Fig. IX.15); therefore it is necessary to attempt to fulfill the surface of airfoil/profile as far as possible smoother.

The geometric form of the airfoil/profiles, intended for motion with high velocities, is characterized by small thickness ratio (to 10-12o/o) with the maximum, delayed by 40-50o/o of chord, by small curvature of center line (less than 2o/o) with the apex/vertex, arranged/located to 40-50o/o of chord, by a small radius of nose section, by a smooth surface. In particular, symmetrical airfoil/profiles are some of the best in the velocity band indicated.

In supercritical zone ($M > M_{kp}$) and at transonic speeds of air foil data undergo the abrupt changes. Those appearing on the airfoil/profile of shock wave (shock waves) change the character of the distribution of the pressure (see Fig. IV.32) and is caused supplementary resistance (Fig. IX.16), which intensely it builds up with an increase in the value ($M - M_{kp}$).

If at the subcritical velocities the evacuation/rarefaction in the forward part of the airfoil/profile, which pulls it forward, is a

little less than the evacuation/rarefaction on the rear end of the airfoil/profile, pulling it back/ago, and drag resistance as a result of this was small, then at hypercritical velocities evacuation/rarefaction on the front of the airfoil/profile decreases (pressure increases), and on tailed, because of the appearance of a supersonic zone, it increases (pressure falls). Thus, the forces, which pull airfoil/profile back/ago, strongly increase and appears considerable resistance (because of pressure difference). This resistance is called wave. The value of wave impedance, according to the experimental investigations

$$\Delta c_{x_{\text{волн}}} = A (M - M_{\text{кр}})^3,$$

where A - coefficient, depending on the form of airfoil/profile and angle of attack ($A=8-12$, the average value $A=11$).

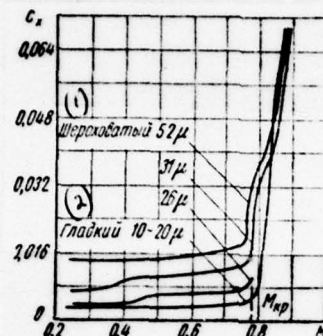


Fig. IX.15. Effect of roughness on $c_x = f(M)$ (airfoil/profile NACA - 0-00-12; $c_y = 0$)

Key: (1). Rough. (2). Smooth.

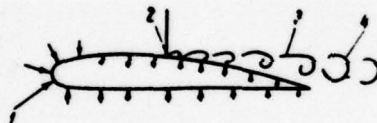


Fig. IX.16. The drag-rise characteristics of pressure after shock stall: 1 - pressure on spout creates resistance; 2 - shock wave; 3 - loss of the balancing thrust on tail; 4 - breakaway.

Page 370.

Experimentally establish/install, that the value of coefficient A is more in those airfoil/profiles, in which is more the value M_{sp} . This means that tightened shock stall in similar airfoil/profiles subsequently (when $M > M_{sp}$) is exhibited in a violent

increase in the wave impedance.

Lift coefficient c_y (to $M = M_{kp}$) somewhat grow/rises because of an increase in the evacuation/rarefaction on upper surface, and then it begins to fall (especially for thick airfoil/profiles), that connected with the education/formation of supersonic zone and increase in the evacuation/rarefaction on lower surface (Fig. IX.17). With further increase in Mach number, the jump on lower surface is rapidly moved back/ago and lift sharply falls, and center of pressure is displaced in direction to leading edge and proves to be sometimes even in front of the airfoil/profile. The consequence of this is the appearance of the destabilizing pitching up torque/moments.

A change in the moment coefficients and center-of-pressure travel in the range $M=0.8-0.9$ adversely affects the longitudinal stability of wing which can be provided via the selection of the rational form of airfoil/profile.

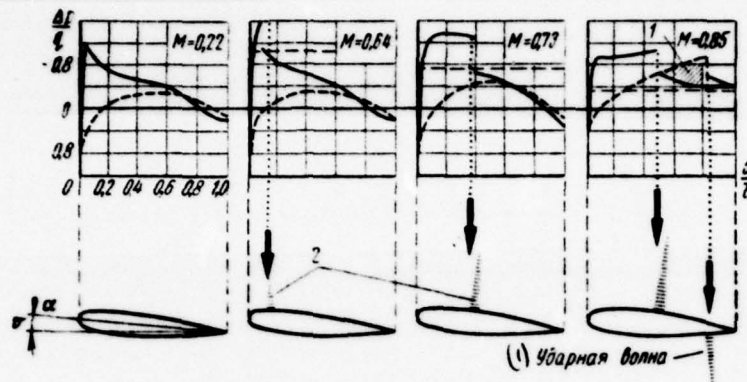


Fig. IX.17. Profile pressure distribution with different Mach numbers (airfoil/profile NACA-0-00-15, $\alpha=4.2^\circ$): 1 - negative lift; 2 - shock wave; - - upper side; - - - lower side.

Key: (1). Shock wave.

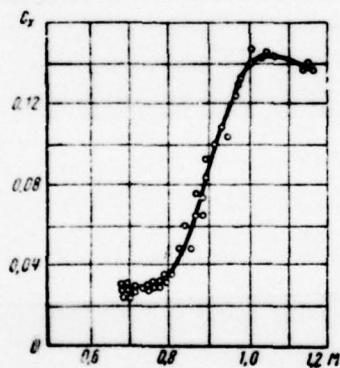


Fig. IX.18. $c_x = f(M)$ for an airfoil/profile in transonic range.

An incidence/drop in the drag coefficient c_x (Fig. IX.18) after its greatest value with $M \sim 1$ is explained by the fact that the extent of the jump before the airfoil/profile in area of critical point decreases, and in distance from it, jump becomes oblique, which decreases the wave losses. At supersonic speeds of flow, the flow around airfoil/profile is connected with the basic properties of such flows.

Flows at supersonic speeds, as was shown in § IV.3, depending on shape of surface, about the which flows the flow, there are two forms: compression and expansion. On the basis of their examination was constructed by Ackeret the theory of the flow around airfoil/profile (infinite-span wing) in the supersonic flow. This theory is valid for low angles of attack ¹ and with the connected head and tailed shock waves.

FOOTNOTE ¹. Leading and trailing edges must be sharp ones, thickness ratio - small. ENDFOOTNOTE.

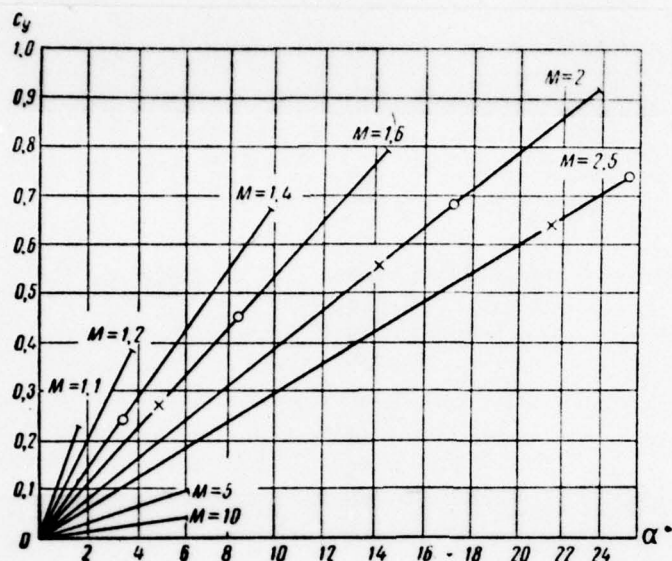


Fig. IX.19. Dependence $c_y = f(\alpha)$ for symmetrical airfoil/profiles with different Mach numbers.

Page 372.

According to Ackeret's theory

$$c_x = \frac{4\alpha^2}{\sqrt{M^2 - 1}}; \quad c_y = \frac{4\alpha}{\sqrt{M^2 - 1}};$$

the slope/inclination of curves $c_y = f(\alpha)$

$$\frac{dc_y}{d\alpha} = \frac{4}{\sqrt{M^2 - 1}},$$

from which it is evident that from an increase in Mach number the slope/inclination curved $c_y = f(\alpha)$ falls (Fig. IX.19).

From expression for c_x it is evident that at supersonic speeds even in the absence of friction, occurs the considerable wave impedance. The lift-drag ratio of airfoil/profile $K = \frac{c_y}{c_x} = \frac{1}{\alpha}$ in the supersonic flow does not depend on Mach number.

More precise values of airfoil characteristics gives the Buzeman theory according to which a change in the pressure (pressure increment Δp) from the local slope/inclination of airfoil/profile is connected by the expression

$$\frac{\Delta p}{\frac{1}{2} \rho v^2} = c_1 \beta + c_2 \beta^2 + c_3 \beta^3 + c_4 \beta^4 + \dots + c_n \beta^n,$$

where $c_1, c_2, c_3, c_4, \dots, c_n$ - functions of Mach number;

β - angle, formed by tangent to the duct/contour of airfoil/profile at the particular point with direction of undisturbed flow.

For routine calculations it suffices to be restricted by one or two members of a series. The values of the Buzeman coefficients are given in table IX.1.

The moment coefficient of symmetrical supersonic

airfoil/profiles, in reference to leading edge, does not depend on the form of the airfoil/profile:

$$m_z = \alpha = \frac{2}{\sqrt{M^2 - 1}} \alpha.$$

Table IX.1. Values of Busemann's coefficients ($\alpha = 1.4$)

M	c_1	c_2	c_3
1.1	4.864	30.32	568.98
1.2	3.015	8.307	54.034
1.3	2.408	4.300	14.247
1.4	2.041	2.919	5.801
1.5	1.798	2.288	3.059
1.6	1.601	1.950	1.937
1.7	1.455	1.748	1.4109
1.8	1.336	1.618	1.1444
1.9	1.238	1.529	1.0050
2.0	1.155	1.467	0.9341
2.2	1.021	1.386	0.8946
2.4	0.9167	1.337	0.91921
2.5	0.8728	1.320	0.94322
2.6	0.8333	1.306	0.97189
2.8	0.7647	1.284	1.0382
3.0	0.7071	1.269	1.1116
3.5	0.5963	1.245	1.3090
4.0	0.5164	1.232	1.5132
4.5	0.4559	1.224	1.584
5.0	0.4082	1.219	1.9250

Page 373.

The center-of-pressure location can be found from the expression

$$\frac{x_{n.z}}{b} = \frac{m_z}{c_y} = \frac{c\alpha}{2c\alpha} = \frac{1}{2}.$$

Hence it is apparent that the center of pressure for all symmetrical supersonic airfoil/profiles lie/rests at the middle of chord, which is aerodynamic focus. In curved profiles the moments with respect to focus are not equal to zero due to different pressure stroke on lower and upper surfaces (Fig. IX.20).

At supersonic speeds are applied the airfoil/profiles of various form: convexo-convex, rhomboid, wedge-shaped and mixel. Fine/thin flat/plane plate from an aerodynamic point of view is the advantageous, but due to its ne-constructiveness it cannot be used in real flight vehicles. Comparative values of aerodynamic characteristics of the various kinds of supersonic airfoil/profiles are given below in table IX.2 and in Fig. IX.21.

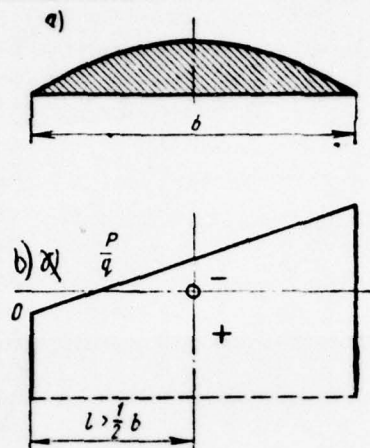


Fig. IX.20. The schematic representation of the distribution of pressures along the chord of curved profile at supersonic speeds (small circle showed the center of gravity): a) airfoil/profile; b) the distribution of pressure.

Table IX.2. Values of coefficients c_y and c_x for supersonic airfoil/profiles.

(1) Профиль	c_y	c_x
(2) Плоская пластинка	$\frac{4\alpha}{\sqrt{M^2-1}}$	$\frac{4\alpha^2}{\sqrt{M^2-1}} + c_f$
(3) Двойковопуклый профиль	$\frac{4\alpha}{\sqrt{M^2-1}}$	$\frac{4\alpha^2}{\sqrt{M^2-1}} + \frac{16}{3} \frac{c}{\sqrt{M^2-1}} + c_f$
(4) Ромбовидный профиль	$\frac{4\alpha}{\sqrt{M^2-1}}$	$\frac{4\alpha^2}{\sqrt{M^2-1}} + \frac{4c^2}{\sqrt{M^2-1}} + c_f$
(5) Каплевидные профили (рис. IX.22)	$\frac{4\alpha}{\sqrt{M^2-1}}$	$\frac{4\alpha^2}{\sqrt{M^2-1}} + \frac{2}{\sqrt{M^2-1}} \left[\frac{c_1^2 + c_2^2}{x_c(b-x_c)} \right] + c_f$ $c_f \approx 0,05$

DOC = 78201107

PAGE

~~24~~ 247

Key: (1). Airfoil/profile. (2). Flat/plane plate. (3). Convexo-convex airfoil/profile. (4). double wedge airfoil. (5). Plane-wedge profiles (Fig. IX.22).

Page 374.

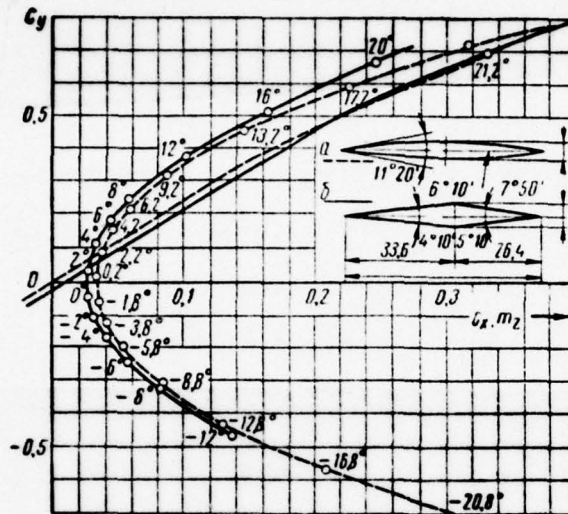


Fig. IX.21. Polars of two airfoil/profiles with $M=1.85$.

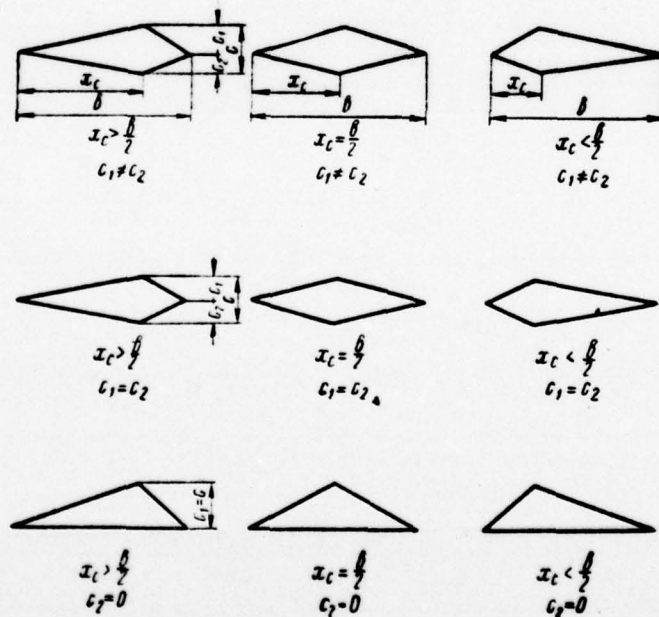


Fig. IX.22.

Fig. IX.22. Plane-wedge profiles.

Page 375.

Small drag have double wedge airfoils with the maximum thickness, arranged/located in the middle of chords. Aerodynamic quality c_y/c_x in flat/plate is equal $\sim 10-15$, in convexo-convex airfoil/profile (without taking into account of friction) - $\sqrt{3/4}c$ in rhombiform - $1/2c$.

§ IX.2. Wing characteristics.

The used in different flight vehicles wings, depending on their designation/purpose and number domains Re and M , for which they are utilized, have different geometric form and are comprised from different types of airfoil/profiles. The geometry of wing is characterized by the following basic parameters.

Planform. The simplest rectangular form is applied in the first on time wings. Contemporary wings for the low speeds of flight have, mainly, trapezoidal planform with the rounded off end/leads of Fig. IX.23). For high subsonic and supersonic speeds are more favorable swept and the low-aspect-ratio wings.

Wing area S . Under wing area, is understood its area in plan/layout.

Span of wing l . This is the distance between the extreme points of wing.

Geometrical mean chord. Under mean geometric chord is implied the ratio/relation to wing area to its spread/scope:

$$b_{cp} = \frac{S}{l}.$$

The aspect ratio of wing. Aspect ratio is called the ratio of the wingspan to its area:

$$\lambda = \frac{l}{b_{cp}} = \frac{l^2}{S}.$$

The mean aerodynamic chord (MAC). The chord of the rectangular in plan/layout wing on which act the same aerodynamic forces and torque/moments, as to the wing in question, it is called the mean aerodynamic chord.

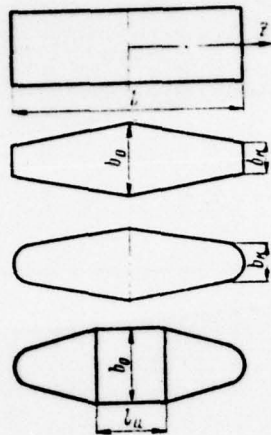


Fig. IX.23. Wings of different planform.

Page 376.

Its length is calculated from the condition of the equality of the torque/moment of airfoil/profile (the rectangular wing) to total torque/moment of this wing, which is equal to the algebraic sum of the longitudinal (relative to Z-axis) torque/moments of the separate cell/elements, in reference to their aerodynamic focus.

The pitching moment of the cell/element of wing with a width of dz

$$dM = m_z q b^2 dz,$$

here m_z - local moment coefficient, in reference to focus; q -

velocity head.

Equalizing resulting moment

$$M = q \int_{-l/2}^{+l/2} m_{z_0} b^2 dz$$

to torque/moment $M = m_{z_{CAX}} b_{CAX} q$, we will obtain

$$m_{z_{CAX}} b_{CAX} = \frac{1}{S} \int_{-l/2}^{+l/2} m_{z_0} b^2 dz,$$

where $m_{z_{CAX}}$ - torque/moment of the rectangular wing of area S , in reference to the mean aerodynamic chord.

Assuming that the moment coefficients of airfoil/profiles are constant on entire spread/scope

$$m_{z_0} = \text{const} = m_{z_{CAX}},$$

it is possible from last/latter equality to find the length of the mean aerodynamic chord:

$$b_{CAX} = \frac{1}{S} \int_{-l/2}^{+l/2} b^2 dz.$$

For the rectangular wing

$$b_{CAX} = b.$$

For the tapered wing the mean aerodynamic chord is equal to the chord, passing through the center of gravity of the area of the half

of the projection of wing (trapezium). For elliptical

$$b_{CAX} = \frac{8}{3\pi} b_{max} = 0,8488 b_{max}.$$

The center-of-gravity location of apparatus (aircraft) usually expresses in the portions of the mean aerodynamic chord. The mean aerodynamic chord is disposed of in such a way that its aerodynamic focus would coincide with the aerodynamic focus of real wing, and chord itself was parallel to the chord of that airfoil/profile, along which are counted off the angles of attack and the zero-lift angles of entire wing.

Page 377.

Wing taper. This is the ratio of the greatest root chord to end wing chord

$$\eta = \frac{b_0}{b_k}.$$

Transverse sweepback. Transverse sweepback is applied for an increase in lateral stability and is characterized by the angle between Z-axis and chord plane.

Wing warp. Torsion is called the relative rotation of wing sections, which leads to the fact that when $c_{y_{\text{np}}} = 0$ the value of local lift coefficients (for separate sections) not equal to zero. If

when $c_y = 0$ the values $c_x = 0$, then wing is called aerodynamically flat/plane. If the chords of all sections lie/rest at one planes, then this wing, being geometrically flat/plane, but being comprised from the airfoil/profiles, which have different zero-lift angles (α_0), it can be aerodynamically twisted. Wing can be twisted positively (angle of attack toward the end of the wing increases) or it is negative, and to also have both of forms of torsion.

Set of airfoil/profiles. The first on time wings have identical airfoil/profiles along the length spread/scope. Recently widely are applied the wings, which have different airfoil/profiles, which is connected with the need of providing the best conditions of their flow for the system of flight vehicle (low resistance, large lift, preventing the premature separation of flow and deterioration in the moment characteristics). Aerodynamic wing characteristics differ significantly from air foil data, from which it is comprised, since the finiteness of the wingspan and the effect of the conjugated/combined with it cell/elements of apparatus changes entire character of flow (speed, pressure, angles of attack, etc.).

Let us examine the wing about which flows liquid or gas and possesses lift. The presence of lift indicates that the pressure on upper surface is less than the pressure on lower. The decrease of pressure in streams on upper surface is connected with an increase in

their velocity an increase of the pressure in the streams, which flow around lower by the wing surface, it is connected with the decrease of their speed. This change in the speeds of flow about wing can be obtained, if besides the incident to wing main flow around wing it will exist by other, which, being added with basic, will lead to an increase in the velocities on the upper wing surface and to their decrease on lower. This flow can be only circulation (Fig. IX.24).

Let us examine some questions, connected with the circulation flow. Let us conduct in fluxion certain closed duct/contour (Fig. IX.24). At any point A on this duct/contour, the liquid will have certain velocity v . Distance S of point A from the initial point O let us consider in direction clockwise the value of positive, and in the opposite direction - negative.

Page 378.

Circulation is called sum $\Gamma = \int v_s ds$, undertaken on entire duct/contour. Here ds - element of line, which contains point with the speed to direction of tangent in this place, by equal to v_s . Circulation is measured in square meters per second. It is closely related with the rotation of liquid.

The rotation of liquid differs significantly from the rotation

of solid body. If for the solid rotating body all points, which lie at a distance of r from rotational axis, will have velocity $v = \omega r$, where ω - an angular velocity, then for a liquid its separate regions can rotate with different angular velocities and it is necessary to speak only about the local angular velocity of the given small particle of liquid. Thus, the rotation of liquid is characterized by the angular velocity in this place.

Eddy/vortices. Eddy/vortices appear during the flow around bodies of real liquid (viscous fluid) and their value in aeromechanics is extremely great. On its physical essence the eddy/vortex represents rotary motion of liquid. The value of angular velocity is closely related with circulation, namely: the angular rate of rotation of liquid ω_n is directly proportional to circulation \mathcal{Q} and it is inversely proportional to the doubled area of duct/contour (2σ), for which it is found \mathcal{Q} :

$$\omega_n = \frac{\mathcal{Q}}{2\sigma}.$$

By analogy with line and tube of flow and other parameters in fluxion, occur the vortex lines and vortex filaments, or vortex filaments. The vortex filaments as this is establish/installed by Helmholtz in theoretical hydromechanics, they cannot terminate suddenly: they either stretch into infinity or they rest on the boundaries of liquid (wall), or they are closed into rings. Very

frequently the boundaries of liquid (wall), or are closed into rings. Very frequently the liquid in flow is not all whirling and swirled regions take the form of the long bodies, the so-called vortex lines. The velocity field, which appears about the vortex line, not arbitrary, but is connected with its circulation. Circulation around rectilinear vortex line (Fig. IX.25)

$$\Gamma = 2\pi r v,$$

whence velocity around the vortex line

$$v = \frac{\Gamma}{2\pi r},$$

where r - radius of any point out of the vortex line.

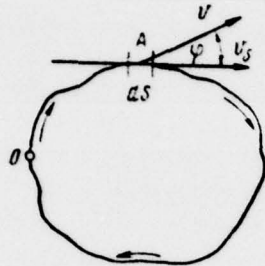


Fig. IX.24. Circulation on duct/contour.

Page 379.

As can be seen from this expression, particle speed with its removal/distance from eddy/vortex will decrease according to hyperbolic law. Within quite vortex line ($\omega = \text{const}$) of velocity, they will change as for rotating solid body. Velocity on any radius r_1 within the vortex line

$$v_1 = r_1 \omega,$$

i.e. is changed according to linear law.

Difference in the motion of liquid within the vortex line and out of it consists not only of the amount of the velocity, but mainly in the fact that within its liquid rotates, and out of cord - it does not rotate. The absence of rotation in the exteriors of the liquid is connected with the fact that the circulation on any duct/contour,

which covers these particles, but which does not include the vortex line, is equal to zero.

ab In experimental aeromechanics high value have the velocities, induced by eddy/vortices in its surrounding liquid, for example during the flow around of the wing of final spread/scope. The induced with vorticity for the incompressible fluid is determined from the formula of Biot and savart by analogy with the action of the cell/element along which flows the current to magnetic pole (Fig. IX.26) :

$$v = \frac{r}{4\pi Y_1} \int_{\varphi_1}^{\varphi_2} \sin \varphi \, d\varphi = \frac{r}{4\pi Y_1} (\cos \varphi_1 - \cos \varphi_2).$$

For the case of infinitely rectilinear eddy/vortex, this formula takes the form

$$v = \frac{r}{2\pi Y_1}$$

(since $\varphi_1 = 180^\circ$ and $\varphi_2 = 0$).

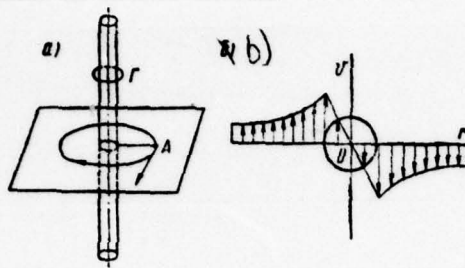


Fig. IX.25. Velocity field of the rectilinear vortex line: a) rectilinear vortex line; b) the velocity field of rectilinear vortex line.

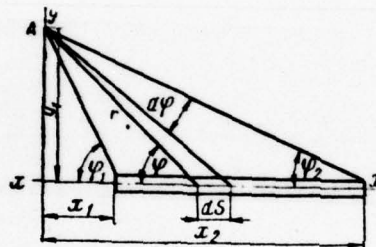


Fig. IX.26. On the calculation of the velocity, induced with rectilinear vortex line.

Page 380.

For half-cord (i.e. the vortex line, which rests by one end/lead on plane, and by other exiting into infinity) of $\phi_1=90^\circ$, $\phi_2=0$ and, therefore,

$$v = \frac{\Gamma}{4\pi Y_1}.$$

Magnus's force. Let us examine the flow around the cylinder of flow, comprised of forward/progressive with a rate of v_0 and circulation with speed $\frac{\Gamma}{2\pi R}$. As a result of cooperating both of flows of the velocity above of cylinders (Fig. IX.27) they will be more, rather than velocity below, i.e., will appear the force, perpendicular to the direction of the incident flow, which is called lift. The amount of this force can be found with the aid of the equation of Bernoulli ¹.

$$p_0 + \rho \frac{v_0^2}{2} = p + \rho \frac{v^2}{2} = H$$

or

$$\begin{aligned} p &= H - \rho \frac{v^2}{2} = \\ &= H - \frac{\rho}{2} \left(2v_0 \sin \theta + \frac{\Gamma}{2\pi R} \right)^2. \end{aligned}$$

FOOTNOTE ¹. As was said in § II.3, velocity on the surface of

cylinder at velocity of incident flow v_0 will compose $2v_0 \sin \theta$. To it it is necessary to add velocity from the circulation flow $\frac{\Gamma}{2\pi R}$.
ENDFOOTNOTE.

To the cell/element of cylinder with a width of dS and by length (on generatrix) 1 will act the force

$$\Delta p = p dS l,$$

projection of which on axle/axis Oy

$$\Delta p_y = - p dS l \sin \theta.$$

For obtaining the complete force p_y , which acts on entire cylinder, it is necessary to conduct the addition (integration) of elementary forces Δp_y , after replacing in this case dS by $R d\theta$ and after substituting for p its value from the equation of Bernoulli. The results of this summation give the value

$$p_y = \rho l v_0 \Gamma.$$

Force p_y , or Magnus's so-called force, is proportional to the air density, velocity of incident flow, to the length of the chosen section of cylinder and circulation around it.

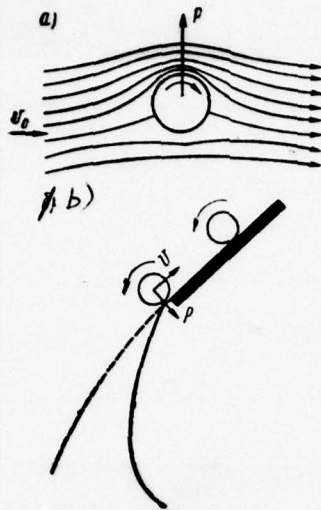


Fig. IX.27. The Magnus force: a - interaction of two flows; b - trajectory of the wheeling cylinder (broken line - without taking into account of Magnus's forces, continuous - taking into account Magnus's forces).

Page 381.

The direction of this force coincides with the sense of the vector of the speed of forward/progressive flow, turned on 90° to the side, reverse/inverse circulations. In practice Magnus's force can be obtained, rotating cylinder in the incident flow, perpendicular to its axle/axis. Cylinder will carry along after itself air and give it in rotation. 1.

FOOTNOTE 1. This type of rotating cylinders were proposed by Flettner for replacing the sails aboard ships. ENDFOOTNOTE.

The rotating artillery shells and the rockets, which fly at certain angle of attack, test the action of Magnus's force, that it is necessary to consider during the calculation of their flight trajectory. If light/lung paper cylinder is rolled up on inclined plane down, then under the action of the force indicated it will change its trajectory. Figure IX.27 by dotted line gives trajectory in the absence of Magnus's force, solid line depicts the trajectory of cylinder in the presence its. To determine the effect of Magnus effect on the longitudinal-behavior characteristics of the rotating bodies is possible by testing the rotating models in wind tunnel. Figure IX.28 gives the diagram of similar installation. Model is fasten/strengthened to six-components balance of duct. The rotation of model is realize/accomplished with the aid of flexible shaft by the engine, not connected with weights. The special feature/peculiarity of such experiments is the smallness of the measured forces and the necessity of the account of the effect of the elasticity of flexible shaft on readings of weights.

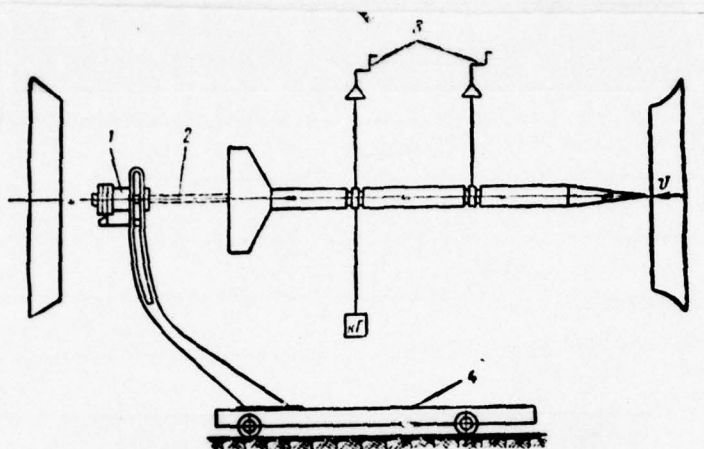


Fig IX.28. The diagram of installation of model in duct for determining the effect of Magnus's force: 1 - electric motor; 2 - flexible shaft; 3 - weights; 4 - frame of balance.

Page 382.

Zhukovskiy theorem. Examining the lift of infinite-span wing in the flow of ideal fluid, N. E. Zhukovskiy will show that wing can be replaced with the so-called bound vortex with the same circulation. This correctly, because once wing has lift, means circulation around this wing it is not equal to zero and the flow, which flows around it, can be presented as forward/progressive, to which as is superimposed the circulation flow. For the points, distant far from wing, the velocity field, caused by the bound vortex is analogous with the velocity field, caused by wing with the same circulation. By

N. Ye. Zhukovskiy was found the lift, acting on the wing:

$$Y = \rho v_0 \Gamma.$$

This theorem was formulated by N. Ye. Zhukovskiy as follows: lift Y , acting on infinite-span wing, was equal to the air density ρ , multiplied by circulation Γ , velocity of flow in infinity v_0 and length of the chosen section of wing l . If velocity vector is turned on 90° to the side, reverse/inverse circulations, then it is possible to obtain line of force. As it is possible to note, Magnus's force exists a special case of the lift, determined according to Zhukovskiy theorem. But this theorem links the amount of circulation and lift, but is not solved a question concerning the very value of circulation, which depends on the form of wing profile and other factors.

The selection of value Γ is realize/accomplished according to zhukovskiy - Chaplygin's postulate in such a way that the descent of flow line from wing profile would occur from trailing edge (Fig. IX.29). If circulation is great or small, then the descent of flow lines will occur from lower or upper surface.

The Joukowski theorem is the important for entire aeromechanics. On its basis are conducted the calculations of wings, propellers, turbines and other aeromechanical apparatuses and equipment/devices. From this theorem it follows that for the wing

$$\Gamma = \frac{Y}{\rho v_0} = \frac{c_y \rho S v_0^2}{2 \rho v_0} = \frac{c_y}{2} b v_0 \quad (\text{equation of relation}).$$

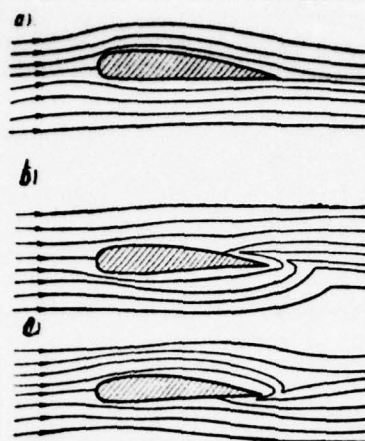


Fig. IX.29. To the selection of value r : a - r is selected correctly; b - r is small; c - r is great.

Page 383.

Value c_y can be found, if is known dependence $\left(\frac{\partial c_y}{\partial \alpha}\right)_\infty$ for an infinite-span wing ¹. this type and the true angle of attack, depending on velocity of incident flow, the actual angle (calculated off zero-lift angle and the vertical velocity, caused by the vortex/eddy system, which disappears from the wing:

$$c_y = \left(\frac{\partial c_y}{\partial \alpha}\right)_\infty \left(\alpha - \frac{v_y}{v}\right).$$

FOOTNOTE ¹. $\left(\frac{\partial c_y}{\partial \alpha}\right)_\infty$ is taken as as the usually equal to 5.6.

ENDFOOTNOTE.

In practice are applied two methods of the experimental determination of circulation. The first method is instituted on Zhukovskiy theorem, according to which for the elementary lift dp of the cell/element of wing on spread/scope dz

$$dp = \rho v \Gamma dz.$$

On the basis of experiments according to the distribution

$$\frac{dp}{dz} = y_1 \cos \alpha - x_1 \sin \alpha = \cos \alpha \int_S (p - p_0) dx_1 - \sin \alpha \int_S (p - p_0) dy_1.$$

We hence obtain expression for circulation in this wing section:

$$\Gamma = \frac{1}{\rho v_0} \left[\cos \alpha \int_S (p - p_0) dx_1 - \sin \alpha \int_S (p - p_0) dy_1 \right].$$

If the distribution of pressure is obtained in a sufficient number of wing sections, then it is possible to find circulation distribution according to entire spread/scope. But circulation on duct/contour S can be found by direct measurements, utilizing the expression

$$\Gamma = \int_S v \cos(v, ds) ds = \int_S u dx + v dy + w dz.$$

Such measurements it is possible to produce by nozzles for determining of value and direction of velocity. In this case, it is necessary to bear in mind, that the measurements of circulation on the duct/contours, which seize wing, must pass in the region of trace (wake zone) approximately in the direction, perpendicular to wake

centerline.

Page 384.

After obtaining from experiments the value of the circulation of sections, that form wing, it is possible to consider the set of airfoil/profiles, the twisted nature and the angles of setting sections, to find with the aid of known integrodifferential equation both the circulation distribution according to wing and its complete value at different angles of attack. Experiments show that the error in the determination of circulation from the measurements of the distribution of pressure or velocities does not exceed 10/o.

In the case of finite-span wing, just as infinite-span wing, it is possible to replace with the attached on the spot vortex line. However so that this cord can exist, it must, according to Helmholtz theorem about eddy/vortices, or be closed to itself or stretch by its end/leads into infinity. The only method to satisfy these conditions is the confirmed by experiments assumption that from wing tips run off the eddy/vortices, which they are seized by flow and go back/ago in the direction of velocity of incident flow. These eddy/vortices are called free vortices or vortex/eddy whiskers.

Real/actually, as a result of pressure difference on the upper

and lower wing surfaces, will occur the overflowing of air from lower surface to upper, and from wing will run off two eddy/vortices. In the simplest case the wing of finite span is aerodynamically equivalent to the U-shaped diagram of eddy/vortices (Fig. IX.30), which, however, in pure form is not realized. In view of the nonuniformity of lift distribution (circulation) according to spread/scope, due to the tip effect, difference between the chords, airfoil/profiles and the like from wing run off many eddy/vortices which after wing are coagulated into the vortex sheet (Fig. IX.31). The vortex sheet is unstable and soon after runoff from wing, it is coagulated into two vortex/eddy whiskers. However, for solving many practical tasks, is examined the diagram of horseshoe vortices.

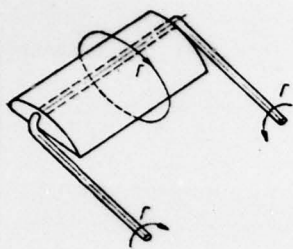


Fig. IX.30. Horseshoe vortices.

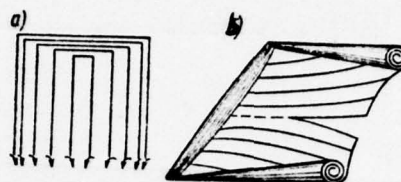


Fig. IX.31.

Fig. IX.31. The vortex sheet: a - diagram; b - film.

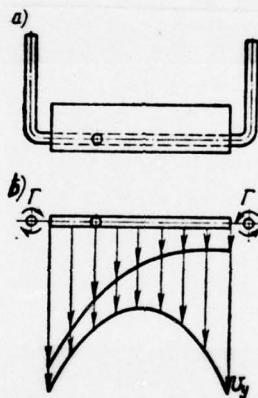


Fig. IX.32. The induced velocity: a - plan view; b - form against flow.

Page 385.

Induced drag. The rotation of trailing vortexes (Fig. IX.32) is directed in inside wing, as a result of which is induced the vertical velocity, which leads to the decrease of true angle of attack and the

appearance of supplementary, so-called, induced drag.

The average speed, induced by the eddy/vortices

$$v_Y = \frac{2\Gamma}{\pi l},$$

where l - wingspan.

Value Γ can be found from the equation of relation between values Γ and c_Y :

$$Y = \rho l v \Gamma = c_Y \rho S \frac{v^2}{2},$$

whence

$$v_Y = -\frac{c_Y}{\pi} \cdot \frac{b}{l} v = -\frac{c_Y}{\pi \lambda} v,$$

sign "minus" it shows that the velocity v_Y is directed down.

The downwash angle $\Delta\alpha$ is obtained by the addition of velocities of flow and inductive (Fig. IX.33), also, in view of its smallness ($v \gg v_Y$):

$$\operatorname{tg} \Delta\alpha = \Delta\alpha = -\frac{v_Y}{v} = \frac{c_Y}{\pi \lambda}.$$

Positive is conditionally considered the rake angle, generatrix in the direction of the induced velocity down. True (effective) angle of attack of the wing, establish/install in flow at geometric angle α :

$$\alpha_i = \alpha - \Delta\alpha,$$

with $\lambda = \infty$ (infinite-span wing)

$$\alpha_i = \alpha.$$

The presence of downwash leads to certain lift convergence and essential increase in the drag. Coefficients of aerodynamic forces, in reference to the velocity of flow at infinity (in wind axes) of the rotation of flow to angle $\Delta\alpha$:

$$c_Y = c_Y' \cos \Delta\alpha - c_{Xp}' \sin \Delta\alpha,$$

$$c_X = c_Y' \sin \Delta\alpha + c_{Xp}' \cos \Delta\alpha,$$

here c_Y' and c_{Xp}' - lift coefficients and frontal (or profile drag) for an infinite-span wing, that correspond to true angle of attack α_i .

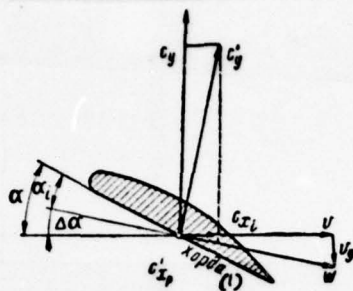


Fig. IX.33. Effect of induced velocity.

Key: (1). Chord.

Page 386.

Counting

$$\sin \Delta \alpha = \Delta \alpha,$$

$$\cos \Delta \alpha = 1,$$

we will obtain ¹.

$$c_y = c_{y_p},$$

$$c_x = c_{x_i} \Delta \alpha + c_{x_p} = c_{x_i} \Delta \alpha + c_{x_p}.$$

FOOTNOTE ¹. Product $c_{x_p} \sin \Delta \alpha$ can be usually disregarded. Primes in this formula it is possible not to place, if to remember that c_y and c_{x_p} they are taken on true angle of attack. ENDFOOTNOTE.

Value $c_{x_i} \Delta \alpha = c_{x_i} = \frac{c_y}{\pi \lambda}$ is called induced drag whose value depends on values c_y and λ . It occurs even in the case of the flow around of the wing of final spread/scope of ideal fluid. Somewhat more precise

formula of induced drag takes the form

$$c_{xi} = \frac{1 + \delta}{\pi} \frac{c_y^2}{\lambda},$$

where δ changes within limits of 0-0.14. ².

FOOTNOTE ². For flat/plane tapered wings δ , it varies within the limits with 0.01-0.08 ($\lambda=5-10$ and $\eta=1-5$). For the twisted tapered wings the value c_{xi} increases approximately by 0.0003. During an increase in the velocity (up to the education/formation of shock waves on wing) induced drag can be found from the expression

$$c_{xi_{cm}} = \frac{1 + \delta}{\pi \lambda} c_{y_{cm}}^2$$

ENDFOOTNOTE.

The values of coefficients A_1 and A_2 in the expressions

$$c_{xi} = A_1 \frac{c_y^2}{\lambda}; \quad \Delta \alpha = A_2 \frac{c_y}{\lambda}$$

for some simplest forms of wings are given in Table IX.3. Induced drag, which is in known sense the value of lift, shows that to energetically more favorably produce delation with the wing down of air with lower speed, but larger mass (under this lift), which is possible during an increase in the spread/scope or wing aspect ratio. This fact is utilized for aircraft with the long range of flight.

The theory of induced drag is well confirmed by numerous experiments. The results of the tests of the wings of different elongations after recalculation for one elongation give the coinciding results (Fig. IX.34).

Table IX.3. Values of coefficients A_1 and A_2 .

(1) Форма крыла	A_1	A_2
(2) Эллиптическое . . .	0,318	0,318
(3) Трапециевидное . . .	0,318	0,318
(4) Прямоугольное . . .	0,335	0,375
(5) Прямоугольное с за- валеными концами	0,318	0,338
(6) Прямоугольное со скругленными кон- цами	0,318	0,365
(7) Ромбовидное	0,363	0,363

Key: (1). Form of wing. (2). Elliptical. (3). Trapezoidal. (4). Rectangular. (5). Rectangular with filled up end/leads. (6). Rectangular with rounded off end/leads. (7). Rhomboid.

Page 387.

The recalculation of the wing characteristics, obtained during one elongation λ_1 , for another λ_2 or infinite elongation $\lambda = \infty$, is conducted, on the basis of the fact that at identical true angles of attack for both of wings all the aerodynamic coefficients will be identical, i.e.,

$$\begin{aligned} C_{Y_1} &= C_{Y_2} = C_{Y_\infty} \\ C_{X_{P_1}} &= C_{X_{P_2}} = C_{X_{P_\infty}} \\ C_{m_1} &= C_{m_2} = C_{m_\infty} \end{aligned}$$

The equality of true angles of attack is determined by the relationship/ratios

$$\alpha_i = \alpha_i^0 - \Delta\alpha_i = \alpha_i^0 - \Delta\alpha_i^0,$$

or

$$\alpha_i^0 - \Delta\alpha_i^0 = \alpha_i^0 - \Delta\alpha_i^0,$$

whence, remembering that

$$\Delta\alpha = \frac{c_Y}{\pi\lambda},$$

$$\alpha_i^0 - \alpha_i^0 = c_Y k,$$

where

$$k = \frac{1}{\pi} \left(\frac{1}{\lambda_1} - \frac{1}{\lambda_2} \right).$$

For the recalculation of curve $c_Y = f(\alpha^0)$ it is necessary each point (for each value $c_{Y_1} = c_{Y_2} = c_Y$) to shift by value $\alpha^0_1 - \alpha^0_2$ (Fig. IX.35).

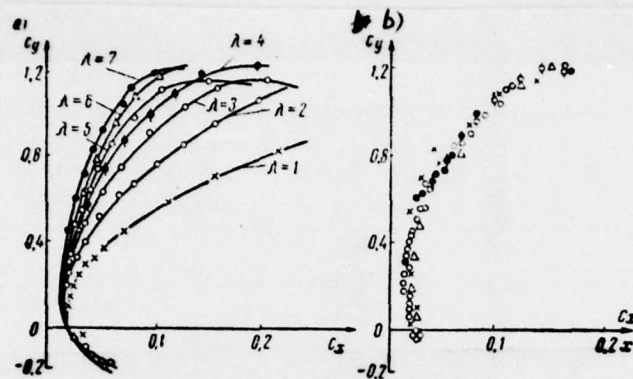


Fig. IX.34. The wing polars of various aspect ratios: a - wing polar of identical airfoil/profile, but different elongations; b - the same curves, converted on $\lambda=5$.

Page 388.

The recalculation of drag coefficients is conducted from the condition

$$c_{X_1} = c_{X_{l_1}} + c_{X_{p_1}},$$

$$c_{X_2} = c_{X_{l_2}} + c_{X_{p_2}},$$

With equality $c_{X_{p_1}} = c_{X_{p_2}}$ for this value c_Y

$$c_{X_1} - c_{X_2} = c_{X_{l_1}} - c_{X_{l_2}} = \frac{c_Y^2}{\pi} \left(\frac{1}{\lambda_1} - \frac{1}{\lambda_2} \right) = c_{X_{\lambda}}.$$

Consequently, moving the points of polar with λ_1 to value $c_{X_{\lambda}}$ we will obtain polar with λ_2 (Fig. IX.36).

If moment curve is assigned/prescribed in the form of dependence $c_m = f(\alpha)$, it remains constant/invariable for different values λ (since

the coefficient c_y of recalculation remains constant/invariable). If moment curve is assign/prescribed in the form $c_m = f(\alpha)$, then it must be corrected to difference $(\alpha_i - \alpha_e) = f(c_y)$ (see Fig. IX.34).

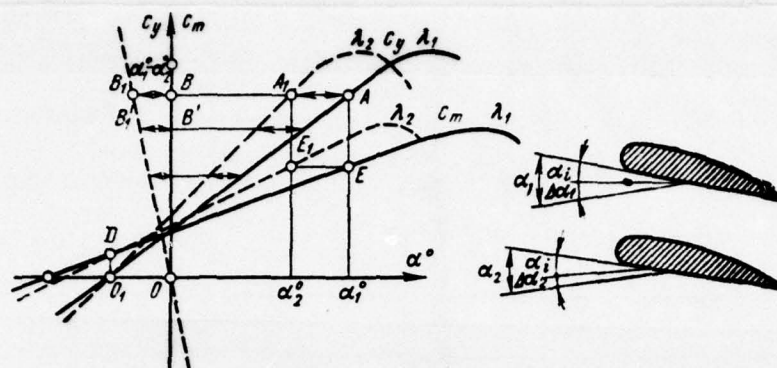
For obtaining the wing characteristics of infinite elongation necessary in finite-span wing λ to deduct entire angle of rake

$$\alpha_i - \alpha_e = 57,3 \frac{c_y}{\pi \lambda}$$

and all induced drag

$$c_{xi} - c_{xi\infty} = \frac{c_y^2}{\pi \lambda}.$$

Simplified theory presented previously of induced drag, without taking into account of compressibility effect, assumes the constancy of downwashes along spread/scope and elliptical circulation distribution at the average values of elongation.



For Fig. IX.35. To the recalculation of characteristics $c_y = f(\alpha)$ wing for another elongation.

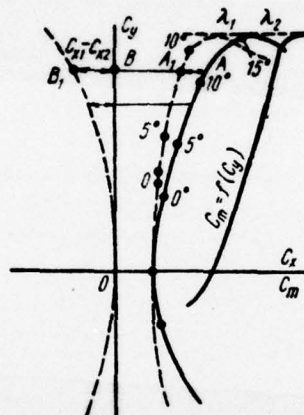


Fig. IX.36. To the recalculation of wing polar for another elongation.

Page 389.

In actuality contemporary wings have a planform, different from elliptical, downwash in spread/scope variable, wing warp, sweepback, etc. All this requires the more precise account of induced drag. This

account is conducted by the careful calculation of circulation and tapers along the wingspan with the aid of the refined theoretical and experimental methods.

If we on curve/graph $c_y = f(c_x)$ finite-span wing plot the curve, obtained from the expression

$$c_{xi} = \frac{c_y}{\pi \lambda}.$$

then the obtained parabola (parabola of induced drag) is the wing polar of final spread/scope in ideal fluid. It makes it possible to divide wing drag on two parts: profile and inductive. The value of profile drag is low (0.004-0.01) and depends on the form of airfoil/profile, Re numbers and M and angle of attack. At high angles of attack, induced drag, proportional c_y , rapidly increases; therefore they attempt wings to make considerable elongation $\lambda > 10-12$ (for example, for the aircraft, which fly at high angles of attack - high-altitude, hyperdistant, etc.), which leads to decrease of induced drag. At subsonic speeds where the compressibility effect yet is not exhibited, aerodynamic characteristics depend, mainly, on elongation, planform, contraction and properties of airfoil/profile.

One of the most important wing characteristics is the spanwise lift distribution, which depends (over a wide range of elongation) only on wing planform.

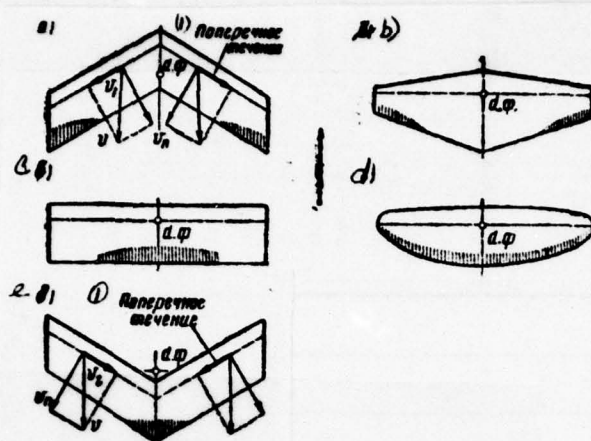


Fig. IX.37. Effect of wing planform on flow separation. The sections where begins flow breakaway from wing, are shaded: a - positive sweepback b - a trapezoid; c - rectangle; d - ellipse; e - negative sweepback.

Key: (1). Cross flow.

Page 390.

The local importance of the lift coefficient c_l of this geometric angle for the tapered wing increase to its end/leads, and values $c_{l_{max}}$ will be reached more earlily in tail pieces, which causes intense flow separation with an increase in the contraction of the tapered wings. In this case, appears the danger of the aileron power loss and stalling of aircraft to wing due to the asymmetry of

disruption/separation on both wings. In the rectangular wing the airfoil/profiles of the middle part work at high angles of attack because the induced velocity, which decreases the angle of attack, increases to wing tips, flow separation appears in its middle (Fig. IX.37), and ailerons retain their effectiveness, also, at high angles of attack. In elliptical, aerodynamically unwarped wings the value $C_{y_{max}}$ end sections due to the decrease of chords and Re numbers somewhat descends on spread/scope and flow separation, beginning in the middle part, rapidly is spread to entire wing.

The adverse phenomena, connected with the nonuniformity of load distribution (lift) according to the wingspan, can be to a considerable degree attenuate/weakened, applying aerodynamic torsion and different means the mechanizations, which increase both the overall and local amount of the lift of wing. Especially this is important for the conditions/modes of the high angles of attack (landing/fitting, maneuver, etc.) of those aircraft whose wing area is selected small for the purpose of an increase in the maximum speed. The provision for safe landing/fitting of this type of apparatuses requires increase $C_{y_{max}}$ for decreasing the landing speed, and minimum speed of the flight:

$$v_{min} = \sqrt{\frac{2G}{\rho C_{y_{max}} S}}$$

where G - weight of apparatus; S - wing area.

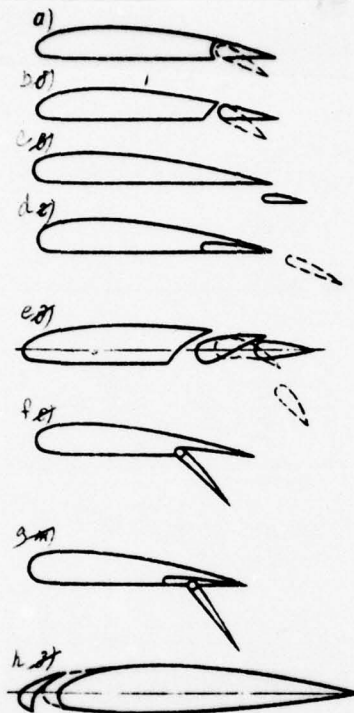


Fig. IX.38. Different forms of the mechanization: a - the plain flap; b - the slotted flap; c - movable flap; d - the extension flap; e - dual-purpose flap; f - the simple wing flap; g - panel with the sliding hinge joint; h - wing with slat.

Page 391.

As the means, which ensure an increase $c_{l\max}$ wing, are utilized mainly the equipment/devices, which increase its area, effective camber, flaps, panels, slats (Fig. IX.38), and also suction and blowing of boundary layer. The character of the effect of

AD-A066 280

FOREIGN TECHNOLOGY DIV WRIGHT-PATTERSON AFB OHIO
EXPERIMENTAL AEROMECHANICS (SELECTED CHAPTERS), (U)
JAN 79 S M GORLIN

F/G 20/4

UNCLASSIFIED

FTD-ID(RS)T-2011-78

NL

4 OF 4
ADA
066280



END
DATE
FILMED

5-79
DOC

mechanization on value $c_{Y_{max}}$ is shown on Fig. IX.39. A selection of one or the other type of mechanization must be produced with consideration a change not only values $c_{Y_{max}}$ but also coefficients c_x and $c_m = f(\alpha)$. Is feasible in principle also the method of an increase in the lift because of a change in the wing area, but in practice due to structural/design difficulties, it still little is applied.

Are recently proposed the jet flaps, in which the emerging from jet engine gases are discharged at certain angle down near trailing wing edge. In this case, the lift, which increases because of the projection of reacting force of jet and the supplementary evacuation/rarefaction, which appears on the upper part of the airfoil/profile, reaches the enormous values: $c_{Y_{max}} \sim 10-12$ (Fig. IX.40).

The character of course by curve $c_Y = f(\alpha)$ in the region of high angles of attack can cause the autorotation of wing around longitudinal axis x .

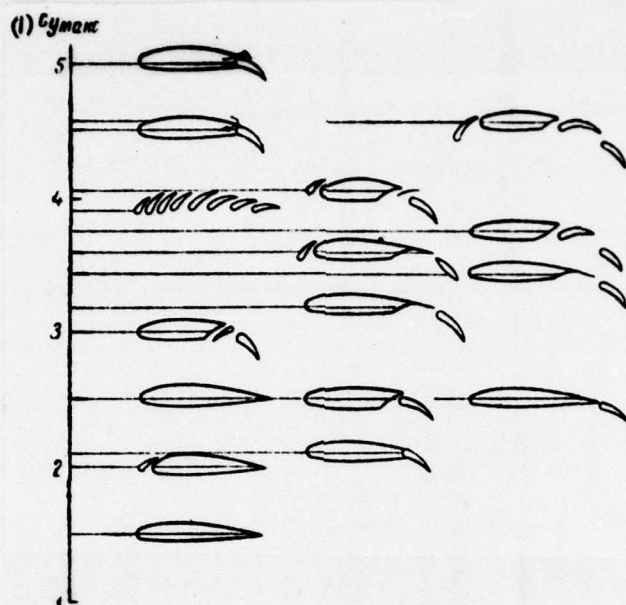


Fig. IX.39. Comparison of different forms of mechanization.

Page 392.

If near the angles, which correspond $c_{y_{max}}$, wing under the effect of external reason starts up, then the angles of attack of left and right half of wings will begin to change, namely: the angle of attack of the discharged wing tip will increase, and heaving - it decreases. In this case, as it follows from dependence $c_y = f(\alpha)$, the lift of the omitted half wing decreases, and heaving - it will remain almost without change, as a result will appear the torque/moment M_x , which increases bank and leading to autorotation (Fig. IX.41). The

intensity of autorotation depends in essence on the value of negative value by derivative $\frac{dc_y}{d\alpha}$ (autorotation begins at the negative value of expression $\frac{dc_y}{d\alpha} + c_x$). Autorotation begins from stalling of aircraft to wing and can lead to spin, i.e., to apiral descent with intense rotation and to the shock of wing about the earth/ground in low altitudes. The fact, which blocks autorotation, is the liquidating or damping moment of wing which falls from an increase in the angle of attack.

The means of decreasing the tendency toward autorotation is the prevention of flow separations at wing tips because of the selection of root airfoil/profiles with coefficients $c_{y_{max}}$ and α_{sp} less than in end airfoil/profiles, and also because of the decrease of contraction, mechanization of end wing sections and washout.

Closely connected to the character of the lift distribution and pressures, is located the distribution of velocities. The field of velocities and downwashes around wing (Fig. XI.42) has great practical value for the selection of the location of tail assembly.

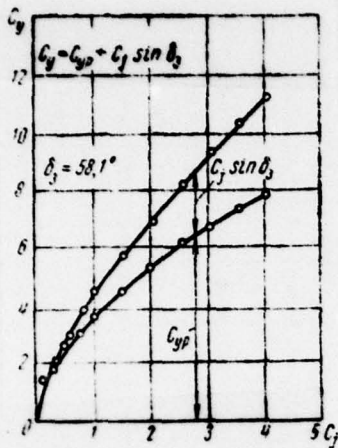
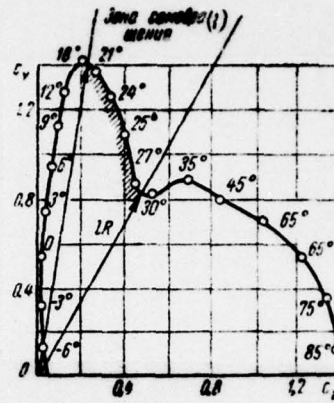
Fig. XI.40. Effect of boundary layer control on $c_{y_{max}}$ 

Fig. IX.41.

Fig. IX.41. Wing polar with the chosen zone of autorotation (autogyration).

Key: (1). Zone of autorotation.

Page 393.

The effectiveness of tail assembly will be greater, the lesser braking velocity 1 . in the location of tail assembly is less local downwash.

FOOTNOTE 1 . Along wing wake from both sides with the intensely developed trace at angles of attack beyond stalling, appear the

narrow zones of the increased velocities, in which value v/v_0 attains values by 1.3-1.4. ENDFOOTNOTE.

The sweptback wings. With an increase in the flight speed (after $M \approx 0.6$) due to compressibility effect resistance of usual wings so grow/rises that their application/use becomes irrational both from the point of view of the power, required for advance and an adverse change in the moment characteristics.

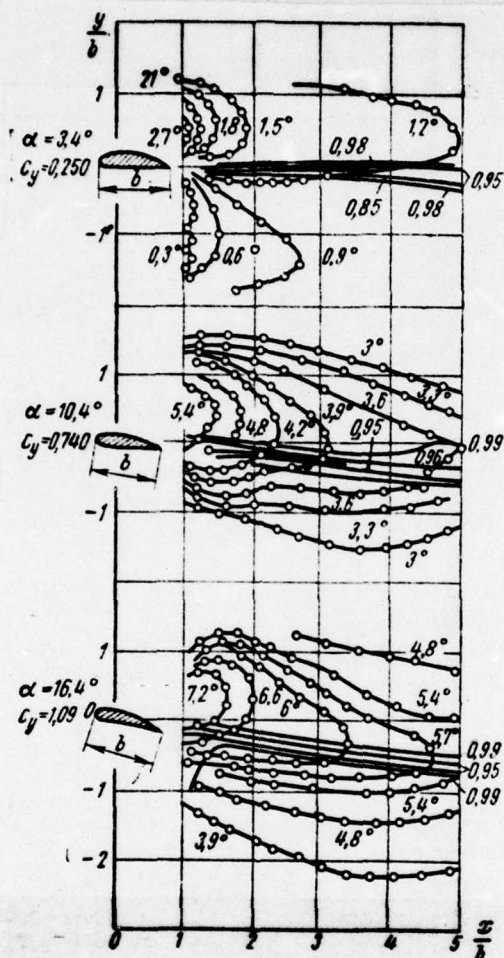


Fig. LX.42. Field of velocities and tapers after wing.

Page 394.

As showed experiments, at high subsonic, transonic and supersonic velocities the wing planform plays not less the significant role, than the form of airfoil/profile. At these velocities had extensive

application wings whose planform gives the possibility to utilize an effect of slip and three-dimensional/space flow, namely: the sweptback wings and low-aspect-ratio wings.

If rectangular infinite-span wing is turned at angle χ to the direction of the incident flow, then velocity v_0 can be decomposed into two components (Fig. IX.43): $v_0 \cos \chi$ that lies at plane of cross-section, and $v_0 \sin \chi$ directed along wing. For lift and drag of wing, streamlined thus, has a value only composing velocities, normal to the leading edge: $v_0 \cos \chi$. Flow in span direction does not have (neglecting of friction) effect on wing pressure distribution and, therefore, on lift.

In view of the fact that the velocity of flow around yawing (swept) wing, which is determining the picture of the distribution of pressures, is decreased in comparison with velocity of incident flow, local pressures on wing also will fall, and value P_{min} , which characterizes the beginning of shock stall, decreases, which will lead to the increase M_{sp} , whose value can be found from the expression

$$M_{sp, \chi} = \frac{M_{sp, \chi=0}}{\cos \chi}.$$

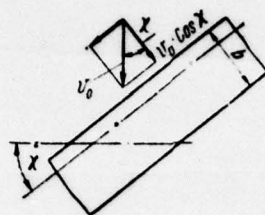


Fig. IX.43. It is slided wing.

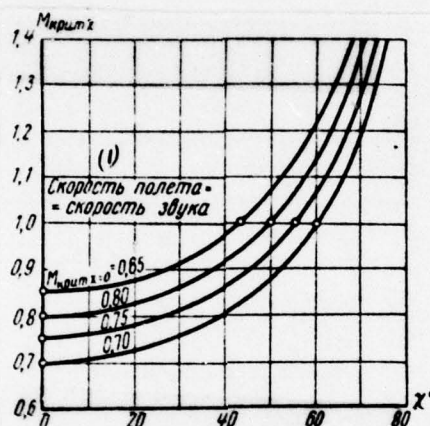


Fig. IX.44. The empirical dependence of critical Mach number of the sweep angle of wing.

Key: (1). Velocity of flight = speed of sound.

Page 395.

In actuality due to the finiteness of the span of the wing, presence of fuselage, bend of center line (middle effect), that leads to the decrease of the effect of slip in center section, change $M_{кр}$

for the sweptback wing of the direct/straight (positive) or reverse/inverse (negative) sweepback (see Fig. XI.37) it occurs not proportionally $\cos \chi$, but it is more complicated:

$$M_{\text{кр}} \chi = M_{\text{кр}} \chi=0 \left(1 + \frac{1 - \cos \chi}{1 + \cos \chi} \right).$$

Experimental dependences $M_{\text{кр}} = f(\chi)$ are given in Fig. XI.44 and $c_x = f(\chi \text{ and } \lambda)$ in Fig. IX.45.

Since the lift (pressure coefficients) of the sweptback wing falls proportional to the square of the cosine of sweep angle ($v_n = v_0 \cos \chi$),

then the aerodynamic coefficients of constant angle of attack can be determined from the following approximations:

$$\begin{aligned} c_{Y_{\text{ср}}} &= c_{Y_{\text{нр}}} \cos^2 \chi, \\ c_{X_{\text{ср}}} &= c_{X_{\text{нр}}} \cos^3 \chi, \\ m_{Z_{\text{ср}}} &= m_{Z_{\text{нр}}} \cos^2 \chi, \\ \frac{dc_Y}{d\alpha_{\text{ср}}} &= \left(\frac{dc_Y}{d\alpha} \right)_{\text{нр}} \cos^2 \chi, \\ k_{\text{ср}} &= k_{\text{нр}} \frac{1}{\cos \chi}. \end{aligned}$$

Experimental data on the measurements of aerodynamic coefficients give, depending on the parameters of wing, somewhat different from computed values of coefficients (within the limits of proportional dependence from $\cos \chi$ to $\cos^2 \chi$). The experimental results of the tests of some sweptback wings are given in Fig. IX.46.

The character of the distribution of pressure in the sweptback wings differs significantly from the distribution of pressure in

usual ones. Transverse currents in boundary layer (from center to end/leads in wings with sweepback and from end/leads to center in wings with the sweepforward) lead to earlier flow separation. This occurs for wings with sweepback not only due to transverse currents, as suction boundary layer from center section and increasing local importance C_r but as a result of changing the effective angle of attack.

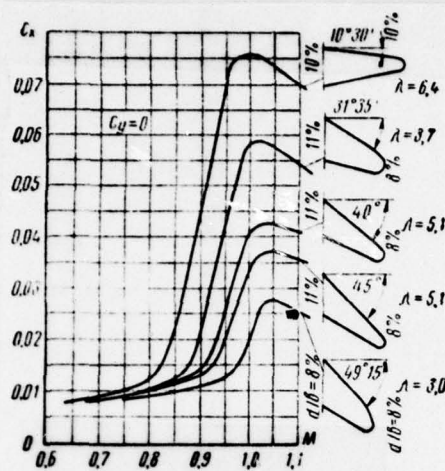


Fig. IX.45. Effect of sweepback and value of elongation on wing drag in transonic range (according to the results of the tests of the symmetrical airfoil/profiles of series NASA 65A).

Page 396.

In wings with sweepback, effective angle toward the end increases, and in the middle part it decreases as a result of the fact that the induced velocity increases in the middle of wing and decreases to its end/leads. On leaving to high angles of attack, the disruption/separation will occur more earlily on tips of the wing where c_l airfoil/profile more earlily it reaches its maximum value (Fig. XI.47).

In wings with the sweepforward, the mean sections have large

lift, transverse currents raise the stability of the flow around end sections, pressure on upper surface falls to the center of wing and disruption/separation begins in mean sections. Moment characteristics and stability in wing with sweepback are less favorable, than in wings with the sweepforward, due to reduction in the aileron-effectiveness derivative and emergence of the moments of yawing of bank and destabilizing torque/moments.

The elimination of the adverse characteristics of the sweptback wings at low speeds (high angles of attack) is possible because of the application/use of the corresponding airfoil/profiles, mechanization, the selection of planform, the contraction and other means, which improve the evenness of course curved $c_y = f(\alpha)$ and prevent/warning premature disruption/separations. In practice for transonic and supersonic velocities, will find more wide application the wings with sweepback, since the exhibited in wings with the sweepforward directional instability and harmful interference with fuselage (at high velocities) with more difficulty was removed than end disruption/separations, but in wings with sweepback.

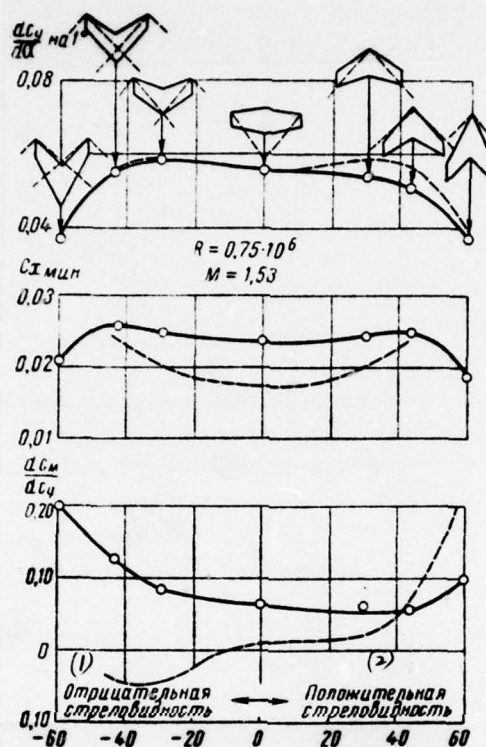


Fig. IX.46. The effect of sweepback on the coefficients of aerodynamic forces ($M=1.53$): — - experiment; --- - linear theory (isolated/insulated wing).

Key: (1). Negative sweepback. (2). Positive sweepback.

Page 397.

The sweep angle of wing for this Mach number must be selected in such a way that entire/all leading edge lie/rests within disturbance

cone, i.e., must be maintained relationship/ratio $\varphi > (90^\circ - \chi)$ (Fig. IX.48). If $\varphi < (90^\circ - \chi)$, then advantages from sweepback will be considerably less. Approximately it is possible to count that the sweepback $\chi = 45^\circ$ gives considerable effect to numbers $M=1.4$, $\chi = 55^\circ$ to $M=1.7$.

Low-aspect-ratio wings. With an increase in the flight mach number (after $M \approx 1.5-1.7$) the sweepback wings not always provide the preservation/retention/maintaining of satisfactory lift-drag ratios. Furthermore, the sweepback wings have some structural/design deficiency/lacks, difficultly surmountable with their form. Due to center-of-pressure travel, back/ago in the sweepback wing appears the large supplementary twisting, which can be structurally removed by the application/use of a wing of triangular form (Fig. IX.49). Therefore for supersonic flight speeds, will have extensive application the low-aspect-ratio wings ($\lambda < 2.5$), having different planform. The basic difference for low-aspect-ratio wings from the wings of usual elongations ($\lambda > 3.5$) lies in the fact that the flow around each section it is not possible to consider being independent of the flow around the adjacent ones (i.e. is inapplicable the hypothesis of "flat/plane sections").

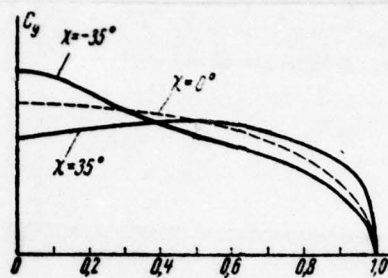


Fig. IX.47. Effect of sweepback on lift distribution along spread/scope.

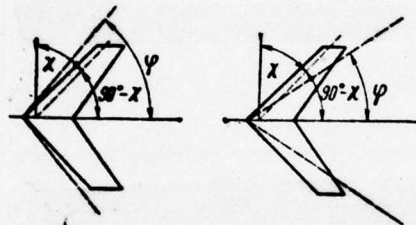


Fig. IX.48. Diagram of the layout of the disturbance cone of the relatively leading edge of the sweptback wing. Broken line showed generatrix of wave cone.

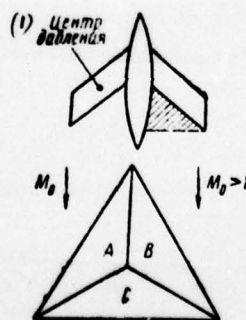


Fig. IX.49. The delta wing (hardness of the sweptback wing will

increase, if it will occupy the shaded region).

Key: (1). Center of pressure.

Page 398.

Finite-span wing and in the supersonic flow flows itself differently, than in subsonic. Zones A (Fig. IX.50), that lie within disturbance cones exist zone of tip effect. Zones B are characterized by the same conditions of flow, kA and infinite-span wing. If zones A are removed (are cut), then tip effect will disappear and the wing of a similar planform will flow itself then just as infinite-span wing. Wing drag of final spread/scope in the supersonic flow is composed of profile drag (pressure drag and friction) and wave, that not depending on elongation and induced drag. ¹.

FOOTNOTE ¹. In expression for induced drag $c_{xi} \frac{1+\delta}{\pi\lambda} c_l$ the value of coefficient δ are equal to 0.5-0.6 - for delta wings and 0.08-0.18 - for the tapered wings. ENDFOOTNOTE.

The overflowing of air with lower to the upper surface and acting only within Mach cone (zone A, see Fig. IX.50) leads (during small wing aspect ratios) to a considerable decrease of evacuation/rarefactions on airfoil/profile and an increase M_{xp} .

Induced drag at supersonic speeds is significantly lower than the wave (Fig. IX.51)

$$C_{X_{\text{DO.18}}} = \frac{c_l \sqrt{M^2 - 1}}{4}$$

depends on the so-called given elongation $\lambda/\overline{M^2 - 1}$, flight mach number and lift coefficient. If we cut the end/faces of wing so that the angle $\tau > \phi$ (Fig. IX.52) with $\sin \phi = c/v$, then induced drag completely disappears.

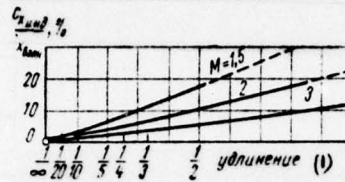
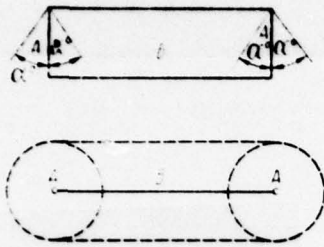


Fig. IX.51.

Fig. IX.50. Flow around the rectangular wing of the supersonic flow.

Fig. IX.51. Dependence of induced drag of the rectangular wing on elongation.

Key: (1) elongation.

Page 399.

From the examination of Fig. IX.53 and IX.54, are visible the considerable advantages of low-aspect-ratio wings at supersonic flight speeds. At low speeds the low-aspect-ratio wings have the aerodynamic characteristics, which differ from the wing characteristics of usual elongations (Fig. IX.55). Is especially noticeable nonlinear character $c_y = f(\alpha)$. In spite of decrease c_y (or displacement $c_{y_{max}}$ at angles to 40°), which requires the application/use of considerable high-lift device of low-aspect-ratio wings for providing the normal landing, low resistance of such wings

at supersonic speeds and their structural/design advantages they provide with them increasing application/use at supersonic speeds both for the aircraft and for rockets.

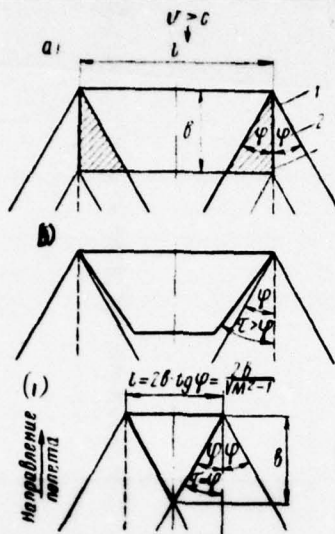


Fig. IX.52. Wing planform at supersonic speed: a - rectangle; are shaded the sections, calling induced drag, which depends on the value of ratio/relation $\frac{b \tan \phi}{l}$ (given elongation); b - trapezoid, by the beveling of the cones of wing at angle $\tau > \phi$ is removed induced drag, this wing equivalently to infinite-span wing (recommended value of $\tau - \phi = 15^\circ$); c - delta wing with spread/scope $l_{max} = \frac{2b}{\sqrt{M^2 - 1}}$ theoretically to equivalently rectangular infinite-span wing. 1 - compression wave; 2 - mach angle.

Key: (1) the direction of flight.

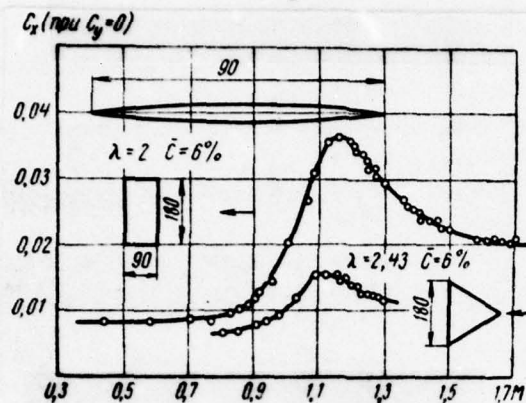


Fig. IX.53. Dependence $c_x = f(M)$ for low-aspect-ratio wings.

Page 400.

In practice will find use of various kinds the wings, combining in themselves the cell/elements of sweepback with a small elongation. Figure IX.56 depicts characteristics at the zero angle of attack of the models of the fine/thin delta wings, tested into four wind tunnels of the gas-dynamic laboratory of Karman (USA) in the range of numbers $M=8-22$ and of Reynolds numbers from 5000 to $4 \cdot 10^6$ at the different values of the ratio of the temperature of wall (T_w) to temperature of stagnation (T_0). As can be seen from results, at hypersonic speeds it is possible to expect a powerful increase in resistance mainly because of liquid resistance, proportional to ratio/relation $\frac{M}{\sqrt{Re}}$.

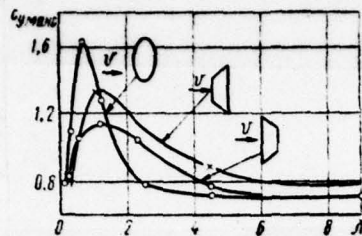


Fig. IX.54. Dependence $c_{y,max} = f(\lambda)$ for the wings of different planform.

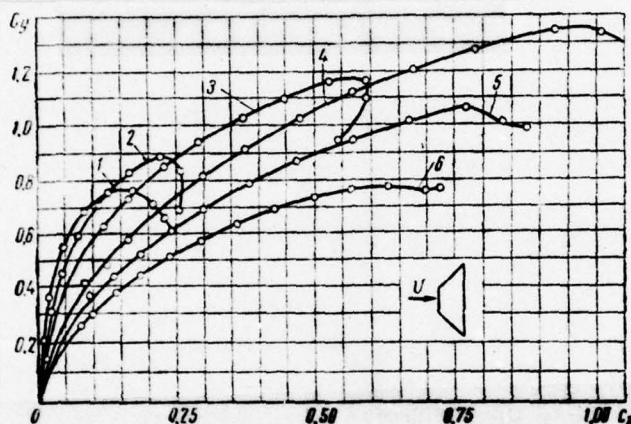


Fig. IX.55. Polars of the plates of trapezoidal planform of different elongations, obtained at the low speed:

1 - $\lambda = 9.0$; 2 - $\lambda = 4.5$; 3 - $\lambda = 2.25$; 4 - $\lambda = 1.125$; 5 - $\lambda = 0.563$;
6 - $\lambda = 0.282$

Page 401.

Low-aspect-ratio wings ($\lambda=1-2$) have a series of other advantages. They are favorable from the point of view of strength and weight due to the small bending moments of wing. An increase in the airfoil chord allows on the same level of technology of production to decrease the relative surface roughness, which favorably affects their aerodynamic characteristics. These wings ($\lambda=1-2$) have a series

of advantages, also, from the point of view of stability and controllability, which is connected with the fact that mean aerodynamic center of wing (i.e. the point relative to which the moment of aerodynamic forces it remains constant during a change in the angle of attack) relatively little it is displaced during transition from subsonic ones to supersonic speeds (Fig. XI.57) and, consequently, also little change longitudinal-behavior characteristics.

Mutual effect. The aerodynamic characteristics of different flight vehicles or bodies of intricate shape, comprised of simple cell/elements, in the first approximation, (when conducting precomputations) are examined under the assumption of the independent flow. Thus, for instance, polar of aircraft is constructed on the basis of the wing polar, characteristics of fuselage, tail assembly and the like considering that is absent the effect of these cell/elements on each other or the interference.

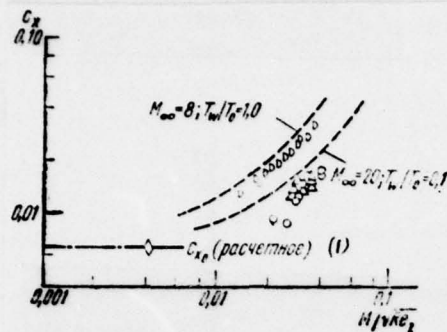


Fig. IX.56. Resistance of delta wing under zero lift.

Key: (1) (calculated).

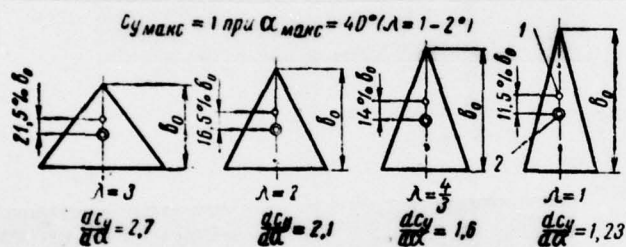


Fig. IX.57. The effect of wing aspect ratio on the displacement of focus at subsonic and supersonic speeds: 1 - aerodynamic focus at subsonic speed; 2 - the same, at supersonic speed.

Page 402.

In actuality fuselage distorts the flow, which flows around wing, and wing, in turn, changes the flow around fuselage. The character of this mutual effect, called interference, depends substantially on mutual location and form of wing and fuselage.

If in the site of the joint of wing and fuselage appears the expanded flow (Fig. IX.58), then as a result of the diffuser effect of flow separations on wing occurs at smaller angles of attack. The elimination of diffuser effect with the aid of "fillets" (Fig. IX.58) leads to the more favorable flow: breakaway begins at high angles of attack, are improved polar and stability characteristics of aircraft (Fig. XI.59). The effect of mutual wing arrangement and fuselage is shown on Fig. IX.60. Downwash from wing exerts a substantial influence on the flow around tail assembly, effectiveness of which depends on their mutual location.

The interference in certain cases can render/show not by "harmful", but "useful", i.e., such, in the presence of which resistance of the combination of cell/elements will be lower than the sum of resistances of components during their isolated/insulated flow. However, in the majority of the cases, interference leads to deterioration in the aerodynamic characteristics. Especially high value it has at high speeds of motion, when an insignificant local increase in the velocity leads to decrease M_{cr} and premature education/formation of supersonic zones, shock waves and increase of wave impedance. On these reasons for the section of fuselage in the region of the connection to it of wing, somewhat adjust (according to

the "rule of areas") and attain because of this decrease of harmful interference (Fig. IX.61).

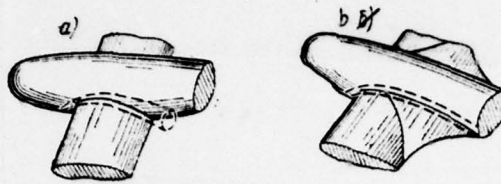


Fig. IX.58. The coupling of wing with the fuselage: a - diffuser effect in coupling; b - fillet decreases the diffuser effect.

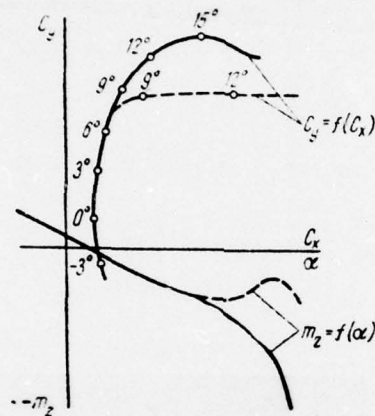


Fig. IX.59. The effect of fillets on the aerodynamic characteristics of the aircraft: — - with fillet; --- - without fillet.

Page 403.

High value has interference, also, for the characteristics bluff bodies. Thus, for instance, drag coefficient of the antenna, comprised of round ducts, proves to be substantially greater than the drag coefficient of cylinders of the same Re numbers.

The theoretical determination of the interference of different

parts of the apparatus is very hinder/hampered. From these reasons the experimental determination of the aerodynamic characteristics of the bodies of intricate shape is necessary even when are known the characteristics of their component elements. Especially high value they have this testing for the determination of moment characteristics and stability characteristics and controllability of the various kinds of flight vehicles, and also during the determination of the power effect of flow on the bodies of complex configuration.

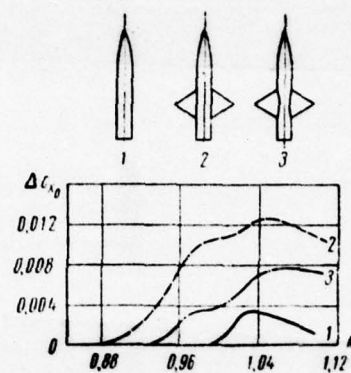
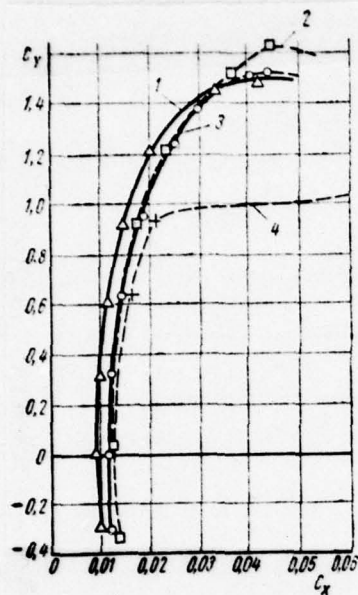


Fig. IX.61.

Fig. IX.60. The effect of mutual wing arrangement and fuselage on the aerodynamic characteristics of the aircraft: 1 - isolated/insulated wing; 2 - upper wing arrangement; 3 - average wing arrangement; 4 - lower wing arrangement.

Fig. IX.61. Effect of the local compression of fuselage.

Flow in channels.

Page 404.

Chapter X.

Flow in channels.

§ X.1. Flow in ducts.

Flow in ducts is one of the most investigated regions of turbulent flow. These obtained during investigations results have important value not only for numerous areas of technology, but also for the understanding of the phenomena, which occur about plate or about bodies with the surface, outlined by flow lines. In the technology of the characteristic of flow in ducts, they are utilized first of all for determining resistance during the motion of liquid, its expenditure/consumption through the duct and required the pressure differential for the realization of flow.

With the inflow of liquid from large reservoir into duct with round cross-section for the extent/elongation of certain section, is formed the initial (input) flow, in which the distribution of the speed across section in proportion to removal/distance from entrance changes. At first the velocity profile uniform, then under the effect of frictional forces is extracted and at certain distance from entrance takes the final form. The length of initial section depends on the pattern of flow and Reynolds number. During laminar flow $l_0 = 0.03 \text{ dRe}$ (more precise, 0.02875 dRe , according to Shiller), with turbulent l_0 is three or four times shorter.

For obtaining assigned rate of flow through the duct, it is necessary to create pressure difference in the beginning and end/lead of the duct. The value of pressure difference depends on the ductility/toughness/viscosity of gas, heat exchange through the walls of duct and surface condition of walls. This value characterizes resisting forces. Consequently, in the general case the required dimensionless pressure differential, referred to velocity head:

$$\frac{\Delta p}{\rho \frac{v^2}{2}} = f\left(\frac{\Delta l}{D}, \alpha, \text{Re}, M, \text{Pr}\right) \quad \text{или} \quad \frac{\Delta p}{\Delta l} = \frac{\rho v^3}{2D} \lambda(\text{Re}, M, \alpha, \text{Pr}),$$

Key: (1). or.

where λ (Re, M, α , Pr) — drag coefficient.

Page 405.

For infinitesimal cut of duct Δl , it is possible to count that the dependence of pressure differentials on the parameters indicated will be linear. If the phenomena of heat exchange can be disregarded, then flow will not depend on number Pr, but with small pressure differentials also on Mach numbers and α , since a change in the temperature along the duct does not affect flow. In this case, the speed and density will be constants, but coefficient λ will depend only on Re number.

In practice, especially for a gravity solution, the pressure differential they replace by pressure head ΔH . The expression of losses of head along the length of conduit/manifold

$$\Delta H = \frac{\lambda}{4} \cdot \frac{S}{F_0} \cdot \frac{\rho v^2}{2} = \lambda \frac{l}{D_r} \cdot \frac{\rho v^2}{2},$$

where D_r — hydraulic diameter ($D_r = D$ for a round duct, $D_r = \frac{4F_0}{U_0}$ — for rectangular cross section, here U_0 — perimeter);

F_0 — cross-sectional area;

S — rubbing surface;

l - length of the section of the conduit/manifold, for which is determined resistance.

During steady viscous motion in cylindrical pipe, the speed in its cross section changes according to parabolic law (poiseuille equation). The pressure differential, expressed through average speed v :

$$\Delta p = 8\mu \frac{lv}{Re^3}$$

or, bearing in mind that

$$Re = \frac{\rho v D}{\mu},$$

we will obtain the formula of the Darcys

$$\Delta p = \frac{64}{Re} \cdot \frac{l}{D} \cdot \frac{\rho v^2}{2} = \lambda \frac{l}{D} \rho \frac{v^2}{2} = \lambda \frac{l}{D} \cdot \frac{\rho v^2}{2},$$

where $\lambda = 64/Re$ - coefficient of friction drag or the "coefficient of friction" during laminar flow of liquid in smooth & round cylindrical pipe.

FOOTNOTE 1. Ducts are considered smooth, if $\epsilon_{\text{npes}} = \frac{k}{D_r} = 17.85 Re^{-0.875}$.

ENDFOOTNOTE.

This theoretical dependence is confirmed well to numbers $Re=2000$ ($\lg Re=3.3$) by numerous experiments (Fig. X.1) and does not depend on the roughness of the walls of duct.

Page 406.

With the large Re numbers, usually occurs the turbulent flow and here for determining the coefficient of friction depending on Re number, widely are applied semi-empirical dependences. For the range of Re numbers from 2000 to $1 \cdot 10^5$ it is possible to use Blasius's formula

$$\lambda = \frac{0,3164}{(Re)^{0,25}}.$$

With numbers $Re=10^5-4 \cdot 10^5$, is suitable the formula of Stanton and Pannel

$$\lambda = 0,00357 + \frac{0,3052}{(Re)^{0,25}}$$

or the formula of Lang

$$\lambda = 0,01 + 1,77 Re^{-0,5}.$$

For calculations over a wide range of Re numbers (from $1 \cdot 10^5$ to $1 \cdot 10^6$) is convenient the formula of Nikuradze and Lis

$$\lambda = 0,0032 + \frac{0,221}{(Re)^{0,237}}$$

or the equation

$$\frac{1}{\lambda} = 2 \lg (Re \sqrt{\lambda}) - 0,8,$$

called the universal law of resistance of Prandtl for smooth pipes. This formula is checked experimentally to numbers $Re=3.4 \cdot 10^6$ and it is possible to use within limits $10^5 < Re < 10^6$. Exemplary/approximate values $\lambda=f(Re)$:

Re	4000	12 000	60 000	180 000	840 000	10 800 000
λ	0,04	0,03	0,02	0,016	0,012	0,008

However, all the given formulas are suitable for smooth pipes. The roughness of the walls of ducts during turbulent flow increases resistance which depends with this not only on Re number, but also on the roughness:

$$\varepsilon = \frac{k}{D} \left(\begin{matrix} (1) \\ \text{или} \end{matrix} \frac{k}{r} \right).$$

Key;: (1). or.

By numerous experiments it is established, that in rough ducts: with the increase of Re number the coefficient of friction approaches the constant value, which depends only on the degree of roughness ξ , i.e., resistance becomes proportional to the square of speed.

FOOTNOTE 1. Roughness is created by deposition on the surface of the duct of grains of sand of the specific size/dimensions. ENDFOOTNOTE.

The quadratic law of resistance in ducts with greater roughness begins to be exhibited with the smaller Re numbers.

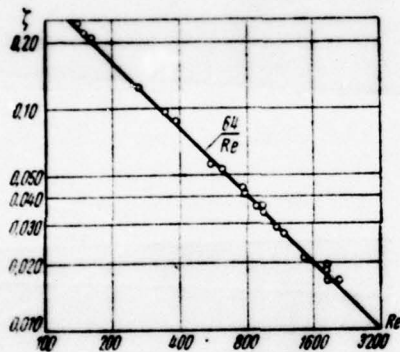


Fig. X.1. Dependence $\zeta=f(Re)$ for a round duct.

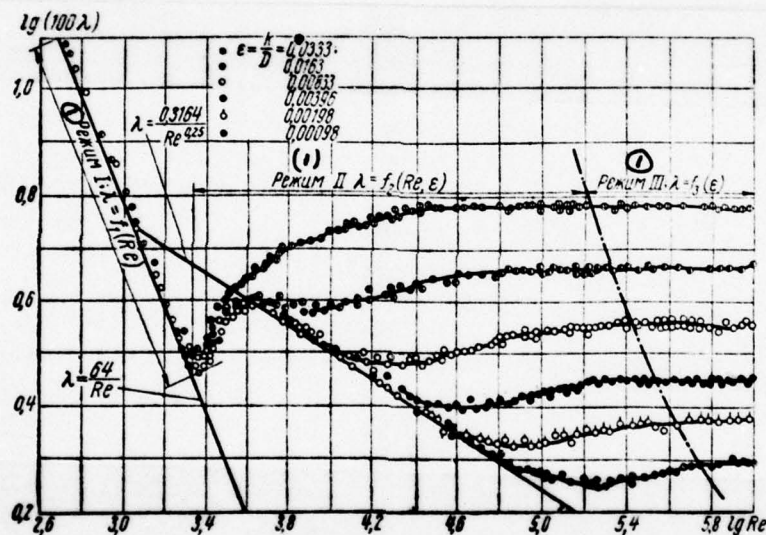
Page 407.

Determination $\lambda=f(Re \text{ and } \xi)$ can be produced on Nikuradze formula

$$\frac{1}{\sqrt{\lambda}} = 1.74 + 2 \lg \frac{1}{\xi}$$

(for $Re > 4.5 \times 10^4$), and also on experimental dependences (Fig. X.2). In real ducts the roughness depends on the quality of finish of surface

and settling of the particles, transferred by liquid. However, as will show experiments of I. Ye. Idel'chik with the ducts, having natural roughness, Nikuradze formula was valid also for real ducts, if we determine according to medium altitude of the prominence/protuberances of roughness.



Page 408.

During transition to the ducts of noncircular cross section, the drag coefficient, other conditions being equal, will change which can be taken into account on the basis of experimental data or on the following formulas (for laminar flow):

- 1) for the ellipse where Re is referred to the minor axis:

$$\lambda = \frac{64}{Re} \cdot \frac{a^2 + b^2}{3a^2 - b^2},$$

here a - semimajor axis; b - semiminor axis;

- 2) for equilateral triangle

$$\lambda = \frac{160}{3Re};$$

- 3) for the rectangle

$$\lambda = \frac{64}{Re} \varphi,$$

where φ - correction factor, depending on the ratio/relation of sides (for $Re < 2000$):

$\frac{a}{b}$	0,1	0,2	0,4	0,6	0,8	1,0
φ	1,34	1,2	1,02	0,94	0,9	0,89

- 4) for the square

$$\lambda = \frac{56,9}{Re}.$$

Re numbers are given relative to a hydraulic radius of duct.

For turbulent flow in noncircular ducts with rough walls, they use different empirical dependence. Thus, for instance, for the duct of the rectangular cross section

$$\lambda_{np} = \varphi \lambda_{np, \text{pyr.}}$$

Values of coefficient φ depending on Re number for a rectangle with the ratio/relations of sides within limits to 0.7-1.0:

Re	$2 \cdot 10^4$	$4 \cdot 10^4$	$6 \cdot 10^4$	10^5	$1.5 \cdot 10^5$
φ	0.89	0.94	0.96	0.99	1.0

Investigations during flow in ducts with high subsonic and supersonic speeds showed that for smooth pipes (in the absence of heat exchange with environment) the drag coefficient does not virtually depend on Mach number (Fig. X.3). As a result of speed change along the length of duct, changes the temperature and, consequently, also the coefficient of ductility/toughness/viscosity and Re number. The coefficient of ductility/toughness/viscosity weakly depends on temperature (for air, for example,

$$\mu \cdot 10^6 = 1.712 \cdot \sqrt{1 + 0.003665 t^\circ \text{C}} \times (1 + 0.0008 t^\circ \text{C})^{(1)} \text{ или } \frac{\mu}{\mu_0} = \frac{T}{273}^{-\frac{3}{4}}$$

Key: (1). or.

The drag coefficient of the high values of Re number changes insignificantly. Thus, during the calculation of the course of gas in ducts it is possible to use the results of the available numerous investigations of the motion of water in ducts.

Page 409.

During the study of flow in ducts, exit cone/diffusers and nozzles whose walls form small angles with the axle/axis of flow, utilize a concept of the average speed (and of average density). Average speed w is determined by the ratio of volumetric flow rate to sectional area

$$w = \frac{\int u dF}{F},$$

where u - true airspeed whose distribution over section makes it possible to find w .

During laminar flow in cylindrical pipe, the average speed is equal to the half the maximum speed in this section. During turbulent flow the velocity distribution law changes and the ratio/relation to the average speed to maximum depends on Re number. According to Nikuradze data, for the incompressible fluid with the large Re

numbers

$$u = u_{\max} \left(1 - \frac{r}{R}\right)^m,$$

where R - radius of duct; r - current radius; u_{\max} - speed on the axle/axis of duct;

Exponent $m=f(Re)$. With $Re=10^5$ $m=1/7$; with $Re=3 \cdot 10^6$ $m=1/10$.

The dependence of the ratio/relation to the average speed to maximum can be obtained from the expression

$$\frac{w}{u_{\max}} = \frac{2}{(m+1)(m+2)},$$

which it is correct at high speeds (Fig. X.4).

The nonuniformity of density has the great value in the absence of heat exchange and can be for gases estimated on formula

$$\frac{\rho}{\rho_{\max}} = \frac{1 - \frac{\kappa-1}{\kappa+1} \frac{u_{\max}^2}{a_0^2}}{1 - \frac{\kappa-1}{\kappa+1} \frac{w^2}{a_0^2}} = \frac{1 - \frac{\kappa-1}{\kappa+1} \frac{(m+1)^2 (m+2)^2 \lambda^2}{4}}{1 - \frac{\kappa-2}{\kappa+1} \lambda^2},$$

where

ρ_{\max} - it corresponds to maximum speed;

ρ - average density over section;

λ - given speed.

Let us note that the nonuniformity of density is considerably less than the nonuniformity of speed over section.

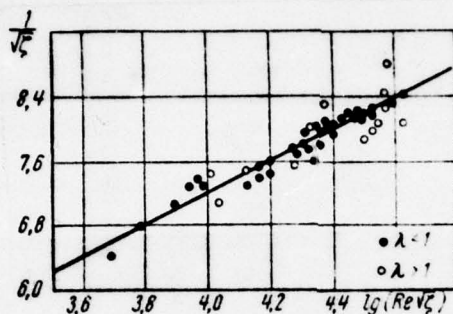


Fig. X.3. Law of resistance for smooth tube during flow of compressible liquid.

Page 410.

Thus, for instance, for air with $Re=3 \cdot 10^4$ and $w/u_{max}=0.87$ ($n=1/10$) for number $M=1$ value $\rho/\rho_{max}=0.93$, for lower speed this difference is still less. On these reasons during the course of the imperfect gas when occurs intense heat exchange and in section is establish/installed constant temperature, density over section (keeping in mind pressure constancy) will also be constant.

The equalization (strain) of the velocity profile produces change the drag coefficient which can be determined depending on the type of duct and character of the distribution of the speed in cross section. Thus, for instance, for round and flat/plane ducts drag

coefficient $\xi = \frac{\Delta p}{\rho v^2}$ depending on exponent m :

m	1	0,74	0,5	0,25	0,147
(1) Круглая труба	0,7	0,36	0,16	0,04	0,02
(2) Плоская труба	0,33	0,19	0,10	0,04	0,02

Key: (1). Round duct. (2). Flat/plane duct.

§ X.2. Flow in exit cone/diffusers and nozzles.

Exit cone/diffusers. As was said earlier (see Chapter VII), exit cone/diffuser serves for converting kinetic energy of flow into energy of pressure and is one of the most widely used and important cell/elements in many aeromechanical equipment/devices and gas machines (wind tunnels, jet engines, turbines, ejectors and so forth). The degree of the perfection of exit cone/diffuser in a decisive manner affects both the efficiency and the quality of gas machines, since usually in exit cone/diffuser in comparison with other cell/elements occur the greatest irreversible energy losses. In diffusers, in contrast to nozzles and nozzles, are created the conditions, favorable for boundary-layer separation (see § V.I) and of emergence of the disruption/separations, which are accompanied by considerable losses.

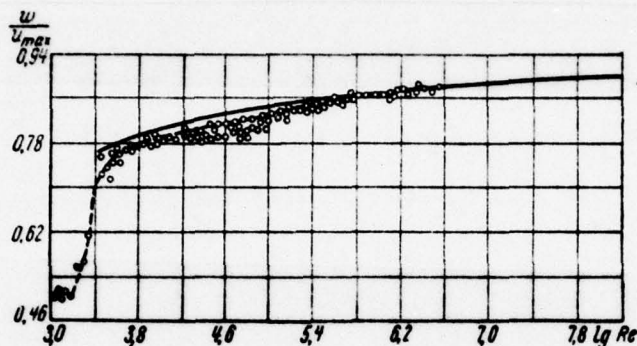


Fig. X.4. Dependence on Re number of the ratio/relation to the average speed to maximum.

Page 411.

As show numerous experimental investigations, the drag coefficient of subsonic exit cone/diffuser does not virtually depend on Mach number at the entrance into it (see Fig. VII.11), but it depends on the expansion ratio of flow (length of exit cone/diffuser), of expansion angle, uniformity of the field of inlet velocities, Re number of surface condition and finally on the form of cross section. In aeromechanical practice are encountered the exit cone/diffusers of diverse types, "working" under varied conditions of the course through them of liquid or gases. Independent of the

designation/purpose of exit cone/diffuser it is always desirable to have not only minimum drag coefficient, but also as far as possible the uniform field of outlet velocities.

The evaluation of diffuser losses it is accepted to produce depending on the speed in them. For exit cone/diffusers with subsonic inlet velocities the drag coefficient of the exit cone/diffuser I could be found from the expression

$$\zeta_x = \frac{2}{\pi M_1^2} \left(\delta - \frac{1}{2} \delta^2 \right),$$

where M_1 - number at the entrance into exit cone/diffuser;

δ - loss factor, equal to $\delta = \frac{p_0 - p'_0}{p_0}$, or, is more precise,

$$\delta = \frac{1}{F} \int \frac{p_0 - p'_0}{p_0} dF;$$

p_0 and p'_0 - total pressure at the entrance also at the end of the exit cone/diffuser (Fig. X.5).

Thus, after measuring total pressures p_0 and p'_0 , it is possible, knowing M_1 , to determine ζ and δ . However, measurements p_0 must be conducted taking into account the nonuniformity of inlet velocity into exit cone/diffuser and compulsorily out of boundary layer the pressure recovery factor

$$v_1 = 1 - \delta = \frac{p_1}{p_0}$$

serves for evaluating the qualities of exit cone/diffuser at high and supersonic speeds.

In view of the diversity of types and forms of exit cone/diffusers, especially used at low speeds, in the practice of the determination of drag coefficient ζ , they use various kinds empirical dependence of the type

$$\zeta = \zeta_{\text{specu}} + \zeta_{\text{trp}}.$$

Values ζ_{specu} and ζ_{trp} are determined depending on the degree of expansion, expansion angle, form of cross section, Re number, of degree of roughness and of degree of uniformity of flow at entrance.

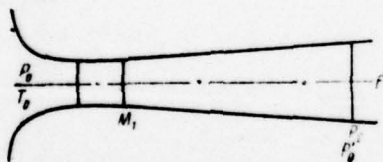


Fig. X.5. Diagram of exit cone/diffuser.

Page 412.

For conical, tapered and pyramidal exit cone/diffusers (Fig.

X. 6)

$$\zeta = \varphi_{pacu} k d + \frac{\lambda}{8} e f,$$

where

$$\varphi_{pacu} = \frac{3}{2} \operatorname{tg} \frac{\alpha}{2} \sqrt[4]{\operatorname{tg} \frac{\alpha}{2}}$$

(for conical diffuser of $0 < \alpha \leq 40^\circ$) or

$$\varphi_{pacu} = 6.2 \operatorname{tg} \frac{\alpha}{2} \sqrt[4]{\operatorname{tg} \frac{\alpha}{2}}$$

(for $0 < \alpha < 25^\circ$ for rectangular and square exit cope/diffusers)

$$\begin{aligned} d &= \left(1 - \frac{F_2}{F_1}\right)^2, & f &= \frac{1}{\sin \frac{\alpha}{2}}, \\ e &= 1 - \left(\frac{F_2}{F_1}\right)^2, & k &= f \left(\frac{w_{max}}{w_0}\right). \end{aligned}$$

Changes k within limits with 1.2-1.8;

$$\lambda = f \left(\frac{w_0 D}{v}; \frac{k}{D_r} \right),$$

moreover λ is defined just as for ducts.

For the plane diffusers (Fig. X.7) value φ_{pacu} usually varies within the limits with 0.1-0.2:

$$\zeta_1 = \varphi_{pacu} k d + \frac{\lambda}{4} \left(\frac{a_2}{b_0} a + \frac{1}{2} e \right) f.$$

The values of coefficients φ_{pacu} , k , d , λ , f are determined to analogously preceding/previous, and the value of the coefficient

$$a = 1 - \frac{F_0}{F_1}.$$

In the case of flat/plane curvilinear cone (Fig. X.8)

$$\zeta \cong \varphi \sigma d \quad \left(\text{для } 0,1 \leq \frac{F_0}{F_1} \leq 0,9 \right),$$

where

$$\varphi_0 = f\left(\frac{l_A}{a_0}\right),$$

$$\sigma_0 = 1,43 - \frac{1,3F_0}{F_1}.$$

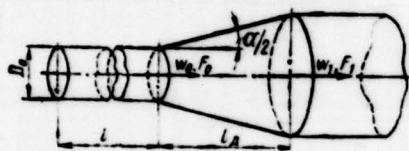


Fig. X.6.

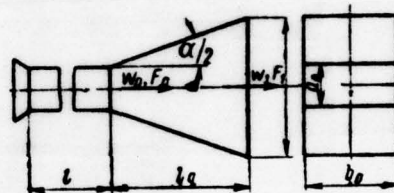


Fig. X.7.

Fig. X.6. The conical diffuser.

Fig. X.7. The plane diffuser.

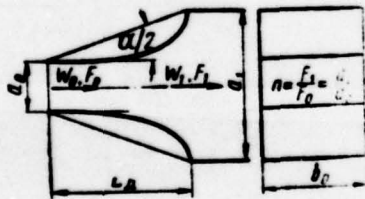


Fig. X.8. Flat/plane curvilinear cone.

For curvilinear cone of round and rectangular cross sections (Fig. X.9) is used the preceding/previous formula, if

$$0 \leq \frac{F_0}{F_1} \leq 0.9,$$

but here

$$\psi_0 = f\left(\frac{l_1}{D_0}\right).$$

In the presence of output resistance from exit cone/diffuser (Fig. X.10)

$$\zeta = \zeta_1 + \frac{\zeta_2}{n^2} \quad (1) \quad (\text{при } \alpha = 0-60^\circ),$$

Key: (1). with.

where ζ_1 - drag coefficient of exit cone/diffuser without equipment/devices at output;

ζ_2 - drag coefficient of equipment/devices at output from exit cone/diffuser.

At $\alpha > 60^\circ$ value $\zeta_2 = 1.2-1.3 \left(\zeta_1 + \frac{\zeta_2}{n^2} \right)$.

The most important design parameters of exit cone/diffuser, which are determining its quality, are aperture angle and expansion ratio of flow in exit cone/diffuser (F_1/F_0). Optimum angle lie/rests

within limits of 4-8°, and expansion ratio can be estimated by the permissible kinetic energy losses. The percent ratio to kinetic energy at the end of the exit cone/diffuser to initial.

$$\left(\frac{F_2}{F_1}\right)^2 \frac{\rho_1}{\rho_2} 100 = \left(\frac{1}{n}\right)^2 \frac{\rho_1}{\rho_2} 100.$$

For rough calculations it is possible to accept $\rho_1 = \rho_2$. Then with $n=4$ loss are 1/16 initial kinetic energies, and with $n=10$ they will be lowered to 1/100. Further increase in the length of exit cone/diffuser for increase n will lead to the considerable increase of losses to friction. The estimation of the power, required for the coating of diffuser losses depending on its drag coefficient ζ_A

$$N = Q \frac{w_1^2}{2} \left(1 + \frac{n-1}{2} M_1^2\right) \zeta_A.$$

where Q - mass flow rate of the gas through the exit cone/diffuser;

w_1 - inlet velocity into exit cone/diffuser.

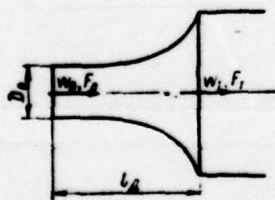


Fig. X.9.

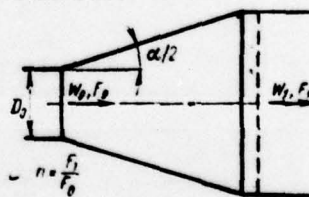


Fig. X.10.

Fig. X.9. Curvilinear circular diffuser.

Fig. X.10. Exit cone/diffuser with output resistance.

Page 414.

If we gear down of supersonic jet, draw down of channel, then in this case is formed virtually normal shock wave after which the speed will be subsonic. Further decrease in the velocity and pressure recovery can be produced in subsonic exit cone/diffuser. However, this method of stagnation of supersonic flow leads to the low pressure recovery factor (for example, see Fig. VII.41). More advisable is equipment/device of the exit cone/diffuser, in which the stagnation of supersonic flow occurs in the system of oblique shock waves.

In connection with development of jet/reactive technology and increase in the velocity of relative motion of bodies and gases, appears the need for decrease of the speed of flow from supersonic to small subsonic. This first of all is related to supersonic and hypersonic wind tunnels and installations, jet engines, gas turbines and compressors, etc.

The method of braking flow in the supersonic diffuser has basic effect on the pressure recovery in it, i.e., on the power, required for the realization of flow in the duct/contour, which includes exit

cone/diffuser. Thus, for instance, required power for operational provisions of supersonic wind tunnel with number $M=2.5$ in test section by the size/dimension of 1 m^2 composes with normal shock in the exit cone/diffuser (after jump it is equal to 0.93) of 8500 kW, with oblique and straight line - only 4500 kW. Pressure recovery factor in exit cone/diffuser when normal shock wave is present, and given speed λ_1 at the entrance

$$v = \frac{q(\lambda_1)}{q\left(\frac{1}{\lambda_1}\right)}$$

At values $\lambda_1 < 1.3-1.4$ ($M_1 < 1.37-1.51$) the normal-shock diffusers give comparatively small losses — $v = 0.75$, but at high values λ_1 , they become unfavorable. With oblique shock in exit cone/diffuser, the pressure recovery factor will be above:

$$v_2 = \frac{q(\lambda'_{2n})}{q\left(\frac{1}{\lambda'_{2n}}\right)},$$

where λ'_{2n} — the given speed in the direction, normal to jump (when $\lambda_{2n} = 1.6$, $v_2 = 0.83$).

Page 415.

If in exit cone/diffuser is realized the oblique shock, after which the speed remains supersonic and its transition to subsonic occurs in normal shock (Fig. X.11), then is the recovery factor of the exit cone/diffuser

$$v = v_2 v_1 v_A = \frac{q(\lambda_{2n})}{q\left(\frac{1}{\lambda_{2n}}\right)} \frac{q(\lambda_1)}{q\left(\frac{1}{\lambda_1}\right)} v_A,$$

here λ_1 - given speed after oblique shock,

v_A - the recovery factor of subsonic exit cone/diffuser after normal shock.

Value v depends on the angle of the slope of oblique shock and, as show calculations, it reaches $v=0.92$ in optimum case ($\sim 15^\circ$). During the deviation of slope angle from optimum within limits of $\pm 5^\circ$ value v remain high, approximately 0.9.

Exit cone/diffusers with several oblique shock waves provide the high values of the pressure recovery factor, also, of hypersonic speeds. Depending on Mach and Re numbers at entrance the exit cone/diffusers have different angles of taper, adjustable neck or angle of wedge shape (for providing the starting/launching of duct with a smaller pressure differential). In a series of cases for decreasing the losses, is applied the boundary-layer bleed (or the bypass of gas from test section into exit cone/diffuser). The typical experimental characteristics of the supersonic diffusers are represented in Fig. X.12.

During the transference of the results of experiments with the models of the supersonic diffusers for nature, one should especially thoroughly consider the conditions of similarity (Re numbers, M , ϵ , etc.), surface condition, condition for the convergence of the state of flow and of inlet boundary layer into exit cone/diffuser, etc. During use in the calculations of the values of the pressure recovery factors, obtained on experiments with models, it is desirable to take known supply on pressures for providing the proper flow through the exit cone/diffuser.

Nozzles. The nozzles and different form nozzles serve for the acceleration/dispersal of flow. The characteristics of these equipment/devices depend on their form, which in turn, is determined by the designation/purpose of nozzle (collector/receptacle). Especially thoroughly are selected wind-tunnels nozzle.

Nozzles, or collector/receptacles, are applied in various kinds machines and equipment/devices.

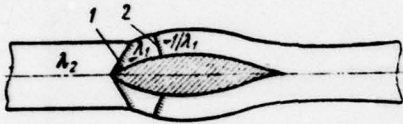


Fig. X.11.

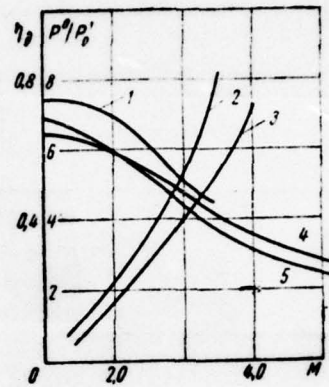


Fig. X.12.

Fig. X.11. The supersonic diffuser with the wedge: 1 - oblique shock; 2 - normal shock.

Fig. X.12. Experimental characteristics of the supersonic diffusers: 1 - exit cone/diffuser with wedge; 2 - open test section; 3 - enclosed test section; 4 - second-throat diffuser; 5 - open nose diffuser.

Page 416.

Nozzle configuration is important for the creation of the uniform field of inlet velocities in various kinds of conduit/manifolds. Figure X.13 shows the picture of flow upon the entrance into

direct/straight duct without collector/receptacle. The drag coefficient in this case attains significant magnitudes. The value of drag coefficient for this entrance equal to 1.0 depends on the ratio of the wall thicknesses of duct to its diameter (Fig. X.14).

Of rounding or equipment/device of conical inlet (Fig. X.15) the drag coefficient substantially decreases. If at the entrance into direct/straight duct are establish/installated washers, lattices or grid from metallic wires, then input losses depend on the clear area of entrance and they reach many tens of velocity heads (Fig. X.16).

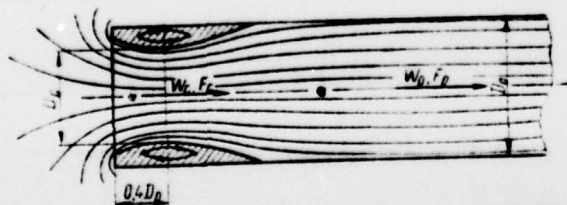


Fig. X.13.

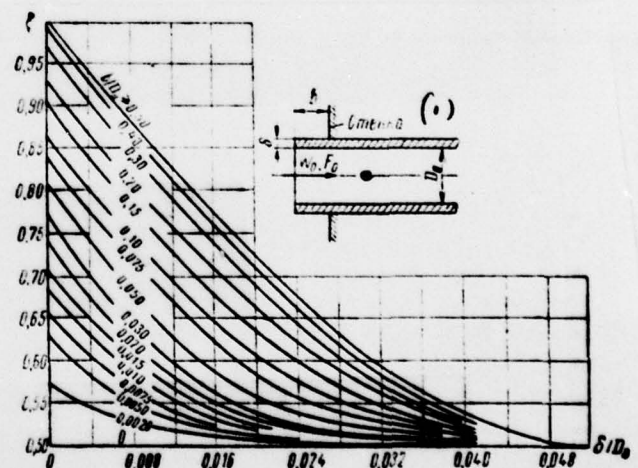


Fig. X.14.

Fig. X.13. Picture of flow upon the entrance into direct/straight

duct.

Fig. X.14. Drag coefficient for an entrance into the direct/straight duct: b - distance of the end/lead of the duct from wall; δ - the wall thickness of duct; D_0 - tube bore.

Key: (1). Wall.

Page 417.

For steady curvilinear nozzles resistance $\zeta = \zeta_{rp}$ can be defined just as ζ_{rp} for flat/plane curvilinear cone or conical diffuser. In the case of rectilinear converging nozzle section (Fig. X.17) drag coefficient

$$\zeta = \zeta_1 \left(1 + \frac{F_0}{F_1} \right) + \zeta_{rp},$$

where

$$\zeta_1 = f \left(\varphi, \frac{l}{D} \right).$$

ζ_{rp} is defined just as for an exit cone/diffuser.

The determination of the drag coefficients of different types of nozzles, converging nozzle sections and of collector/receptacles has high value for those cases when it is necessary to determine the

required head of fan for providing the flow of the gas through the system and when the specific gravity/weight of input losses and losses in transient sections is significant.

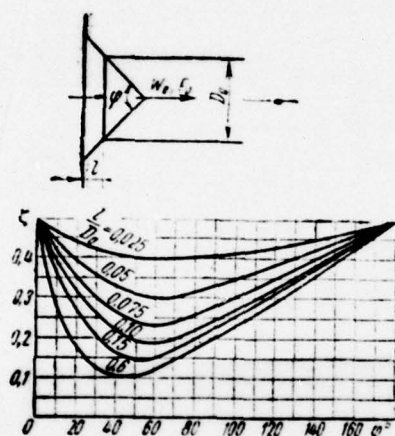


Fig. X.15. Conical entrance into duct.

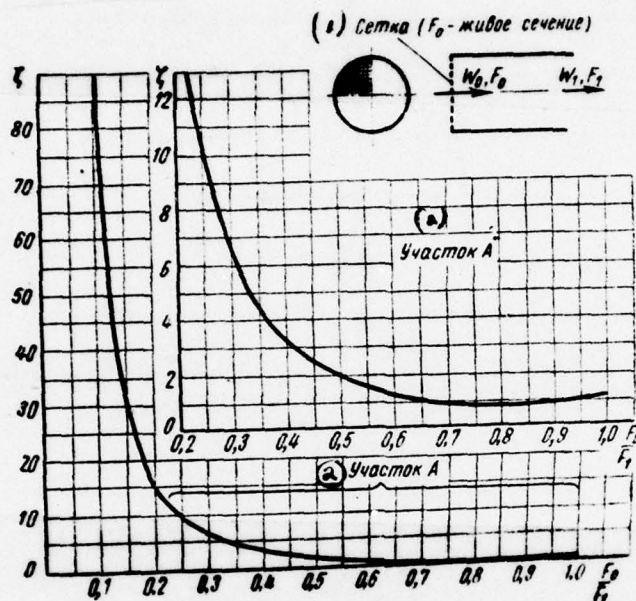


Fig. X.16. Grid at the entrance into direct/straight duct.

Key: (1). Grid (F_0 - clear opening). (2). Section.

Page 418.

For large jump/drops in the pressures, which occur in wind tunnels, the losses in nozzles comprise very low portion. So, for the rationally carried out subsonic nozzles magnitude of losses $\delta=1-\eta$ does not exceed 0.005, but for supersonic ones - 0.02. To wind-tunnels nozzle on these reasons is presented one requirement:

obtaining the uniform field of outlet velocities.

For low speeds the nozzle configuration can be carried out, for example, according to the Vitoshinskiy equation (see §VII.1). For obtaining supersonic speeds, are applied the Laval nozzles. For given speed (λ), on the basis of value, to which it is necessary to select the area of output F , on the basis of the equation of the constancy of the expenditure/consumption

$$F = \frac{F_x}{q(\lambda)},$$

where F_x - nozzle throat area, which it can be found for expenditure/consumption of Q :

$$Q = F_x \left(\frac{2}{\kappa + 1} \right)^{\frac{1}{\kappa - 1}} \sqrt{\frac{2\kappa}{\kappa + 1} p_0 \rho_0}.$$

Using the equation of adiabatic flow, it is possible to calculate the pressure

$$p = p_0 \left(1 - \frac{\kappa - 1}{\kappa + 1} \lambda^2 \right)^{\frac{\kappa}{\kappa - 1}},$$

where p_0 - the total pressure at the nozzle entry.

Decompression at the nozzle outlet lower than the calculated does not affect flow in nozzle. At design pressure the gas escape/ensues by parallel jet. During an increase in the pressure at output in nozzle edge, are formed the oblique shock waves, which

convert into the complex system of oblique and normal shocks with an increase in the pressure at output (Fig. X.18). With a considerable increase in the pressure at the output of gallop, they are formed already within nozzle, ever more approaching straight line, that causes the decrease of exit velocity (up to subsonic) and the deviation of flow from the direction of the axle/axis of nozzle, accompanied usually by boundary-layer separation, especially for nozzles with large angle of taper. In nozzles with small angle of taper, the jump even with small pressure differentials completes considerable oscillation/vibrations.

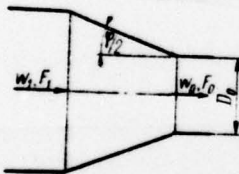


Fig. X.17.

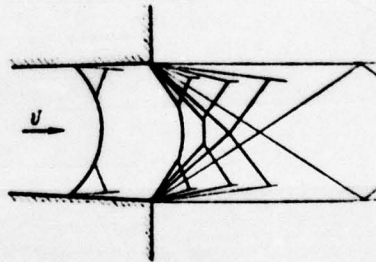


Fig. X.18.

Fig. X.17. Rectilinear converging nozzle section.

Fig. X.18. System of jumps at the nozzle outlet and within it.

Flow in nozzles at high speeds frequently is disrupted due to the education/formation of the condensation shocks, which represent actually sudden heat supply in certain section of nozzle and entailing a change in the temperature, density, pressure and gas velocity. Thus, for instance, at the outlet velocity, which corresponds $M=2$, the temperature of air descends to -113°C (for $T_0=15^{\circ}\text{C}$), in this case, the impurity/admixtures of water vapors, always available in gas, are condensed in the form of drops of liquid or small pieces of ice.

The condensation of vapors, as is shown experiment, occurs abruptly it leads at subsonic speeds to an increase in the velocity, and at supersonic speeds - to its decrease. The position of condensation shock in nozzle depends on relative humidity. With an increase in the relative humidity it it is displaced to critical section. Thus, for instance, with 50o/o of relative humidity jump is located from throat at a distance of two critical throat diameters, and with 25o/o of humidity, - at a distance of three diameters. On the reasons indicated for obtaining the qualitative flow on output from high-speed/velocity ones, it is necessary to decrease the humidity to the limits, by which will be guaranteed the absence of condensation shocks (approximately for numbers $M \leq 4-4.5$).

For hypersonic nozzles, as has already been mentioned earlier, for the purpose of the prevention of the liquefaction of the components of gas, is applied the intensive preheating. If in nozzle is formed normal shock wave, then is the pressure recovery factor after the normal shock

$$v_1 = \frac{q(\lambda)}{q\left(\frac{1}{\lambda}\right)},$$

where λ - the given speed before the jump.

After normal shock wave the speed in nozzle is subsonic. This nozzle divergent section of nozzle will serve as exit cone/diffuser with the recovery factor, equal to v_1 . The speed at the end of the nozzle can be determined, using the expression

$$q(\lambda) = \frac{F_0}{v_1 v_2 F}.$$

Pressure p_0 at the end of the nozzle is connected with pressure at entrance by the dependence

$$p = p_0 v_1 v_2 \left(1 - \frac{\kappa - 1}{\kappa + 1} \lambda^2\right)^{\frac{\kappa}{\kappa - 1}}$$

The account of the build-up of boundary layer along nozzle

liners has the important value for providing the uniformity of flow at high supersonic and hypersonic speeds of discharge.

Page 420.

At supersonic speeds it is necessary depending on form and length of the nozzle of speed and Re number additionally to increase flow areas after throat. As showed experiment, thus is provided the "nucleus" of constant velocity, which differs little in intake area.

For the wind tunnels of hypersonic speeds and the low density (see § VII.3) the build-up of boundary layer remains so/such considerable, that the useful nucleus of uniform flow comprises low portion of discharge area. Thus, for instance, in duct with numbers $M \approx 10$, at total pressure $p_0 = 1.25 \text{ atm (tech)}$ and $T_0 \approx 3000^\circ \text{K}$ the diameter of the "nucleus" of conical nozzle (30°) will prove to be equal to 25 mm, with exit diameter, - equal to 148 mm and $d_{\text{ex}} = 2.59 \text{ mm}$. For obtaining the flow core of similar high size/dimensions in ducts it is expedient to increase the size/dimensions of nozzle exit section.

349

REFERENCES.

1. А. К. МАРТЫНОВ. Экспериментальная аэродинамика. Оборонгиз, 1968.
2. Н. А. ЗАКС. Основы экспериментальной аэродинамики. Оборонгиз, 1953.
3. Я. Е. ЛЕВИНСОН. Аэродинамика больших скоростей. Оборонгиз, 1948.
4. У. Ф. ХИЛТОН. Аэродинамика больших скоростей. ИЛ, 1955.
5. Н. ГОШЕК. Аэродинамика больших скоростей. ИЛ, 1954.
6. Л. И. СЕДОВ. Методы подобия и размерности в механике. ГТТИ, 1957.
7. Р. ПЭНКХЕРСТ и Д. ХОЛДЕР. Техника эксперимента в аэродинамических трубах. ИЛ, 1955.
8. Г. Н. АБРАМОВИЧ. Прикладная газовая динамика. Гостехиздат, 1963.
9. И. Е. ИДЕЛЬЧИК. Справочник по гидравлическим сопротивлениям. Госэнергоиздат, 1960.
10. С. М. ГОРЛИН, И. И. СЛЕЗИНГЕР. Аэромеханические измерения. Изд-во «Наука», 1964.
11. С. Г. ПОПОВ. Некоторые задачи и методы экспериментальной аэромеханики. ГТТИ, 1952.
12. Г. ШЛИХТИНГ. Теория пограничного слоя. ИЛ, 1956.
13. Н. Я. ФАБРИКАНТ. Аэродинамика. Изд-во «Наука», 1964.
14. Н. Ф. КРАСНОВ. Аэродинамика тел вращения. Изд-во «Машиностроение», 1964.
15. У. Д. ХЕЙЗ, Р. Ф. ПРОБСТЕЙН. Теория гиперзвуковых течений. ИЛ, 1962.
16. Современное состояние аэродинамики больших скоростей, т. II. Под ред. Л. Хоуарта. ИЛ, 1962.
17. Исследование гиперзвуковых течений. Под ред. Ф. Р. Риддела. Изд-во «Мир», 1964.
18. Г. Г. ЧЕРНЫЙ. Течение газа с большой сверхзвуковой скоростью. Физматгиз, 1959.
19. Л. Г. ЛОЙЦЯНСКИЙ. Механика жидкости и газа. Физматгиз, 1959.

DISTRIBUTION LIST

DISTRIBUTION DIRECT TO RECIPIENT

<u>ORGANIZATION</u>	<u>MICROFICHE</u>	<u>ORGANIZATION</u>	<u>MICROFICHE</u>
A205 DMATC	1	E053 AF/INAKA	1
A210 DMAAC	2	E017 AF/RDXTR-W	1
B344 DIA/RDS-3C	9	E403 AFSC/INA	1
C043 USAMIIA	1	E404 AEDC	1
C509 BALLISTIC RES LABS	1	E408 AFWL	1
C510 AIR MOBILITY R&D	1	E410 ADTC	1
LAB/FIO			
C513 PICATINNY ARSENAL	1	FTD	
C535 AVIATION SYS COMD	1	CCN	1
C591 FSTC	5	ASD/FTD/NIIS	3
C619 MIA REDSTONE	1	NIA/PHS	1
D008 NISC	1	NIIS	2
H300 USAICE (USAREUR)	1		
P005 DOE	1		
P050 CIA/CRB/ADD/SD	1		
NAVORDSTA (50L)	1		
NASA/KSI	1		
AFIT/LD	1		
LLL/Code L-389	1		